

https://dspace.org/

The nature of hydrothermal fluids associated with granite-hosted, polymetallic mineralisation in the Eastern lobe of the bushveld complex

Freeman, Lauren Anne

1998
https://hdl.handle.net/10539/24747

Downloaded from a DSpace repository. https://dspace.org/

DISCUSSION

The results of the Raman analysis indicate the presence of H_2O, CO_2, N_2 and CH_4 in the fluids. The Raman responses in inclusions, where microthermometry had suggested the presence of volatiles, were not as good as was expected. Microthermometry suggested that gases other than CO_2 were present in the fluids. Many inclusions formed clathrates which melted at temperatures above 0°C, and some even had clathrate melting temperatures above 10°C. Furthermore, $T_{final\ melting}$ (CO_2) in fluid inclusions containing both liquid and vapour CO_2 occurred at temperatures below -56.6°C (the temperature at which final melting in pure CO_2 fluids occurs). When some of these inclusions were analysed, the Raman responses for most gases, including CO_2, was generally poor. Thus, the evolution of the gas content of the fluids could not be accurately assessed using this method.

The information that was obtained, however, does provide some insight into the nature of the fluids. The samples from Spoedwel and Houtenbek contain fluids associated with the sulphide paragenesis, and in addition to them containing significant amounts of solutes (indicated by PIXE analysis), the presence of N_2, CO_2 and CH_4 has been detected. The fluid inclusions from Grass Valley were associated with the precipitation of hydrothermal cassiterite and small amounts of galena, sphalerite and chalcopyrite. These fluids contained $CO_2 \pm N_2 \pm CH_4$. Thus, these gases were certainly present in the fluids associated with stage 2 (i.e. the precipitation of the sulphide assemblage) in the paragenetic sequence. In addition, the methane peak position served as an external geobarometer, from which pressure estimates of the true entrapment temperature of the fluids is possible. At Spoedwel, the pressure at which the fluids in fluorite were trapped was approximately 450 bar. At Grass Valley the late stage Type 5 fluid inclusions were trapped at pressures between 110bar and 450 bar. The entrapment pressure for fluids at Spoedwel and Grass Valley are identical in samples SP6 and GV02, and are relatively low, reflecting the fact that the fluids were not under high pressure as they were channelled along the fracture systems.

The results of the Raman analysis prompted further study of the gas chemistry of the fluid inclusions, and attempts to identify, and quantify the volatiles associated with the different stages in the paragenetic sequence were made by means of Quadrupole Mass Spectrometry.

6.3 QUADRUPOLE MASS SPECTROMETRY

Quadrupole Mass Spectrometry (QMS) of fluid inclusion gases was chosen in order to determine the gas/volatile content of fluids associated with each of the three mineral assemblages recognised in the Bushveld granites. Analytical techniques such as microthermometry and Raman spectroscopy have indicated the presence of CO_2, N_2 and CH_4 in the fluids, but reliable quantitative data from these techniques was not obtained. In addition, several questions were raised by the fluid inclusion microthermometry which required detailed spectrometric analysis to be answered. For example,

1) Clathrate melting temperatures above 10 °C cannot be accounted for by the presence of CO_2 alone. Are CH_4 and/or N_2 clathrates, which affect phase equilibria (Murphy and Roberts, 1996), responsible for these elevated final melting temperatures?
2) CO_2 seldom occurs unaccompanied by N_2 and/or CH_4 (van den Kerkhoff, 1990). In what proportions are these volatiles present in the fluids?
3) Can the fluids be categorised in terms of their volatile content?
4) Is it possible to determine at what stage in the evolution of the magmatic fluid that N_2 and CH_4 became significant, and can this be used to recognise the point at which the external fluid was introduced?

OVERVIEW

Quadrupole Mass Spectrometry is a destructive technique used for analysis of the volatile content of fluid inclusions. The fluid inclusion gases are released by crushing or decrepitating (heating the sample until the fluid inclusions burst) small samples under vacuum. The gases are passed through an inlet system to the ionizing filament. Most gases are "cracked" into smaller fragments at the quadrupole analyzer source, and these ionized molecules and molecular fragments are detected by a secondary electron multiplier. Determination of the relative abundances (mole fractions) of gases in a complex gas mixture requires the use of a matrix fitting procedure, provided as part of the operating software of the quadrupole (Jones and Kesler, 1992). The theory behind

into account cracking patterns (relative intensities of parent and "cracked" peaks at a particular pressure) for each gas in an analysis and delineates multiple contributions to masses by a series of simultaneous equations in a matrix. A correlation coefficient determined for each analysis defines how well the final composition fits the original raw data (Jones and Kesler, 1992)

EQUIPMENT

Analyses were carried out in the Department of Geological Sciences, University of Michigan, using a VG SXP600 quadrupole mass spectrometer (Figure 6.28). The system used in the laboratory is described by Graney and Kesler (1995), and is briefly reviewed here. The system has dual inlet ports, a closed electron source, and a secondary ectron multiplier (SEM) detector. The number of masses (1 to 16) monitored by the Quad94 software package, and the number of counts made at each mass are operator controlled.

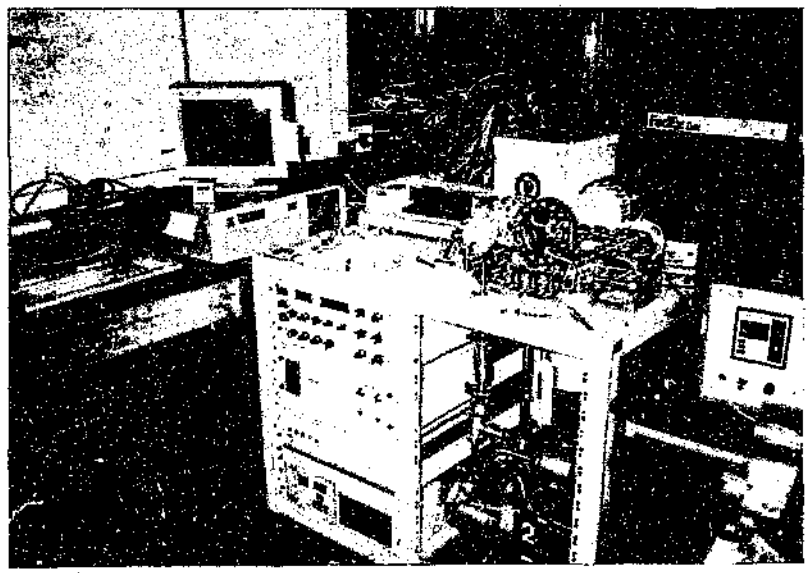


Figure 6.28 Photograph of the Quadrupole Mass Spectrometer at the University of Michigan.

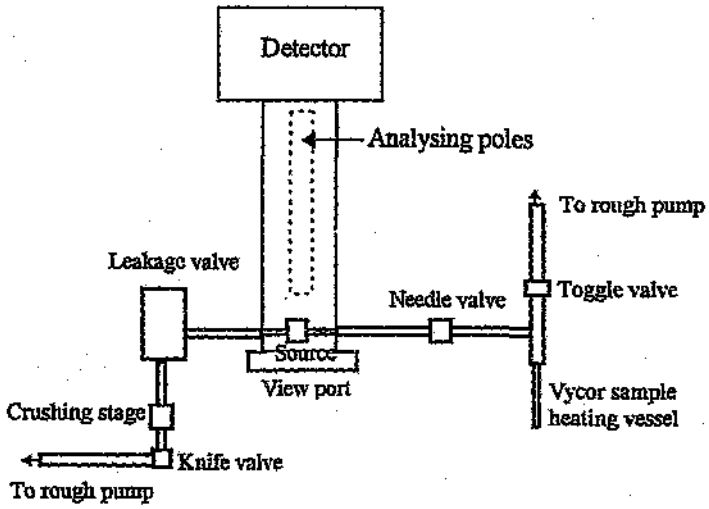


Figure 6.29 Schematic diagram of the inlet systems on the University of Michigan quadrupole mass spectrometer (re-drawn from Jones and Kesler, 1992).

SAMPLE MATERIAL

The samples chosen for crush and decrepitation analyses were ones on which petrography and microthermometry had already been carried out. A list of the samples from each deposit is shown below (Table 6.7).

Table 6.7 List of samples chosen for QMS from Grass Valley, Spoedwel, Albert, Leeufontein and Houtenbek.

DEPOSIT	SAMPLE	SAMPLE DESCRIPTION
Grass Valley	MF3A	Subsolvus granite.
	GV01	Quartz vein associated with hematite. CO_2 fluid inclusions present.
	GV02	Quartz associated with hydrothermal cassiterite.
	GV04	Massive, pegmatitic quartz associated with pyrite and chlorite.
	GV05	Quartz vein.
	GV07A	Euhedral quartz crystals lining walls of open fracture -generation 1.

Table 6.7 continued List of samples chosen for QMS from Grass Valley, Spoedwel, Albert, Leeufontein and Houtenbek.

DEPOSIT	SAMPLE	SAMPLE DESCRIPTION
	GV07B	Euhedral quartz crystals in open fracture -generation 2.
	GV08	I te stage fluorite.
Spoedwel	SP4	Medium-grained hypersolvus granite with minor quartz.
	SP5	Quartz vein material with massive hematite.
	SP6	Graphic granite.
	SP9	Fine-grained granite.
	SP13	Massive sulphide ore with late stage fluorite veins.
	L1	Vein quartz associated with chalcopyrite.
Albert	RP11 11A	Vein quartz.
	RP1 11B	Vein quartz.
	RP2 20B	Fluorite containing fluid associated with sulphide and hematite/fluorite assemblages.
	RP2 27A	Quartz vein associated with hematisation and chloritisation of the host rock.
	RP2 29	Subsolvus granite which has been mildly hematised.
	AS25 10C	massive, quartz vein material with stringers of hydrothermal arsenopyrite, sphalerite and chalcopyrite.
	RP1 11A	Vein quartz.
Leeufontein	BF2	Tourmaline spheroid.
	TB	Tourmaline spheroid.
	KK03	Vein quartz associated with hematite.
	KK01	Tourmaline crystals.
	BBK1	Coarse-grained Klipkloof Granite.
	WG35	Fine-grained Klipkloof Granite.
	NEBO	Nebo granite.
	WG03	Albitised Klipkloof Granite.
	WG43	Fine-grained Klipkloof Granite
	ALB	Albitised Klipkloof Granite
Houtenbek	HBF	Fluorite.

METHODS

Samples for the crush analyses were prepared by separating quartz and fluorite from the other minerals, using a magnetic separator and then hand picking grains to ensure purity of the sample. In most cases, material where different quartz generations could be separated by hand (e.g. quartz veins with multiple growth stages) was selected.

Samples of between 5mg and 50mg, which had been baked in an oven (at 60°C) to drive off excess surface water, were placed in a stainless steel sample holder. The sample holder was bolted to the base of the modified Nupro valve. Pressure in the sample chamber is then reduced using roughing and turbomolecular pumps until the pressure at the pump is $<10^{-7}$ torr. The sample was then crushed with the turbomolecular pump on-line (Graney and Kesler, 1995).

The samples selected for the decrepitation analyses were fragments of doubly polished thin sections which had been mapped, and on which microthemometry had already been done. Wherever possible, fragments containing only one known fluid inclusion assemblage were chosen. However, this proved to problematic, because the samples contain numerous inclusions, and on such a small scale it was difficult to be certain that no fluid inclusions from other assemblages were present. The samples was placed in quartz tubes which are connected to the inlet system with Teflon seals. The inlet system is then evacuated and the tubes are heated with a resistance furnace. The rate of heating was controlled by a Variac rheostat in line with a temperature controller connected to a thermocouple inside the furnace. The fluid inclusions burst when the internal pressure exceeds the strength of the host mineral and the gases are liberated. The masses analysed for were: 2 (H_2); 12 (C^+); 14 (N^+); 15 (CH_3^+/NH^+); 16 ($O^+/CH_4^+/NH_2^+$); 18 (H_2O^+); 28 ($N_2/C_2H_4^+/CO^+$); 33 (H_2S); 34 ($H_2{}^{32}S^+/{}^{34}S^+$); 36 (HCl); 40 (Ar^+); 44 (CO_2^+/N_20^+); 48 (SO^+).

The spectra generated are plots of SEM current (mA) (or Intensity expressed at the negative logarithm of the SEM current) against time. In crush analyses, all the gas is liberated simultaneously and an abrupt increase in detector response occurs

milliseconds after crushing, which is observed as a sharp jump in the spectrum. With time, the response decays until all masses return to background levels. The number of cycles varied between 300 and 500 depending on how long it took for the sample to return to background.

In the decrepitation analyses, temperature was gradually increased and recorded in connection with time and number of cycles, so that the temperature of individual inclusion bursts could be determined and the amounts of each gas liberated from an inclusion could be measured.

RESULTS

The results of the crush analyses are shown in Table 6.8 The samples are tabulated according to deposit. The results have been normalised and are reported in mole %.

The fluids are predominantly aqueous, consisting of between 92 to 99 mole % water (Figure 6.30). The samples containing the lowest amount of water are those associated with the late stage precipitation of quartz-hematite veins at Spoedwel and Grass Valley, and contain considerable amounts of CO_2 (2 to 6 mole %). In addition to CO_2, most samples contained minor amounts of N_2 CH_4, C_2H_6, Ar, HCl, and SO_2.

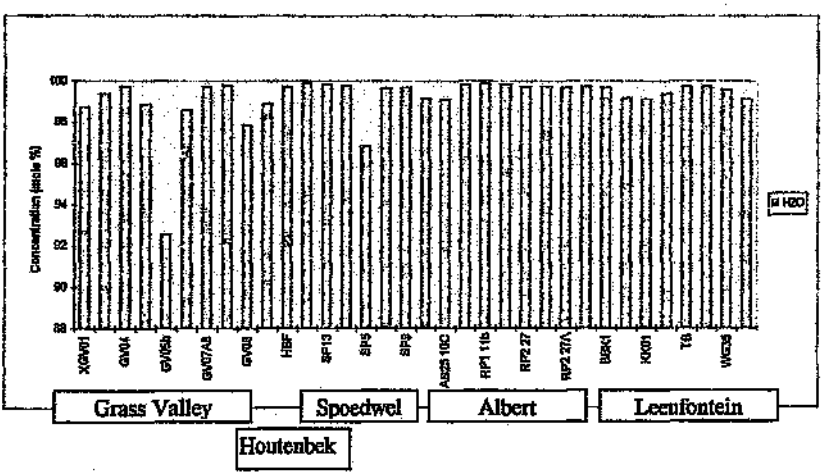


Figure 6.30 Bar chart showing the percentage of water in fluid inclusions from Grass Valley, Houtenbek, Spoedwel, Albert and Leeufontein.

Table 6.8 Results of crush analyses (mole %)

Filename	H2O	N2	H2S	SO2	SO2+H2S	CH4	C2H6	C3H8	CnHn	Ar	CO2	HCl	H2
GRASS VALLEY													
GV04	99.75942	0.017724	0.005622	0.001526	0.007149	0.007255	0.00213	0	0.009385	0.000408	0.13803	0.000872	0.067014
GV05a	98.87713	0.077294	0.004002	0.004917	0.008919	0.014995	0.003414	0	0.018409	0.001617	0.988661	0.00198	0.025991
GV05b	92.58427	0.322211	0.003515	0.007741	0.011256	0	0.004643	0.040011	0.044955	0.003629	6.995985	0.002687	0.03501
GV06d	98.58107	0.164452	0.004351	0.009117	0.013468	0.014001	0.003218	0	0.017219	0.002363	1.174066	0.001922	0.045003
GV07A8	99.73043	0.146396	0.006028	0.0019	0.007929	0.005509	0.004794	0	0.010304	0.000228	0.046011	0.000602	0.058014
GV07B8	99.78592	0.06678	0.002246	0.003005	0.005251	0.00823	0.002799	0	0.011029	0.000696	0.094028	0.001281	0.03501
GV08	97.88761	0.034596	0.004324	0.001353	0.005677	0.075252	0.003522	0	0.078774	0	1.795007	0.000677	0.197662
MF3A	98.90125	0.111795	0.008759	0.024008	0.032766	0.022007	0.005871	0	0.027878	0.002058	0.920291	0.003961	0
XGV01	98.73211	0.104574	0.004144	0.005992	0.010135	0.009314	0.003717	0	0.013032	0.001554	1.110147	0.002445	0.026003
XGV02	99.37996	0.120137	0.003495	0.003426	0.00692	0.009338	0.003054	0	0.012393	0.001473	0.436206	0.001895	0.041019
ALBERT													
AS25 10c	99.16976	0.067212	0.00219	0.003371	0.005561	0.011002	0.003104	0	0.014106	0.001379	0.703126	0.001847	0.037007
AS25 10C	99.12162	0.074736	0.00361	0.006708	0.010318	0.00203	0.002387	0.009072	0.013489	0.000667	0.742162	0	0.037008
RP1 11a	99.86307	0.058732	0.003072	0.006633	0.009705	0.006408	0.002532	0	0.00894	0.001792	0.056012	0.00175	0
RP1 11b	99.88866	0.050089	0.003156	0.004605	0.00776	0.005254	0.002409	0	0.007663	0.001489	0.043008	0.00133	0
RP11 11	99.83318	0.061256	0.003155	0.001704	0.004859	0.008751	0.00257	0	0.011321	0.001142	0.043011	0.001221	0.044012
RP2 27	99.73691	0.069615	0.004489	0.008927	0.013416	0.011002	0.003815	0	0.014817	0.001822	0.116025	0.00338	0.04401
RP2 28B	99.76633	0.033105	0.003447	0.002927	0.006374	0.035026	0.002865	0	0.037891	0.000182	0.035026	0.001999	0.119089
RP2 27A	99.71825	0.073	0.012	0.011	0.023	0.015	0.004344	0	0.019344	0.003468	0.102	0.003939	0.057
RP2 29	99.73476	0.073	0.009737	0.018	0.027737	0.013	0.006564	0	0.019564	0.004114	0.136	0.004823	0

Table 6.8 Results of crush analyses (mole %)

Filename	H2O	N2	H2S	SO2	SO2+H2S	CH4	C2H6	C3H8	CnHn	Ar	CO2	HCl	H2
SPOEDWEL													
L1	99.88967	0.033967	0.003043	0.000916	0.003959	0.009829	0.002195	0	0.012024	0.000764	0.059012	0.0006	0
SP13	99.8423	0.127649	0	0.003097	0.003097	0.023016	0.003936	0	0.026952	0	0	0	0
SP4	99.80551	0.052776	0	0.001435	0.001435	0	0.003335	0	0.003335	0.000902	0.136042	0	0
SP5	96.82295	0.179822	0.004503	0.00306	0.007563	0.028003	0.004262	0	0.032265	0.001897	2.91436	0.002142	0.039005
SP6	99.6323	0.078	0.002328	0.002443	0.004771	0.019	0.002987	0	0.021987	0.001358	0.260001	0.001579	0
SP9	99.70441	0.030094	0.005906	0.00159	0.007495	0.024011	0.002184	0	0.026195	0.000227	0.113051	0.00047	0.118054
HOUTENBEK													
HBF	99.73708	0.021335	0.005596	0.003532	0.009128	0.030021	0.003116	0	0.033138	0	0.098063	0.001174	0.110078
LEEUFONTEIN - EAST OF MARBLE HALL													
ALB	98.8548	0.637992	0.005122	0.012	0.017122	0.028	0	0	0.028	0.019	0.438995	0.004088	0
BBK1	99.72005	0	0.003595	0.004205	0.007799	0.06801	0	0	0.06801	0	0.202028	0.002108	0
BF2	99.20734	0.556201	0.002532	0.004096	0.006629	0.027016	0.003474	0	0.03049	0.007751	0.165095	0.002481	0
KK01	99.14088	0.092336	0	0.001645	0.001645	0.014002	0.002892	0	0.016895	0.001543	0.745127	0.001575	0
KK03	99.41086	0.1308	0.004295	0.003697	0.007993	0.16974	0	0	0.16974	0	0.278574	0.002033	0
TB	99.74531	0.072	0.002552	0.002417	0.004969	0.051	0.002842	0	0.053842	0.004683	0.119	0	0
WG03	99.74914	0.094507	0.002305	0.002914	0.005219	0	0.003701	0	0.003701	0.0044	0.142101	0.000928	0
WG35	99.59523	0.160282	0.004257	0.004056	0.008313	0.022006	0	0	0.022006	0.009112	0.205054	0	0
WG43	99.13435	0.578628	0.004013	0.004661	0.008674	0.066049	0	0	0.066049	0.008456	0.201149	0.002697	0

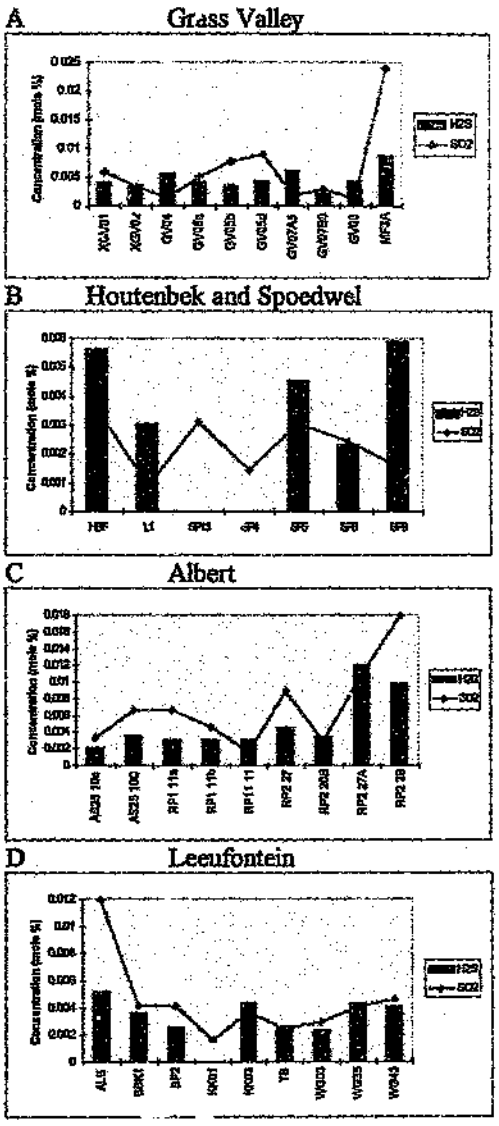


Figure 6.31 Bar charts showing the concentrations of H_2S and SO_2 (mole %) in samples from Grass Valley (A), Houtenbek and Spoedwel (B), Albert (C) and Leeufontein (D).

At Grass Valley, the early fluids associated with cassiterite precipitation (XGV02) contain equal amounts of H_2S and SO_2. However, fluids associated with late stage quartz veins (XGV01, GV05 and GV07) tend to contain greater amounts of SO_2. Samples GV04 and GV07a (first vein quartz generation) which is associated with pyrite, contain greater amounts of H_2S. The fluids associated with the subsolvus granite (MF3a) contain approximately three times more SO_2 than the fluids associated with sulphide-bearing quartz veins.

The fluorite samples from Houtenbek (HBF) and Spoedwel (SP13), and the late stage hematite-quartz sample from Spoedwel (SP5), contain more SO_2 than the hematitised hypersolvus granites hosting disseminated sulphide mineralisation. The H_2S content of the fluids in all samples associated with mineralisation, except the late stage fluorite (SP13), is greater than the SO_2 content.

At Albert, the subsolvus host granites (RP2 29) contain comparable amounts of SO_2 and H_2S as the subsolvus granite at Grass Valley (MF3a). Quartz vein material with no sulphides (RP1 11a and b) contains more SO_2 than H_2S, while the opposite is true for veins containing sulphide mineralisation.

The fine-grained (WG03, WG35, WG43) and coarse-grained (BBK1) Klipkloof Granites contain similar sulphur contents. Altered Klipkloof Granite i.e. tourmalinised and albitised material (BF2 and WG03), contains higher SO_2 concentrations than the unaltered rock. The fluids associated with quartz-hematite veins contain slightly more H_2S (KK03), and the fluids in tourmaline crystals (KK01) contain no H_2S.

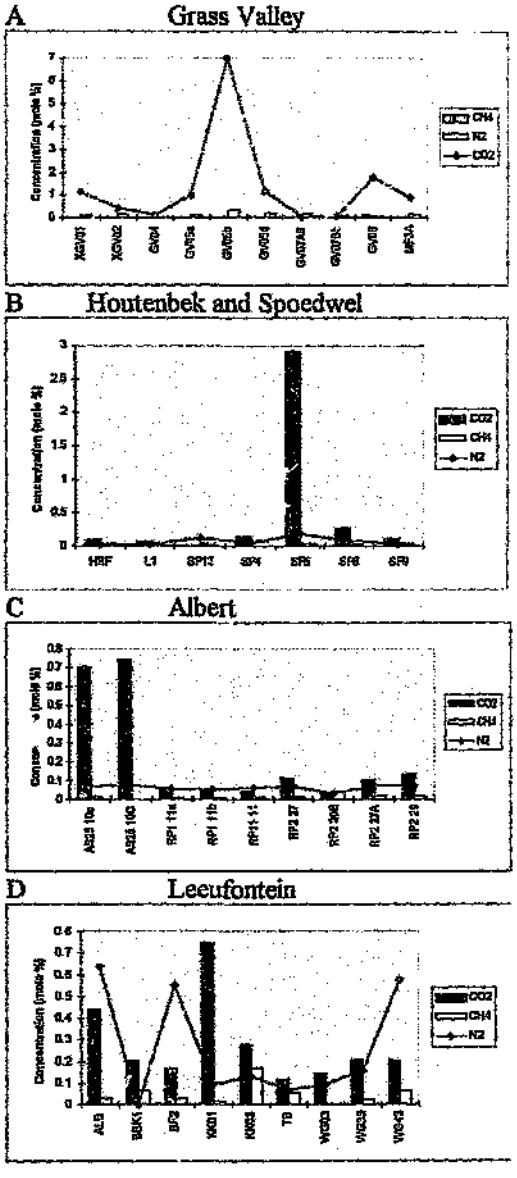


Figure 6.32 Bar charts showing the CO_2, CH_4 and N_2 concentrations (mole %) of fluids in samples from Grass Valley (A), Houtenbek and Spoedwel (B), Albert (C) and Leeufontein (D).

The concentration of CO_2 in the fluids associated with mineralisation at Grass Valley, and with the subsolvus granites, is minor in comparison with the high concentrations in the fluids associated with hematite precipitation in quartz generations 7 and 8 in vein quartz (GV05b). These fluids are trapped as secondary trails of inclusions in fluorite (GV08). N_2 ($\pm$ CH_4) are more abundant in the subsolvus granite (MF3a) and in the late stage fluids trapped in vein quartz (GV05a, b and d). The fluids associated with hydrothermal cassiterite and sulphide mineralisation contain small amounts of N_2 and CO_2.

The late stage quartz-hematite veins at Spoedwel contain large amounts of CO_2 in comparison with the earlier fluids associated with sulphide mineralisation and which are trapped in earlier generations of quartz veins. The N_2 content of these fluids is also greater than the earlier fluids.

The concentration of N_2 is relatively uniform in the samples from Albert. The host granite (RP2 29) contains similar amounts of N_2, CO_2 and CH_4 as the quartz veins. The late stage fluorite contains greater amounts of N_2 than the quartz veins and host granite. Sample AS25 10C contains significant amounts of CO_2.

The N_2 content of the fluids increases from the hydrothermally altered Nebo Granite (Coarse-grained Klipkloof Granite) through to the fine-grained Klipkloof Granite, and is most abundant in the altered granite (tourmaline spheroids). The fluids in tourmaline crystals contain abundant CO_2 , and the fluids associated with the late stage quartz-hematite veins contain significant amounts of CO_2, N_2 and CH_4.

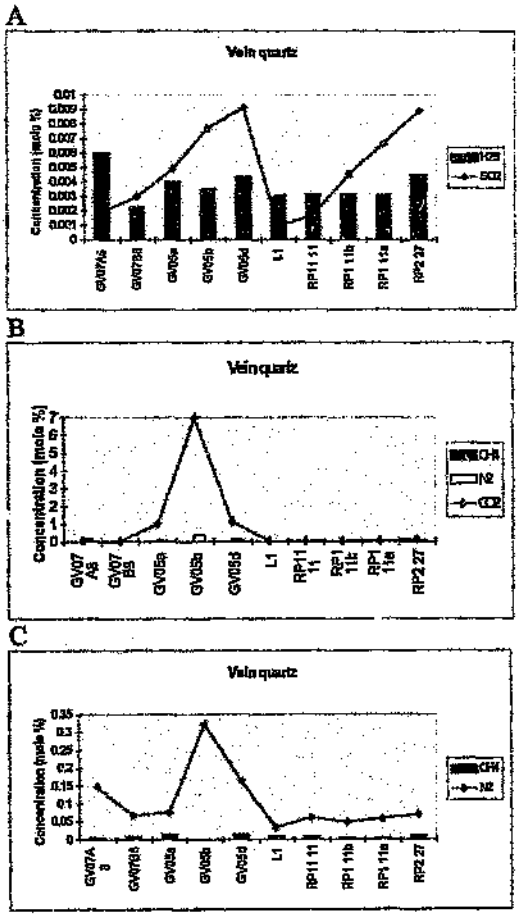


Figure 6.33 Bar charts showing the H_2S, SO_2 (A), CO_2, CH_4 and N_2 (B and C) concentrations (mole %) of fluids in samples of vein quartz from Grass Valley, Spoedwel, and Albert .

The vein quartz samples from each of the deposits have been selected and are compared in Figure 6.33 A-C. The H_2S content of vein material does not vary considerably. The fluids associated with the first vein quartz generation (GV07A8) contain the highest H_2S concentration, and the fluids in subsequent quartz generations contain slightly less H_2S. The SO_2 content of these fluids increases with time at each deposit. The fluids in the earliest quartz vein material have the lowest SO_2 values, and the highest values were recorded in the youngest quartz vein material.

The concentration of CO_2 in the vein-hosted fluid inclusions overshadows that of CH_4 and N_2, and for this reason a separate plot of just CH_4 and N_2 is shown. The fluids containing abundant CO_2 at Grass Valley also contain significant amounts of N_2. The N_2 content of the fluids preceding the late stage CO_2-N_2-rich fluids at Grass Valley, increases from Spoedwel (L1) to Albert (RP2 27).

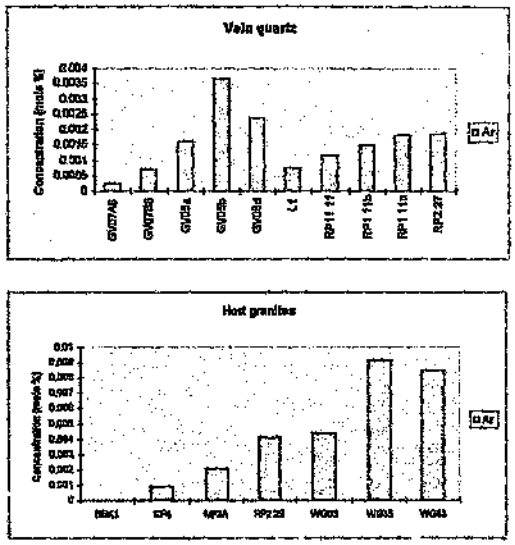


Figure 6.34 Bar charts showing the Ar concentration (mole %) in samples of (A) vein quartz from Grass Valley, Spoedwel and Albert and (B) hypersolvus and subsolvus granites.

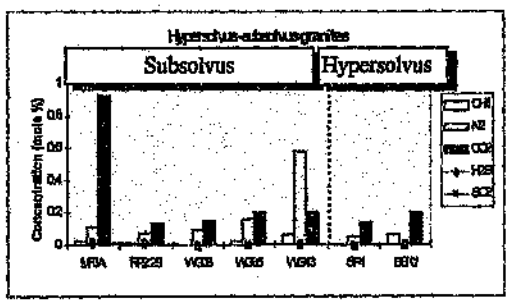


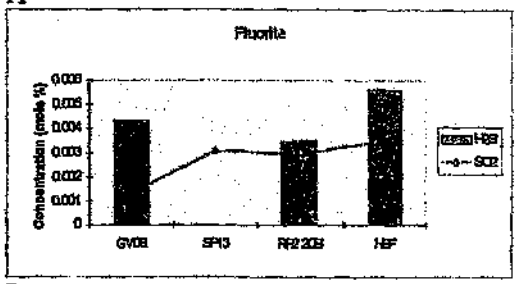
Figure 6.35 Bar chart showing the difference in concentrations of the major volatiles in hypersolvus and subsolvus granites

The Ar content of the fluids in vein quartz follows a similar pattern to SO_2. At each deposit, the earliest fluids have the lowest concentration of Ar. In addition, there is an overall increase in Ar in the fluids associated with quartz veins from Grass Valley, to Spoedwel and Albert.

The Ar content of the host granites varies depending on the nature of the granite. The hydrothermally altered Nebo Granite (or Coarse-grained Klipkloof Granite) contains no Ar, and the hypersolvus granite at Spoedwel contains only a small amount of Ar. The fluids associated with the subsolvus granites at Grass Valley (MF3a), Albert (RP2 29), and Leeufontein (WG03, WG35 and WG43), contain progressively greater amounts of Ar.

The hypersolvus and subsolvus granites can be differentiated in terms of their volatile content. The hypersolvus granite (Nebo) contains virtually no SO_2, while the subsolvus granites contain small amounts of SO_2 and H_2S. In addition, N_2 is not as abundant in the hypersolvus as it is in the subsolvus granites.

A



B

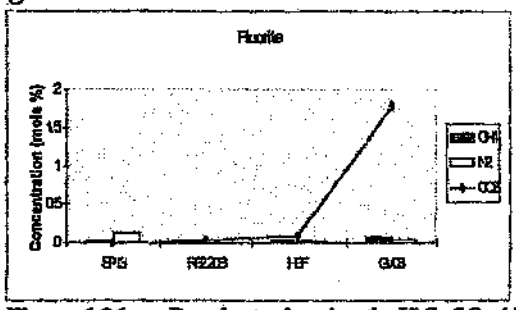
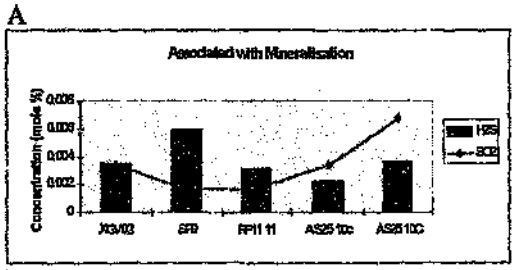


Figure 6.36 Bar charts showing the H_2S, SO_2 (A) CO_2, CH_4 and N_2 (B) concentrations (mole %) of fluids in samples of fluorite.

The fluorite at Grass Valley, Albert and Houtenbek contain greater amounts of H_2S than SO_2, while at Spoedwel no H_2S was detected.

The late stage fluorite at Spoedwel contains the greatest N_2 concentration of all the fluorite samples analysed. CO_2 and CH_4 at Spoedwel are minor in comparison with the concentrations measured in the fluorite sample from Grass Valley. However, it should be noted, that the fluid inclusions containing high concentrations of these components are not related to fluorite precipitation, but rather were derived from fluids associated with the younger quartz-hematite veins.

A



B

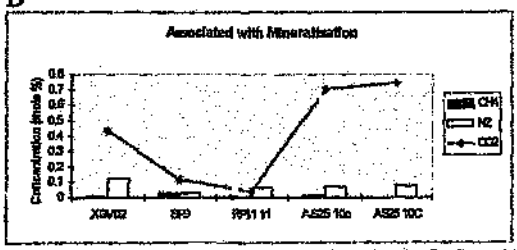


Figure 6.37 Bar charts showing the H_2S, SO_2,(A) CO_2, CH_4 and N_2 (B) concentrations (mole %) of fluids associated with mineralisation.

The sulphur content of fluids associated with mineralisation at Grass Valley (XGV02), Spoedwel (SP9) and Albert (RP1 11, AS25 10C) are broadly similar. Equal amounts of H_2S and SO_2 are present at Grass Valley, while H_2S is more abundant in the samples containing sulphides at Spoedwel and Albert. The high SO_2 content of the duplicate analyses of AS25 10C may be due to contamination by later fluids as secondary inclusions within the sample. AS25 10C also contains large amounts of CO_2. The N_2, CO_2 and SO_2 content of this sample compares favourably with sample XGV02.

The results of the thermal decrepitation analyses are filed in the Appendix. At Grass Valley, three distinct episodes of fluid inclusion decrepitation were recorded in samples associated with cassiterite precipitation. The lowest temperature fluids ($T_{decrepitation}$ 85 to 118°C) contain only CO_2 and N_2 molecular fragments. The first water-containing inclusions decrepitated at temperatures above 206°C, and also contained CO_2 and N_2 and H_2S/SO_2 fragments. The highest temperatures for decrepitation were at 363°C and consisted of CH_4, CO_2 and N_2 fragments.

At Spoedwel a sample of vein quartz associated with sulphide precipitation contained three main episodes of decrepitation. The first is in approximately the same range as the low temperatures fluids in the Grass valley sample associated with cassiterite (i.e. 83 °C to 100°C). These fluids contain Ar, H_2O, CO_2 and N_2 fragments. Between 138 °C and 150°C, the peaks for Ar, H_2O, and N_2 fragments return to background levels and large CO_2 peaks dominate. Another population of fluid inclusions containing Ar, H_2O, CO_2 and N_2 fragments, began to decrepitate at 245°C and continued until 300°C.

In quartz veins containing sulphides at Albert, in addition to the fluids which decrepitated between 85 °C and 110 °C (CO_2 and N_2 fragments), a broad water plateau was observed between 256 °C and 314°C. At 350°C H_2S and HCl became evident. A second generation of CO_2-bearing fluid inclusions decrepitated at 381 °C, and a third generation decrepitated at 450°C. Thus, three distinct fluids containing CO_2 are present at Albert.

Decrepitation temperatures of fluids in multiple generations of vein quartz at Grass Valley indicate that the lowest temperature fluids (85°C) are not preserved in the early quartz generations and that the maximum decrepitation temperature is 473°C. These are carbonic fluids, and no water peaks were detected. The first water peaks are preserved in the seccond quartz generation, in an assemblage that decrepitated at temperatures below 400°C, and contain Ar, CO_2 and N_2 . The low temperature (80°C) fluids were detected in quartz generation 3, and contain CH_4, CO_2 and N_2. An assemblage of CO_2-rich inclusions

began to decrepitate at 194°C, and the first water and Ar peaks were observed at 250°C. A second assemblage began to decrepitate at 285°C and continued until 500°C. In the fourth quartz generation the lowest temperature aqueous inclusions were encountered (100°C). N_2 and CO_2 were liberated from an assemblage which decrepitated between 200 °C and 220°C, and a second batch of water peaks appeared 293 °C and 322°C. The last quartz generations associated with hematite precipitation contain N_2, Ar, CO_2 and minor amounts of water. These inclusions decrepitated over a broad temperature range, beginning at 97°C and continuing until 500°C. Thus, three CO_2 generations are also preserved at Grass Valley.

DISCUSSION

The results of the quadrupole mass spectrometry show that complex gas mixtures are present in the fluids from all the study areas and that these fluids are somewhat similar at each deposit.

In terms of the sulphur content, the fluids associated with mineralisation are distinguished from the subsolvus granites at the ore deposits, in that they contain greater amounts of SO_2 and H_2S than the orebodies themselves (Figure 6. 38). A possible explanation for this is that as the residual melt approached water saturation, the sulphur content was also increased by being partitioned into the residual melt. Thus, as crystallisatior of the subsolvus granites proceeds, the sulphur is incorporated into the feldspars. In addition, the high concentration of SO_2 in the fluids in these subsolvus granites compared with the low SO_2 concentrations in the barren Nebo Granite and coarse-grained Klipkloof Granite, suggests that the oxidation potential of the fluids had been increased by the time crystallisation of subsolvus granite took place. The oxidation potential of the fluids may have been increased by the introduction of an external, oxidised fluid. In the model proposed for the occurrence hypersolvus and subsolvus granites, Martin and Bonin (1976) attributed the change in textures to the incursion of meteoric water. Considering the high SO_2 concentrations in the subsolvus granite, this hypothesis does indeed seem feasible.

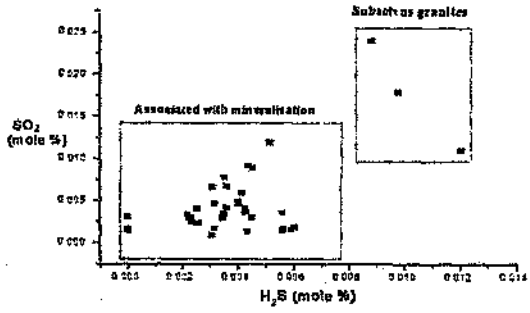


Figure 6. 38 SO_2 (mole %) versus H_2S (mole %) of fluids associated with the subsolvus granites, and with mineralisation from Grass Valley, Houtenbek, Spoedwel and Albert.

In addition to the high SO_2 concentrations in the fluids associated with the subsolvus granites at the ore deposits, these fluids contain greater concentrations of N_2, CH_4 and CO_2 than the hypersolvus granites (see Fig 6.35). Although N_2 and CO_2 may be derived from a magmatic source, the presence of hydrocarbons in the fluid usually implies that an external (connate) fluid was introduced at some stage.

In order to determine at which stage in the paragenetic sequence the external fluid was introduced, the Ar content of the fluids was examined. Norman and Musgrave (1992) have shown that the Ar content of magmatic fluids is low compared with the Ar contents of deep (and shallow) circulating meteoric waters. In Figure 6.34, samples of hypersolvus and subsolvus granite are arranged from the first formed to the last formed. A gradual increase is observed in the Ar content from the hypersolvus granites, through to the late stage Klipkloof Granite dyke material. The subsolvus granites associated with mineralisation have intermediate concentrations of Ar, which according to Norman and Musgrave (1992) indicates mixing between magmatic and deep circulating meteoric fluids. The higher Ar content in the fluids in the fine-grained Klipkloof Granite dykes implies that the magmatic fluids were diluted by the increasing meteoric component.

The origin of the fluids can be predicted using N_2/Ar ratios (Giggenbach, 1986). The N_2/Ar ratio in air saturated water is approximately 36, but may be as high as 50 as a result of entrained air. Crustal rocks contain low but significant concentrations of N_2 that average 30ppm in basalts, 21ppm in granites, 73ppm in carbonates, 120ppm in sandstone and 602ppm in shales. In comparison, geothermal fluids associated with recent magmatic activity have N_2/Ar > 100 (Norman and Musgrave, 1992). N_2/ Ar ratios were determined for the samples of hypersolvus and subsolvus granites, as well as for the fluids associated with mineralisation. These ratios are shown in the bar charts in Figure 6.39. No ratio could be calculated for the Nebo Granite since no Ar was detected. The ratios for vein quartz associated with mineralisation at Spoedwel and Albert fall in the range for air saturated water. The fine-grained Klipkloof Granite at Leeufontein and the subsolvus granite at Albert also fall in this range. The ratios for the late stage fluids associated with quartz-he- 'e veins contain high N_2/Ar ratios. The samples associated with sulphide precipitatio.. also contain higher N_2/Ar ratios than that for air saturated water, possibly suggesting th"t magmatic gases were involved. Comparing the histograms in Figure 6.39, is appears that the quartz veins have higher N_2/Ar ratios than the granites. However, when taking into account the position of each sample within the crystallisation history of the pluton, it is evident that the early quartz vein generations associated with cassiterite precipitation contain fluids with more of a magmatic ratio than samples associated with later stage sulphide mineralisation. The granite samples for which ratios could be calculated were samples of subsolvus and transsolvus granite, where the introduction of meteoric/connate water has been shown in Chapter 4, and therefore, show lower N^2/Ar ratios than quartz veins formed early in the paragenetic sequence, before the incursion of an external fluid component became significant.

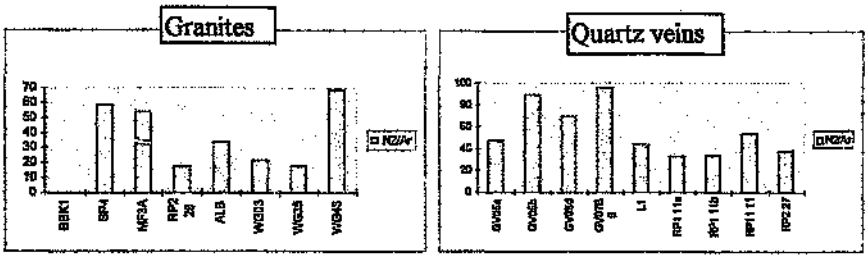


Figure 6. 39 Bar charts of N_2/Ar in host granites and in vein quartz associated with mineralisation.

The sulphur content of the late stage Klipkloof Granite is similar to that in the fluids associated with mineralisation and quartz veins. Binary plots of SO_2 versus H_2S are shown in Figures 6.40 to 6.43. The data points have been labelled for easy reference, and boxes drawn around samples associated with mineralisation. At Grass Valley, Spoedwel and Albert, the fluids associated with sulphide mineralisation plot in similar ranges. These fluids contain less SO_2 than the subsolvus granites that they are associated with, since the sulphur was extracted from the melt and incorporated into the sulphide minerals. The fluids post-dating sulphide precipitation are thus depleted in sulphur relative to the host subsolvus granite.

The fluids associated with late-stage fluorite precipitation at each of the deposits contain greater amount of SO_2 than the fluids associated with the sulphide assemblage. At Spoedwel and Houtenbek in particular, the late stage fluorite contains significantly more SO_2. This enrichment in SO_2 is also observed in the late stage quartz-hematite veins at Grass Valley, Spoedwel and Albert. The source of the additional sulphur is uncertain, but it seems likely that it was transported into the system, by the same fluid associated with the elevated CO_2, CH_4 and Ar concentrations .

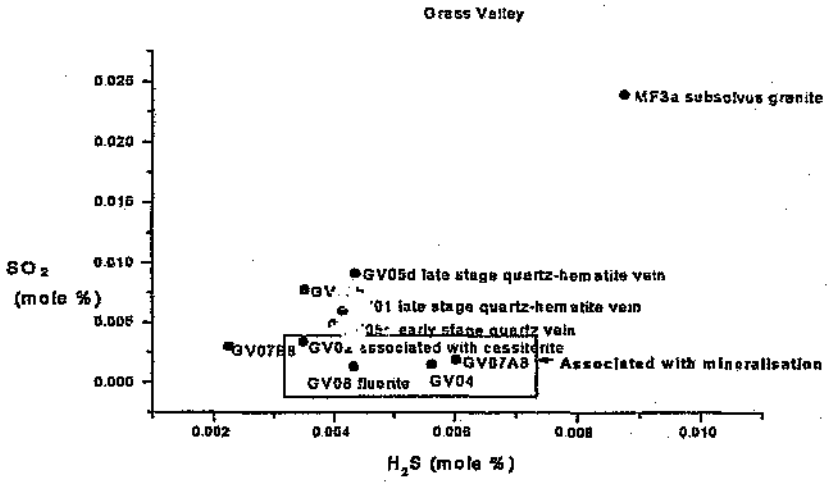


Figure 6.40 SO_2 (mole %) versus H_2S (mole %) in fluids at Grass Valley.

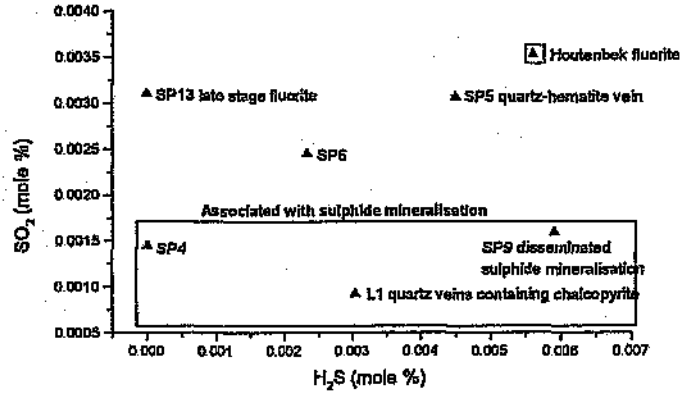


Figure 6.41 SO_2 (mole %) versus H_2S (mole %) in fluids at Houtenbek and Spoedwel.

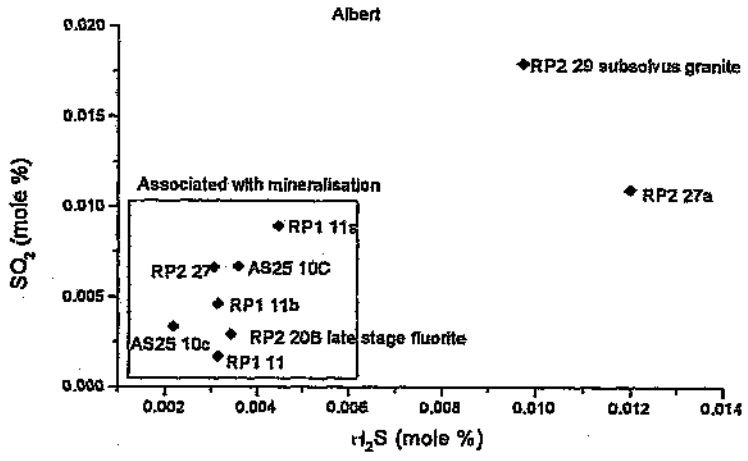


Figure 6.42 SO_2 (mole %) versus H_2S (mole %) in fluids at Albert.

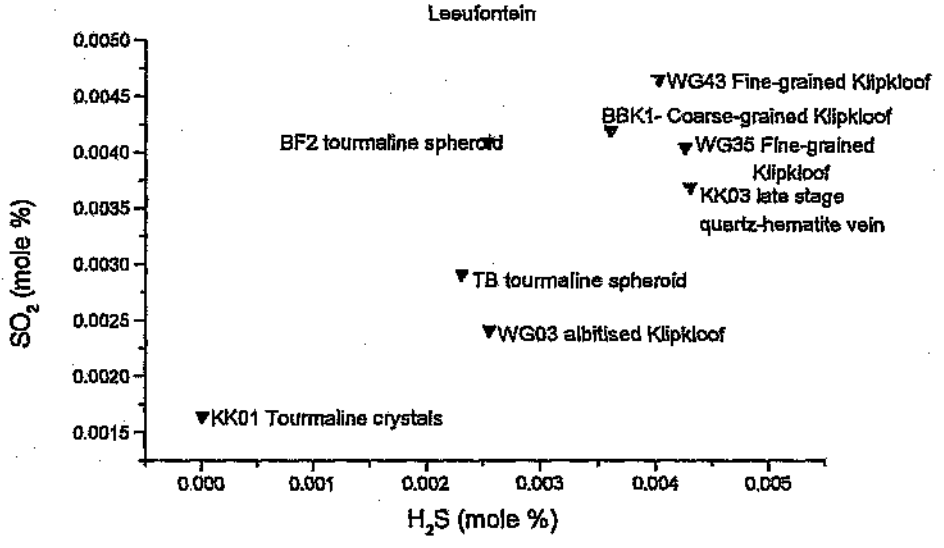


Figure 6.43 SO_2 (mole %) versus H_2S (mole %) in fluids at Leeufontein.

CHAPTER 7

STABLE ISOTOPES

In previous chapters, numerous lines of evidence pointing toward the involvement of an external fluid in the mineralising system have emerged. For example, during microthermometry, two distinct end member fluid types were recognised in terms of their compositions and homogenisation temperatures. PIXE analysis revealed that lower temperature fluid contain significant amounts of a variety of metals, in contrast with the relatively barren, higher temperature fluid. The volatile composition of the metal charged fluids (determined by quadrupole mass spectrometry and Raman spectroscopy), indicated the presence of N_2, CH_4 and CO_2, the concentrations of which increase with time, being more abundant in the late stage veins and aplite dykes. In addition, a steady increase in Ar contents in the fluids was observed, along with N_2/Ar ratios which indicate the presence of N_2 derived from both magmatic and meteoric origins. Thus, a study of stable isotopic signatures of the fluids associated with mineralisation in the Bushveld granite was undertaken, in order to provide unambiguous evidence regarding the origins of fluids and the validity of fluid mixing.

OVERVIEW

The application of stable isotope geochemistry to ore deposit research has been based on an understanding of mechanisms, and magnitudes of isotopic fractionation that accompany various geological processes; such as knowledge of equilibrium isotopic fractionation factors between compounds as a function of temperature and other geochemical parameters and the kinetic effects accompanying a conversion of one substance to another under a variety of conditions (Ohmoto, 1986).

H, O, C and S isotopes provide useful information on aspects of ore forming processes which include: thermal conditions of ore formation; the origin and mass of ore forming fluids, geometry of plumbing systems, duration of hydrothermal activity; sources of ore constituents (especially sulphur, carbon and metals); redox state, metals/sulphide ratios, pH, and CO_2/CH_4 ratios; mechanisms of metal and sulphur transport and ore

deposition; and the origin and evolutional processes of ore-forming magmas. However some isotopic systems are more useful than others in particular circumstances. Sulphur isotopes are generally more useful in constraining formational temperatures of sulphide ore deposits, while analysis of hydrological aspects of ore formation rely more heavily on H and O isotopic data. Sulphur and C isotopes assist in understanding chemical aspects of ore formation (Ohmoto, 1986).

Hydrogen and Oxygen Isotopes

The origin of ore-forming fluids and the hydrologic nature of plumbing systems has been estimated by comparing the H and O isotopic compositions of ore forming fluids with those of natural waters such as sea water, meteoric water, magmatic water, connate water and metamorphic water, and by comparing the H and O isotopic compositions of minerals and rocks surrounding ore deposits with those of "normal" rocks (Ohmoto, 1986).

δD and $\delta^{18}O$ of fluids may be determined by extracting fluids from inclusions in minerals (Rye and O'Neil, 1968), or by determining δD and/or $\delta^{18}O$ of a mineral and then calculating the δ value of the fluid, using an estimated temperature of mineralisation and an equation for the isotopic fractionation factor between the mineral and H_2O.

According to Clayton *et al.*, (1989), uncertainties in mineral-water fractionation factors make it difficult to estimate the oxygen isotopic compositions of hydrothermal fluids in ore deposits. Differences of 1 to 2‰ between experimental and theoretically calculated estimates of fractionation factors imply that an uncertainty of that magnitude is introduced in the estimate of the isotopic compositions of hydrothermal fluids.

Experimental determinations of equilibrium oxygen isotopic fractionation has been carried out for quartz-water (O'Neil and Clayton, 1964; Clayton *et al.*, 1972, Matsuhisa *et al.*, 1979; Matthews and Beckinsale, 1979; and Clayton *et al.*, 1989). Linear equations defined by least-squares regressions have been published by Clayton *et al.* (1972) (Equation 1), Matsuhisa *et al.* (1976, 1978)(Equation 2) and Matthews

and Beckinsale (1979) (Equation 3) for the temperature range 200 °C to 500°C. By substituting an appropriate temperature T in the equation, solving for α, and then substituting the value for α in Equation 4, the δ value of the water may be determined.

Clayton *et al.* (1972): $10^3 \ln \alpha = 3.38 \times 10^6 T^{-2} - 2.90$ (1)

Matsuhisa *et al.* (1976, 1978): $10^3 \ln \alpha = 3.31 \times 10^6 T^{-2} - 3.26$ (2)

Matthews *et al.* (1979): $10^3 \ln \alpha = 3.05 \times 10^6 T^{-2} - 2.09$ (3)

$$\alpha_{\text{quartz-water}} = \frac{1000 + \delta_{\text{quartz}}}{1000 + \delta_{\text{water}}} \qquad (4)$$

In addition, the effect of fluid chemistry on mineral-water fractionation factors introduces another degree of uncertainty. Truesdell (1974) and Ohmoto and Oskvareck (1985) suggest that salinity has a significant effect on O isotopic fractionation factors. Oxygen isotope fractionation factors between minerals and aqueous solutions may vary by as much as 3‰ at temperatures as high as 600°C, depending on solute chemistry. A similar salinity-dependent effect was suggested for H isotopic fractionation factors with errors as large as 10‰ in the temperature range 150 to 300°C (Kazahaya and Matsuo, 1986).

The isotopic signatures of fluid inclusions are less problematic, provided that the minerals hosting the inclusions are non-oxygen bearing minerals. If the host mineral contains oxygen, isotopic exchange occurs between the host crystal and the fluids, thus producing incorrect values of $\delta^{18}O$ for the original fluid. Therefore, quartz is an unsuitable mineral on which to analyse fluid inclusion stable isotopic signatures. Interpretation of data involves simple comparison with experimentally determined ranges of values for fluids derived from particular sources. Figure 7.1 shows the approximate $\delta^{18}O/\delta D$ ranges for magmatic water, meteoric water, organic water, metamorphic water and sea water, as well as the mixing trends between magmatic and meteoric waters.

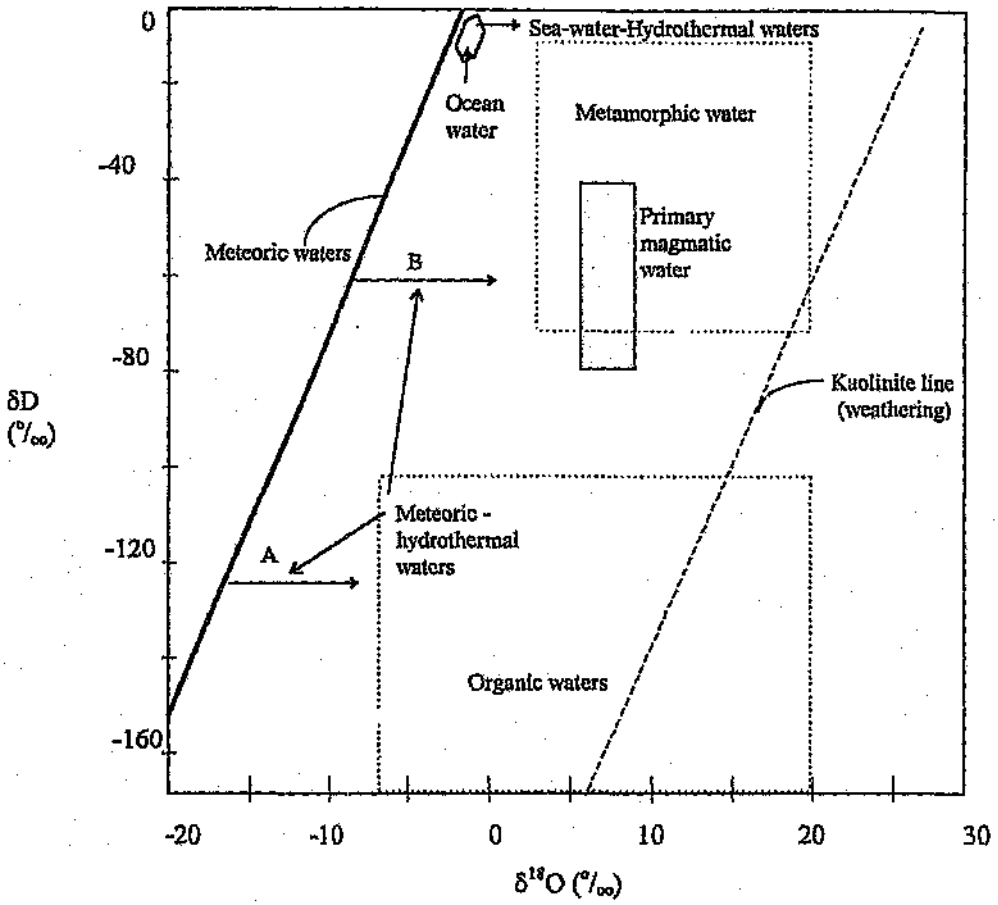


Figure 7.1 Isotopic compositions and fields for sea water meteoric water, primary magmatic water, metamorphic water and organic water. The kaolinite weathering line is given for reference. The ^{18}O-shift trends due to water rock interaction and exchange in hydrothermal systems are shown for sea water and meteoric waters of compositions A and B (After Sheppard, 1986).

Seawater, meteoric water and juvenile water (water derived from the mantle that has never existed as surface water) have been termed reference waters because they have uniquely defined isotopic composition at their source. All other types of subsurface waters (i.e. connate, geothermal, metamorphic, magmatic, organic and ore-forming waters) are considered to be derived from one or more reference waters. The H and O isotopic composition of present-day seawater is relatively constant ($\delta D = 0 \pm 10‰$

and $\delta^{18}O = 0 \pm 1‰$). The δD and $\delta^{18}O$ values for meteoric water are linearly related, and are approximately -70‰ for δD and -10‰ for $\delta^{18}O$ in most places. The δ values become more negative with increasing distance from the sources of water vapour in the atmosphere. The estimated values for juvenile waters are $\delta D = -65 \pm 20‰$ and $\delta^{18}O = 6 \pm 1‰$. Juvenile water is distinguished from magmatic water (water that has coexisted with magma at some stage) in that it was derived from the mantle and has never existed as surface water.

The δD and $\delta^{18}O$ of hydrothermal fluids, pore fluids and connate waters, sedimentary basin brines, metamorphic fluids and magmatic waters deviate significantly from those of the reference waters. These deviations may results from the formation of hydrous minerals, shale membrane filtration, fluid mixing and unmixing, and isotopic exchange with rocks (Ohmoto, 1986). Most geothermal fluids have δD values identical to the local meteoric water but are enriched in $\delta^{18}O$. The magnitude increases with temperature and salinity of the fluid, and is interpreted by Craig (1963) to mean that the fluids were merely recycled meteoric waters, which had acquired heat and salts, and exchanged O isotopes with deeply buried rocks.

In sedimentary brines, the δD and $\delta^{18}O$ values increase with increasing temperature and salinity. A wide range of values have been recorded for brines in different sedimentary basins ($\delta D = -150$ to 20‰ and $\delta^{18}O = -20$ to 10‰), but in any one basin the values are relatively uniform. The isotopic composition of metamorphic fluids (fluids formed by dehydration of minerals during regional metamorphism) vary from one area to another depending on the initial rock type and the history of water-rock interaction. The range for metamorphic waters is approximately $\delta D = 0$ to -70‰ and $\delta^{18}O = 3$ to 20‰. The typical range for magmatic fluids is $\delta D = -75$ to -30‰ and $\delta^{18}O = 7$ to 13‰, and is strongly influenced by the type of rock that is partially melted.

In Figure 7.1, the term "organic waters" refers to the waters whose D/H ratio is derived from the direct or indirect transformation of organic matter, bitumen, coal, kerogen, petroleum, organic gases, etc. by processes such as dehydration, dehydrogenation oxidation and/or exchange (Sheppard and Charef, 1986). The range for H in these waters is δD =-90 to -250‰, while the $\delta^{18}O$ values are determined by the reservoir rocks and the temperature of exchange, and are similar to metamorphic water values (Sheppard, 1986).

Carbon isotopes

Carbon isotopes have not been used as extensively as hydrogen, oxygen and sulphur isotopes in the study of ore deposits because carbon-bearing minerals usually post-date the main stages of mineralisation (Ohmoto, 1986). Apart from being components of the atmosphere and oceans, fixation of carbon species as limestone, and organic matter is common. $\delta^{13}C$ values of modern marine limestone fall in the range -1 to 2‰ (average 1‰) and for marine organic carbon in the range -30 to -10‰. Methane produced by biogenic reduction of HCO_3^- near the sediment water interface has values between -110 and -55‰. Thermal decomposition is the primary source of natural gas at temperatures greater than 50°C. $\delta^{13}C$ values of CH_4 formed by thermal cracking are between -55 and -35‰. CO_2 generated by thermal decomposition of organic matter may have been an important source of carbonate in some sediment-hosted sulphide deposits. The $\delta^{13}C$ values of aqueous carbonate produced by dissolution or thermal decarbonatisation fall in the range -8 to 4‰. The isotopic signatures of carbon which has been derived from the above mentioned sources are shown in Figure 7.2.

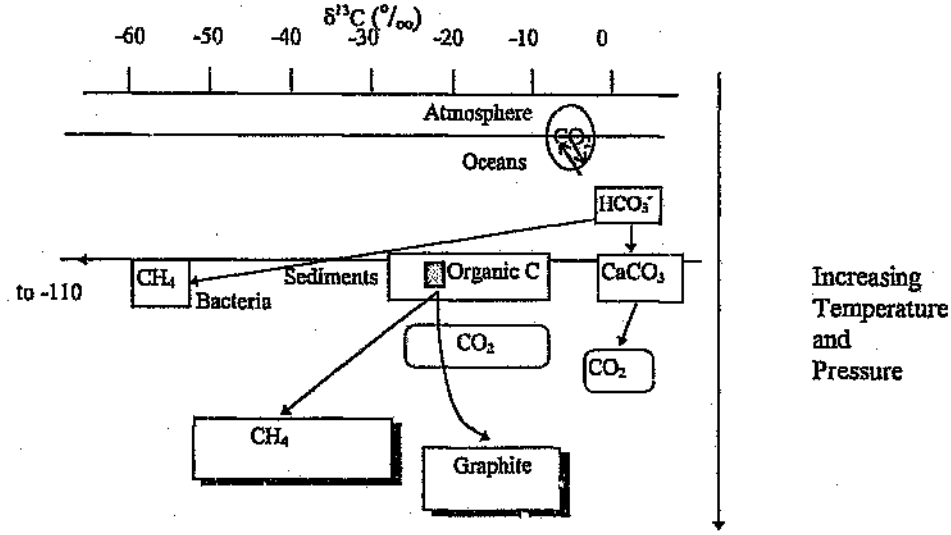


Figure 7.2 Schematic diagram showing $\delta^{13}C$ values of carbon-bearing compounds in near surface environments (after Ohmoto,1986).

As with δD and $\delta^{18}O$, the $\delta^{13}C$ value is diagnostic of its source. The $\delta^{13}C$ values of ΣCO_2 can be calculated from the $\delta^{13}C$ of the carbonate mineral using 1) fractionation factors between the mineral and H_2CO_3 (CO_2 + H_2CO_3) or HCO_3^- and between aqueous carbonate species, and 2) the relative abundance of H_2CO_3 and HCO_3^- in the fluid. Fractionation factors are a function of temperature only because the assumption of isotopic equilibria in carbonate species is usually valid (Ohmoto, 1986).

Stable isotopes in meteoric-hydrothermal systems

In modern meteoric-hydrothermal systems on continents and islands, virtually all the water is of meteoric origin (Craig *et al.*, 1956). Although the $\delta^{18}O$ and δD values of meteoric water are linearly related, the $\delta^{18}O$ values of the geothermal waters are higher than the local meteoric waters. This ^{18}O-shift reflects isotopic exchange between heated meteoric waters and ^{18}O-rich rocks, which, after interaction, become depleted with respect to ^{18}O. As a result of the very large mineral-water fractionation factors,

the $^{18}O/^{16}O$ ratios of the rocks can be increased by low temperature interactions with meteoric waters, as observed during weathering and in the low temperature parts of some meteoric-hydrothermal systems (Criss *et al.*, 1984). The actual response of isotopic systems to fluid rock exchange depends on the initial isotopic composition of the fluid and rock, on the temperature as reflected by the water-rock fractionation factor, on the relative proportions of fluid and rock involved in the exchange, on the degree of approach to isotopic equilibrium, and on the boundary conditions (Criss and Taylor, 1986).

Oxygen isotopic studies have identified a number of areas where ancient meteoric-hydrothermal system have caused pervasive and widespread alteration, isotopic exchange and often economically significant mineralisation. The most important epithermal deposits are simple fissure veins of quartz or chalcedony containing precious metals (Au/Ag) that may be free or associated with sulphide minerals. Other epithermal deposits are valued for base metals, mercury, antimony, and alunite. They may occur as stockworks and pipes, below impervious zones and in subhorizontal stratigraphic beds (Criss and Taylor, 1986). The δD and $\delta^{18}O$ values for fluids associated with these epithermal deposits usually plot very close to the meteoric water line, or to the right, reflecting the ^{18}O-shift observed in modern geothermal waters. Other examples of ore deposits formed by the meteoric hydrothermal fluids include the Pb-Zn replacement bodies at Bluebell, British Columbia (Ohmoto and Rye, 1970), and the rich Main Stage veins at Butte (Sheppard and Taylor, 1974), where relatively high salinities and temperatures were recorded. At Climax, Colorado, meteoric waters were involved in the formation of the Mo porphyry (Hall *et al.*, 1974)

Studies of the light stable isotopes associated with mineralisation in the Bushveld granites has received very little attention to date. The only reference literature available is an oxygen isotope study by Pollard *et al.* (1991) at the Zaaiplaats Tin Mine. Pollard *et al.* (1991) found that whole rock samples from the Zaaiplaats Tin Mine had oxygen isotopic compositions between 9.2 and 9.9 per mil. The $\delta^{18}O$ values of quartz from granites and the marginal pegmatite range from 7.3 to 9.4 per mil, whereas those of quartz from cavities, low-grade ore bodies, pipes and veins range from 7.8 to13.5 per

mil (Pollard *et al.* 1991). Pollard *et al.* (1991) modelled the isotopic exchange between granites and magmatic fluid phase in isotopic equilibrium with average Bobbejaankop Granite quartz at 600°C and found that whole rock compositions result from final exchange at temperatures less than 400°C, with fluid compositions in the range 4.2 to 5.2 per mil at 300°C and 0.8 to 1.8 per mil at 200°C. Pollard *et al.* (1991) maintain that these results are consistent with fluid compositions calculated from $\delta^{18}O$ and pressure-corrected fluid inclusion homogenisation temperatures, and indicate that oxygen isotope variation at Zaaiplaats reflects exchange between the granite and the magmatic fluid phase at temperatures down to 200°C.

EQUIPMENT AND METHODS

The oxygen isotopes of quartz, as well as carbon, oxygen and hydrogen isotopes, of fluid liberated from fluid inclusions from the Grass Valley, Spoedwel, Houtenbek and Albert deposits were analysed at the Department of Geological Sciences, University of Michigan. The procedure is described by Vennemann and O'Neil (1993). A schematic diagram of the experimental set-up of the fluid inclusion line is shown in Figure 7.3.

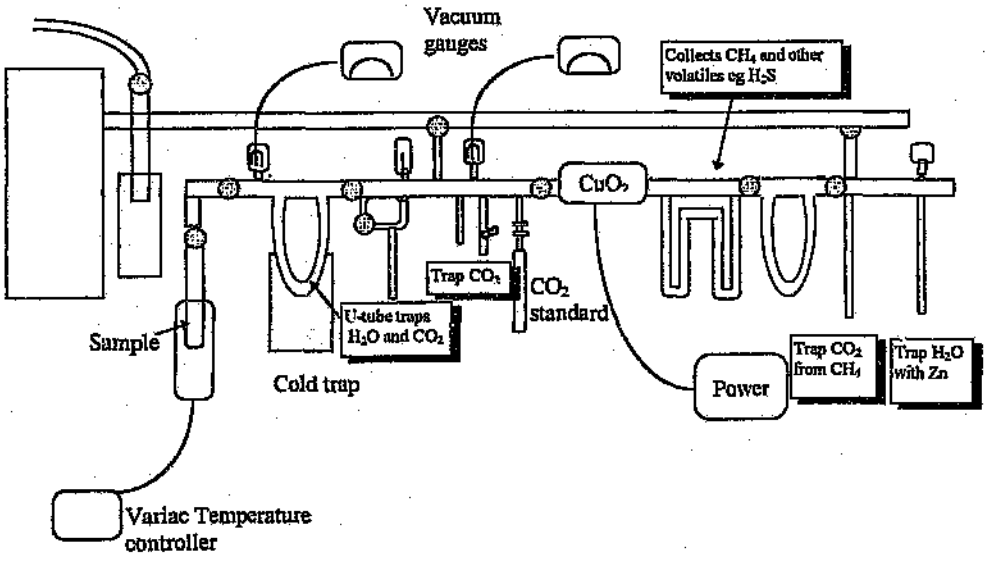


Figure 7.3 Schematic representation of the experimental set-up for separating CO_2, CH_4, H_20 liberated from fluid inclusions.

The fluid inclusion contents were released from the sample by gradual heating within a furnace. The fluid inclusion line at the Deptartment of Geological Sciences, University of Michigan, is designed in such a way that all CO_2, CH_4 and H_2O liberated from each sample can be trapped and the C, O and H isotopic signatures determined. Initially, the H_2O and CO_2 released is frozen into a U-tube cold trap, and the other gases, chiefly CH_4 are allowed to pass through the CuO_2 chamber. The CH_4 is converted to H_2O and CO_2, which is subsequently frozen into the U-tubes behind the CuO_2 chamber. The CO_2 is separated out first and collected in a 6mm Pyrex safety tube, which is then removed from the line for analysis. The water is released next and is trapped in a quartz tube containing Zn. Zinc is used to react with the water on heating, producing ZnO and H_2. The tubes are then cracked under vacuum on the mass spectrometer and the hydrogen isotope composition analysed.

CO_2 is liberated from the U-tube containing H_2O and CO_2, frozen into a Pyrex tube and removed from the line. The water is then trapped in a detachable cold finger and stored in a water bath for two days, to allow for equilibration of ^{18}O and ^{16}O.

SAMPLE MATERIAL

Samples of non-oxygen-bearing minerals (i.e. fluorite and sphalerite) were selected for analysis of the isotopic signatures of fluid inclusions. One quartz sample was included for comparison. The samples are tabulated in Table 7.1. With the exception of SP2, the samples were prepared by separating the fluid inclusion-bearing host minerals from the feldspar and other rock forming minerals by means of magnetic separation and hand picking. Insufficient sample material of fluorite from Albert Silver Mine could be gathered, and, therefore, no analyses could be made.

Table 7.1 List of samples chosen for isotopic analysis of fluid inclusion decrepitates.

DEPOSIT	SAMPLE	SIZE (g)	CHARACTERSITICS
Spoedwel	SP2	17.99	Interstitial fluorite and quartz (whole rock).
	SP13	3.75	Massive fluorite post-dating sulphide mineralisation
Grass Valley	GV02	3.82	Quartz
	GV08	5.91	Fluorite filling a vug in granite
Houtenbek	HBF	9.6	Purple fluorite
	ZNS	9.65	Sphalerite

The quartz samples analysed for $\delta^{18}O$ are listed in Table 7.2. The samples were chosen specifically to represent fluids associated with barren hypersolvus (samples NEBO and BBK1) and subsolvus granites at Albert (RP2 29) and Grass Valley (MF3a), as well as the fluids associated with cassiterite mineralisation (GV02), and late stage quartz-hematite veins (GV01a and b) at Grass Valley. Admittedly, one sample of mineralisation is not representative, but problems encountered with H_2S liberated from mineralised samples inhibited extensive analysis of such sample material.

Table 7.2 List of samples chosen for oxygen isotope analysis of quartz.

SAMPLE	CHARACTERISTICS
GV01a	Second generation of quartz filling fracture at Grass Valley.
GV01b	First generation of quartz filling fracture at Grass valley.
GV02	Quartz associated with hydrothermal cassiterite at Grass Valley.
BBK1	Hydrothermally altered Nebo Granite (Bobbejaankop granite equivalent).
RP2 29	Coarse-grained subsolvus granite from Albert Silver Mine.
NEBO	Unaltered Nebo Granite.
MF3a	Medium-grained subsolvus granite from Grass Valley.

RESULTS

The $\delta^{18}O$ and δD values from fluid inclusions are shown in Table 7.3. The δ values from the fluid inclusion H_2O are shown in the first two data columns, and the δ values from the water converted from CH_4 are shown in the second two data columns. The $\delta^{18}O$ of samples GV02 and SP2 should be treated with caution, since they were derived from quartz-hosted fluid inclusions. However, the δD values of these samples are reliable. Unfortunately, in some of the samples where CO_2-rich fluid inclusions are abundant, both $\delta^{18}O$ and δD values were not obtained because one or other of the isotopes was not detected. The samples where both values were obtained are plotted in Figure 7.4. The δ values associated with mineralisation and fluorite at Houtenbek and Grass Valley have similar $\delta^{18}O$ signatures, but the δD values vary between -52 and -96 ‰. The values obtained from water converted from methane for the fluorite at Grass Valley plot separately.

Table 7.3 Stable isotopic data for $\delta^{18}O$ and δD from fluid inclusion water and methane.

SAMPLE	$\delta^{18}O_{water}$ (‰)	δD_{water} (‰)	$\delta^{18}O_{methane}$ (‰)	$\delta D_{methane}$ (‰)
HBF	1.2	-52.7	21.4	not detected
ZNS	1.6	-93.0	55.6	not detected
GV02	1.0	-96.2	15.5	not detected
GV08	17.3	not detected	19.1	-150.6
SP2	not detected	-60.8	not detected	-167.3
SP13	72.1	not detected	not detected	not detected

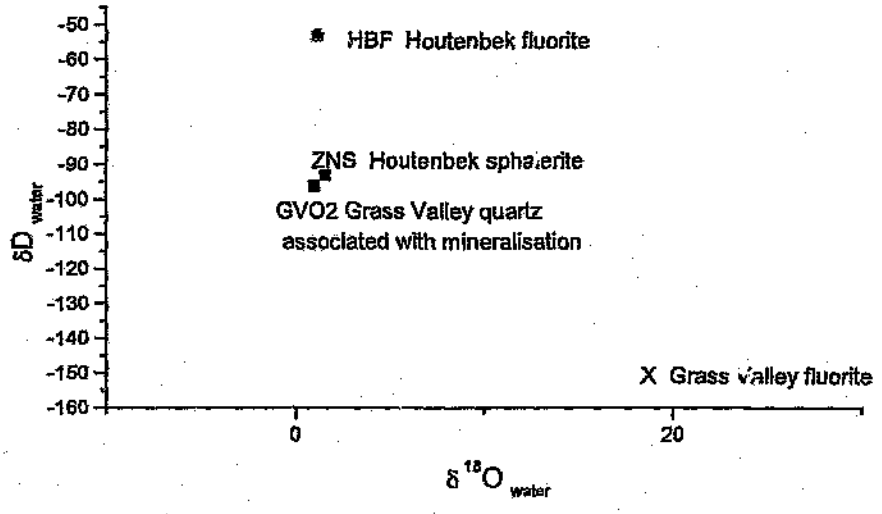


Figure 7.4 $\delta^{18}O$ and δD values from fluid inclusion water (■) and water converted from methane (X) for samples from Houtenbek, and Grass Valley.

The results of the $\delta^{18}O$ determinations of quartz from host granites, and quartz associated with veins and mineralisation are shown in Table 7.4. Calculations of the $\delta^{18}O_{fluid}$ using the equations of Clayton *et al.* (1972) and Matsuhisa *et al.* (1979) for T= 300°C are also tabulated. Figure 7.5 plots the measured $\delta^{18}O_{(quartz)}$ values and the calculated $\delta^{18}O_{fluid}$ (Matsuhisa *et al.*,1979). The host minerals cluster together at lower values of δ than the fluids associated with mineralisation and late stage quartz veins.

Table 7.4 $\delta^{18}O_{(quartz)}$ and $\delta^{18}O_{(fluid)}$ values for quartz . $\delta^{18}O_{(fluid)}$ ‰ values were calculated using the equations of Clayton *et al.* (1972) and Matsuhisa *et al.* (1979) for T= 300°C.

SAMPLE	$\delta^{18}O_{quartz}$ ‰	$\delta^{18}O_{fluid}$ ‰ Clayton *et al.* (1972)	$\delta^{18}O_{fluid}$ ‰ Matsuhisa *et al.* (1979)
GV01a	10.28	3.34	3.38
GV01b	10.34	3.40	3.44
GV02	10.14	3.20	3.24
RP2 29	7.31	1.12	1.15
MF3a	8.51	0.39	0.43
BBK1	8.04	1.22	1.25
NEBO	8.14	1.59	1.62

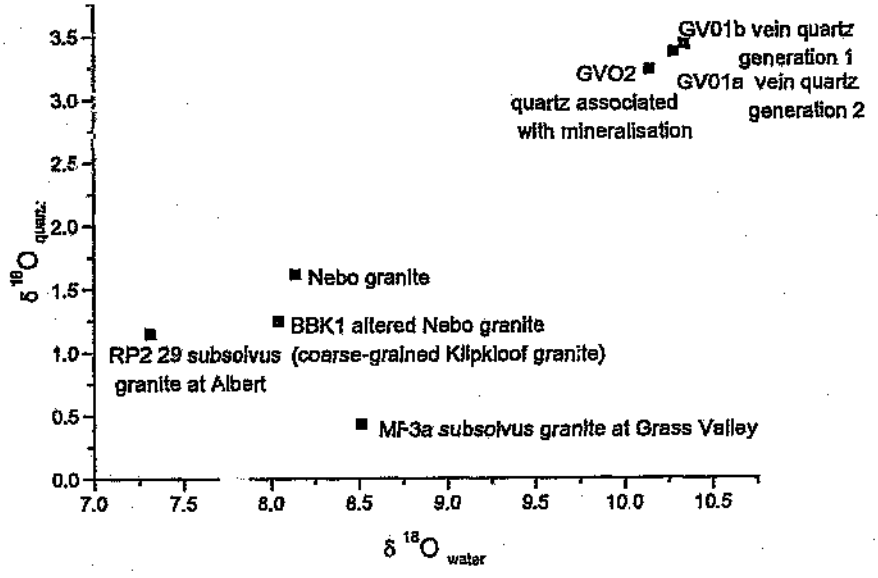


Figure 7.5 Graph of $\delta^{18}O_{quartz}$ versus $\delta^{18}O_{water}$ of unmineralised host granites and quartz associated with veins and mineralisation at Grass Valley.

The $\delta^{13}C$ values obtained from fluid inclusion CO_2 are shown in Table 7.5 DI-CO_2 values represent the CO_2 used for determining the fractionation factor between fluid inclusion CO_2 and the CO_2 standard. The $\delta^{18}O$ values of the CO_2 are also shown in Table 7.5. The data are plotted in Figure 7.6. The $\delta^{13}C$ values fall in the range of approximately -8 to 3.5‰. The samples of late stage fluorite from Spoedwel and sphalerite from Houtenbek are enriched in $\delta^{18}O$ relative to the fluorite samples from Houtenbek and Grass Valley.

Table 7.5 $\delta^{13}C$ and $\delta^{18}O$ from CO_2 in fluid inclusions from Houtenbek, Grass Valley and Spoedwel.

SAMPLE		$\delta^{13}C$ ‰	$\delta^{18}O$ ‰
HBF	CO_2	-7.5	21.4
	DI-CO_2	-3.9	38.1
ZNS	CO_2	1.4	55.6
	DI-CO_2	-3.4	40.1
SP13	CO_2	2.4	72.1
	DI-CO_2	?	?
GV02	CO_2	-2.6	15.6
	DI-CO_2	-3.8	39.1
GV08	CO_2	3.5	17.8
	DI-CO_2	-30.8	19.1

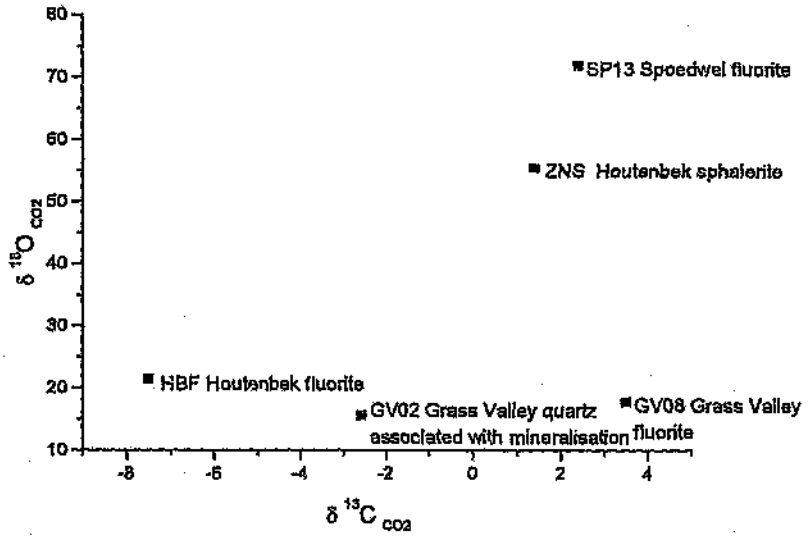


Figure 7.6 Plot of $\delta^{13}C$ and $\delta^{18}O$ from CO_2 in fluid inclusions from Houtenbek, Grass Valley and Spoedwel.

DISCUSSION

Oxygen and Hydrogen Isotopes

The results of this study are consistent with those of Pollard *et al.* (1991) which are summarised in Figure 7.7. Calculations of $\delta^{18}O_{fluid}$ at 300 °C (at lower temperatures, errors in fractionation factors are unacceptable) using the equations of Clayton *et al.* (1972) an Matsuhisa *et al.* (1979) yielded values in the same ranges as found by Pollard *et al.* (1991) for the low temperature hydrothermal quartz. Furthermore, the oxygen isotopes indicate that the fluids associated with crystallisation of the Nebo Granite and the hydrothermally altered Nebo Granite (Bobbejaankop Granite equivalent) can be distinguished from the subsolvus granites and from late- stage quartz veins associated with mineralisation (Figure 7.5) . The subsolvus Verena Granites hosting the Albert Silver deposit have the lowest $\delta^{18}O$ quartz value (7.31per mil), followed by the Bobbejaankop Granite (8.04 per mil), Nebo Granite (8.14 per mil) and subsolvus granite from Grass Valley (8.51 per mil). The hydrothermal quartz

associated with hydrothermal cassiterite at Grass Valley and late-stage quartz veins associated with hematite precipitation have values which are considerably higher (10.14, and 10.28 to 10.34 per mil, respectively). The ranges of $\delta^{18}O$ values obtained from quartz, as well as the calculated values of $\delta^{18}O_{fluid}$ (at 300°C) are compared with the data of Pollard *et al.* (1991) in Figure 7.7. The data from Zaaiplaats are indicated by the narrow lines, while the data obtained in this study are indicated by heavy lines. The boxed captions indicate $\delta^{18}O$ values from quartz and the others indicate ranges for fluids.

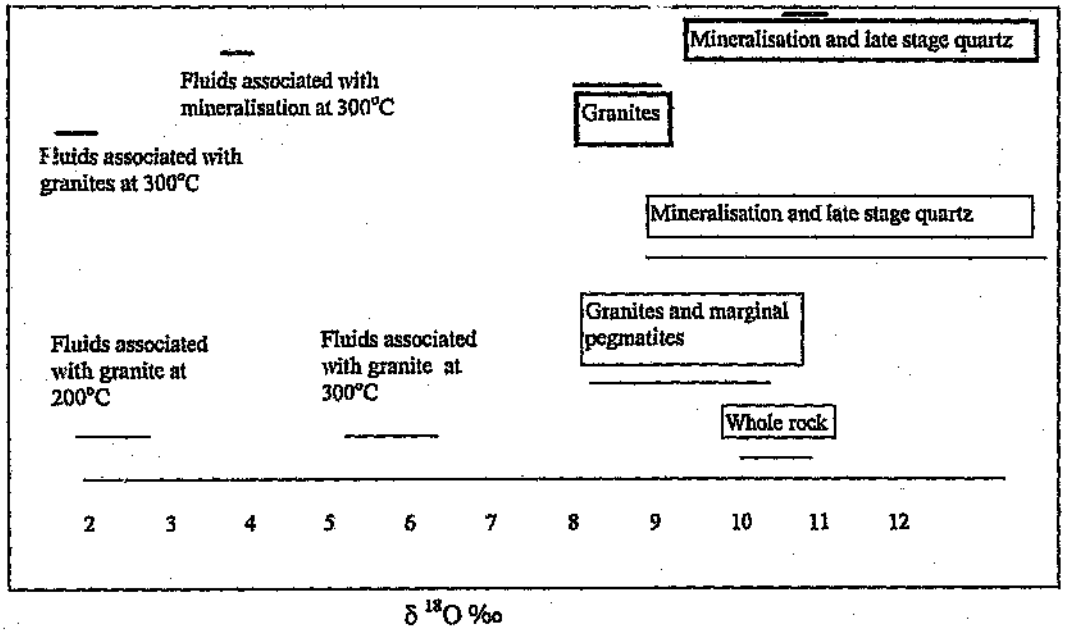


Figure 7.7 Comparison of $\delta^{18}O_{fluid}$ and $\delta^{18}O_{quartz}$ (narrow lines) from Zaaiplaats (Pollard *et al.*, 1991) and the Grass Valley, Albert, Houtenbek and Spoedwel deposits (this study) (heavy lines).

It appears that the fluids have become enriched in ^{18}O with time. However, the depletion of ^{18}O in the host granites compared with the enrichment of ^{18}O in the fluids associated with mineralisation and late stage quartz veins, is reminiscent of the ^{18}O-shift described in meteoric-hydrothermal systems. Furthermore, the gradual enrichment of ^{18}O in fluids of hydrothermal systems was interpreted by Mullis *et al.* (1994) as

indicating retrograde fluid evolution, which is controlled by uplift and cooling, and the involvement of meteoric water.

Evidence for the involvement of meteoric water is provided by comparing the data points with established δ ranges for fluids derived from different sources (Figure 7.8). The fluids associated with sulphide mineralisation, such as those trapped within sphalerite at Houtenbek, plot in between the meteoric water line and the field for primary magmatic water. Fluids that plot in this area of the graph are derived from mixing of meteoric and magmatic fluids. The $\delta D/\delta^{18}O$ plot of fluids associated with mineralisation (Figure 7.8) shows a large range of δD values, but $\delta^{18}O$ remains relatively constant. According to Taylor and O'Neil (1977) this trend reflects an increasing component of meteoric water. High δD values imply the involvement of connate water. The late-stage purple fluorite from Houtenbek shows the highest δD values and fluids associated with sulphide mineralisation have lower δD values. Thus, the δD values became progressively more positive with time, as the external fluid component became more dominant.

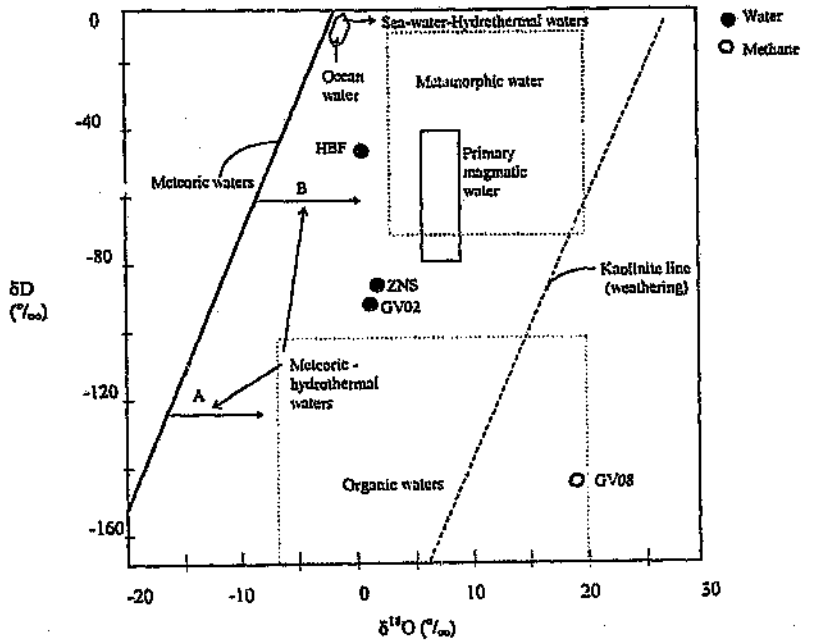


Figure 7.8 Duplication of Figure 7.1 showing the ranges of δD and $\delta^{18}O$ values for fluids derived from different sources, with data points from this study superimposed.

Carbon Isotopes

The carbon isotopic signatures prove irrefutably that an external fluid component was introduced into the system. The majority of values indicate that the carbon was derived from a carbonate source (Figure 7.9). The fluorite at Grass Valley and Spoedwel, as well as the sphalerite at Houtenbek, contains C which was derived from a carbonate source. The fluorite from Houtenbek falls in the overlap between mantle derived fluids and carbonate derived fluids. Since no evidence for C derived from an external organic carbon reservoir was found, and considering that the geological setting of the Houtenbek deposit suggests that it represents a hydrothermal vent, the C in sample HBF is interpreted as being mantle derived.

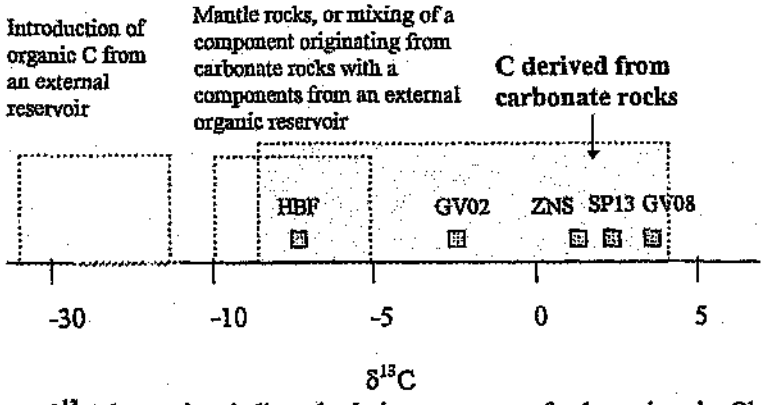


Figure 7.9 $\delta^{13}C$ data points indicated relative to ranges of values given by Ohmoto (1986) for C derived from an external reservoir, mantle or carbonate source.

CHAPTER 8

SYNTHESIS AND MODEL

The results of this study on the nature of hydrothermal fluids associated with granite-hosted mineralisation in the eastern lobe of the Bushveld granites has revealed that fluid mixing was a major factor governing the deposition of metals in favourable structural traps within the granites and surrounding country rock.

In the previous chapters, various analytical techniques have shown that the associated hydrothermal fluids are complex mixtures of various metals and volatiles, which were derived from at least two different sources, one being magmatic and the other an external meteoric/connate source.

Evidence pointing towards a fluid component of a magmatic origin includes the following:

- N_2/Ar ratios in the range stipulated by Norman and Musgrave (1992) for fluids of magmatic origin.

- A gradual increase was observed in the Ar content in fluids from the hypersolvus granites, through to the late stage Klipkloof Granite dyke material. The higher Ar content in the fluids in the fine-grained Klipkloof Granite dykes implies that magmatic fluids were progressively diluted by an increasing meteoric component (Norman and Musgrave, 1992).

- Two of the major factors governing the formation of fluorite deposits are the dilution of mineralising fluids by ground water and the change in temperature gradient on contact with excess groundwater (Deer *et al.*, 1962). However, Plumlee *et al.* (1995) have shown that the interaction of magmatic fluids/gases with Ca, Mg and SO_4-rich brines results in the formation of acidified brines which precipitate fluorite on cooling from 150°C to 140°C. Progressive mixing of this brine with the original brine leads to further precipitation of significant amounts of fluorite. The model proposed by Plumlee *et al.*

(1995) involves the migration of magmatic gases upwards and along fractures in the crystalline basement, where titration of these gases into basinal brines at depth led to preferential mineralisation of these structures. Similarly, in the Bushveld granites, basinal brines, which were channelled along regional fractures, interacted with the magmatic fluids and precipitated fluorite at temperatures between 300°C to 150°C. According to Plumlee *et al.* (1995), a second episode of fluorite precipitation takes place at lower temperatures (<150°C) The presence of two generations of fluorite associated with mineralisation at Spoedwel and Albert, which were formed at similar temperature conditions as that found by Plumlee *et al.* (1995), suggests that fluid mixing was responsible for the precipitation of the fluorite, and is assumed to be an important factor in the development of sulphide and fluorite-hematite assemblages.

- Copper was detected by PIXE analysis in Type 5b (CO_2-rich) fluid inclusions, which is consistent with the theory that copper is transported in the vapour phase (Heinrich *et al.*, 1992). Thus, the source of copper in the fluids is most likely magmatic, and migrated with HF-rich gases emanating from the crystallising magma.

The external fluid component was derived from two sources, namely, a meteoric source and a connate source. The fluid inclusion studies clearly indicated that two distinctly different fluids coexisted at similar temperatures in quartz associated with the sulphide paragenesis. The fluid inclusion evidence for the mixing of two fluids include:

- Variable phase proportions, wide ranges of homogenisation temperatures and wide ranges of final melting temperatures within single fluid inclusion assemblages indicate that entrapment of a heterogeneous fluid took place.

- Dissolution of halite daughter crystals after homogenisation of the liquid and vapour phases indicates that the heterogeneous fluid was the result of fluid mixing rather than boiling.

- The overlap of homogenisation temperature ranges of saline and non-saline fluid inclusion assemblages in the first fluorite generation implies that both fluids were circulating at the same time and that mixing probably took place.

- The presence of two distinctly different fluid inclusion assemblages (one highly saline and the other relatively unsaline) coexisting a similar temperatures indicates the presence of two contrasting parental fluids.

- The fluids associated with the sulphide assemblage became progressively more saline, peaking with the deposition of sphalerite, and then decreasing in salinity with the precipitation of chalcopyrite. The high salinity of the external fluid suggests that the source of this fluid was not purely meteoric, but rather, that it was a basinal brine or connate fluid, derived from the Transvaal sedimentary rocks into which the granites were intruded. Thus, initially, mixing between a magmatically derived fluid and a connate fluid occurred. The magmatic fluid component would have dominated the system, but as the magmatic fluids waned, the connate fluid became the dominant fluid, which is reflected by the increasing salinity of the fluids from the precipitation of arsenopyrite to sphalerite. Thereafter, the fluids became progressively less saline as dilution of the magmatic and connate fluids by meteoric fluids, which entered the system along fractures in the granite, proceeded.

- Two distinct fluid types have been detected in terms of their solute composition. These fluid types may be correlated with the two end-member fluids recognised during microthermometry. The fluids with the lowest salinity and highest temperature are those which PIXE analysis has shown to be relatively barren with respect to ore-forming components. These fluids are represented by the early fluids at Grass Valley which precede cassiterite precipitation. In contrast, the highly saline, lower temperature fluid preserved in primary inclusions hosted by a second generation of quartz at Spoedwel contain significant amounts of all the ore-forming components. The sample material from Albert represents the intermediate category of fluids recognised by microthermometry, where the temperature and solute content is moderate, reflecting partial interaction between the two parental fluid types.

- The fluid inclusions from Grass Valley associated with the precipitation of hydrothermal cassiterite and small amounts of galena, sphalerite and chalcopyrite contained $CO_2 \pm N_2 \pm CH_4$. Thus, these gases were certainly present in the fluids associated with Stage 2 (i.e. the precipitation of the sulphide assemblage) in the paragenetic sequence.

- The high concentration of SO_2 in the fluids in the subsolvus granites compared with the low SO_2 concentrations in the barren Nebo Granite and coarse-grained Klipkloof Granite, suggests that the oxidation potential of the fluids had been increased by the time crystallisation of subsolvus granite took place.

- The fluids associated with subsolvus granites are less saline than the hypersolvus granite fluids, providing supporting evidence that the incursion of meteoric water triggered the change from hypersolvus to subsolvus granite textures, and that the magmatic fluids were diluted by meteoric/connate fluids.

- N_2/Ar ratios indicate that nitrogen from both magmatic and meteoric sources is present in the fluids associated with mineralisation and in late stage quartz veins. The ratios for vein quartz associated with mineralisation at Spoedwel and Albert fall in the range for air saturated water. The fine-grained Klipkloof granite at Leeufontein and the subsolvus granite at Albert also fall in this range. The ratios for the late stage fluids associated with quartz-hematite veins contain high N_2/Ar ratios. The samples associated with sulphide precipitation also contain higher N_2/Ar ratios than that for air saturated water, possibly suggesting that magmatic gases were involved.

- Sphalerite precipitation at Grass Valley, Albert, and Spoedwel occurred over a temperature range of approximately 100°C, but the compositions of the fluids were very similar. Assuming that mineralisation was triggered by mixing of two fluids, the similar fluid compositions associated with sphalerite deposition suggests that fluid mixing occurred at different stages in the paragenetic sequences.

- Although N_2 and CO_2 may be derived from a magmatic source, the presence of hydrocarbons, such as CH_4 and C_2H_6 and C_3H_8, in the fluid usually implies that an external fluid (meteoric and /or connate) was introduced at some stage.

- At Spoedwel and Houtenbek in particular, the late stage fluorite contains significantly more SO_2 than H_2S. This enrichment in SO_2 is also observed in the late stage quartz-hematite veins at Grass Valley, Spoedwel and Albert. The source of the additional sulphur is uncertain, but it seems likely that it was transported into the system, by the same fluid associated with the elevated CO_2, CH_4 and Ar concentrations.

- High δD values and the enrichment in $\delta^{18}O$ with time indicate the involvement of meteoric/connate water.

- The fluid inclusions hosted by quartz and tourmaline in the tourmaline spheroids show that Fe, Zn and Pb (as well as trace elements- Br, Ga, Rb, Sr) are present in the late stage fluids. The presence of these elements in the fluids at such a late stage in the system suggests that, in addition to enrichment of the residual fluid in incompatible elements, some of these components may have been leached from the Transvaal Supergroup and transported into the Bushveld granites by the connate fluid.

- The majority of $\delta^{13}C$ values indicate that the carbon in the fluids was derived from a carbonate source. The Malamani dolomites of the Transvaal Supergroup, into which the Bushveld granites were intruded, are thus a possible source of some of the carbon introduced by the external fluid.

Thus, fluid inclusion studies of the fluids associated with the various stages of mineralisation in the eastern lobe of the Bushveld complex have demonstrated that magmatic, meteoric and connate fluids were involved in the mineralising process. Further evidence of the interaction between these fluids, recognised during mineral petrography, include:

- Petrographic studies of the granites hosting mineralisation in the eastern lobe of the Bushveld Complex have revealed that these granites can no longer simply be described as hypersolvus granites. In addition to hypersolvus granites, subsolvus and transsolvus granites have been also been recognised, the implications of which are significant in constructing any model for the evolution of the Bushveld granites and associated mineralisation. The hypothesis proposed by Martin and Bonin (1976) to explain the hypersolvus-subsolvus granite association incorporates the concepts of water saturation of the magma, with the ingress of meteoric water as the circulation of magmatic fluids wanes. The petrographic evidence (muscovitisation, local fusion of perthites, albitisation of feldspar, and precipitation of late albite) suggests that water saturation occurred during the final stages of the crystallisation of the hypersolvus granite, coinciding with the onset of subsolvus granite crystallisation. This is supported by evidence from Ollila (1981), who conducted a study of the structural state and composition of the alkali feldspars in the Bushveld Granites, and found that the alkali feldspars in the Bobbejaankop Granite (coarse-grained Klipkloof Granite) exhibit the highest degree of ordering and are maximum microcline, indicating the lowest thermal state. The alkali feldspars from the Lease Granite (Fine-grained Klipkloof Granite) are intermediate microcline, indicating a higher thermal state, or less ordered state, which is due to the rapid cooling rate of this granite (Ollila, 1981). The Nebo (or "Main") Granite alkali feldspars are monoclinic, reflecting a state of greater disorder in the lattice. Ollila (1981) explained this phenomenon as the result of volatile deficiency during initial crystal growth stages, which may have prevented the later development of triclinic alkali feldspars. The variation in the structural state of the alkali feldspars is directly related to the availability of hydrothermal fluids during their cooling history (Parsons, 1978). Thus, the absence of volatiles during the crystallisation of the Nebo Granite is reflected in the monoclinicity of the K-feldspars, even though the rate of cooling was sufficiently slow for the formation of large interlocking crystals. As the degree of fractionation of the host rock increases, the water content of the residual melt increases, causing increased order in the younger K-feldspar crystals. Thus, the higher degree of order observed in the coarse-grained Klipkloof Granite reflects the increasing water content of the residual melt. This trend would have continued during the formation of the Lease Granite (Fine-

grained Klipkloof Granite) were it not for the rapid cooling of this material (Kleemann and Twist, 1989).

- The overall paragenetic sequence in the Bushveld granites suggests that mineralisation took place in three discrete episodes. The first episode of mineralisation resulted in the formation of cassiterite-scheelite-wolframite-molybdenite-specularite and possibly arsenopyrite. The mineralisation is disseminated and formed by processes related to fractional crystallisation of the magma. Fluctuations in the pH of the late magmatic fluids as they interacted with the wall-rocks and with the externally derived meteoric/connate fluids channelled along the fractures, resulted in the deposition of a second episode of mineralisation, which is represented by the sulphide paragenesis pyrite-galena-tetrahedrite/tennantite-sphalerite-chalcopyrite. The occurrence of this assemblage is fracture-related, with sizeable deposits located on the flanks of large-scale regional faults. These fracture systems acted as conduits for mineralising fluids. As the external fluid component became progressively more dominant, the paragenesis changed, and deposition of hematite, pitchblende and large amounts of fluorite took place. The introduction of this third assemblage along the same fracture systems which localised the sulphide assemblage, resulted in alteration of the sulphides, to secondary minerals such as bornite, chalcocite, digenite, covellite and limonite. The extended nature of this three stage paragenetic sequence is considered to reflect widespread mixing between and an early fluid derived by H_2O-saturation of the granitic magma, and an external meteoric/connate fluid.

- The volatiles associated with the final fractionated portion of the granitic melt caused deuteric changes such as the hematitisation of the feldspars, chloritisation of mafic minerals, albitisation of perthite and precipitation of secondary albite. These deuteric changes have the effect of increasing the iron content of the fluids, priming the system for the deposition of the late-stage massive hematite in the third stage of mineralisation. The deuteric alteration marks the interface between fluids with high iron sulphide activity from those with low iron sulphide activity. The iron enriched fluids caused alteration of the primary sphalerite by ion exchange of Fe and Zn, producing iron-rich opaque sphalerite as alteration rims and fracture planes within the transparent sphalerite.

The colour of the chlorite also reflects an increase in the iron content of the fluids. Chlorite associated with sulphide mineralisation is grass-green and highly pleochroic. In contrast, the chlorite associated with the orthomagmatic cassiterite mineralisation is olive-green to brown.

- Covellite overprinting occurred at some stage after consolidation of the sulphide minerals, since alteration of the copper-bearing minerals occurs along grain boundaries and micro-fractures. This phenomenon is characteristic of retrograde processes, i.e. the older minerals remain stable while the younger ones overgrow or fill fractures within them (Hemley and Hunt, 1992). According to Hemley and Hunt (1992), when dissolution and replacement occurs, they are the result of the imposition of a contrasting chemical environment, and not simply lower temperatures. The petrographic evidence suggests that the sulphide mineralisation followed a prograde thermal path, which was then changed to a retrograde thermal path as the external meteoric/connate fluid component became more pronounced.

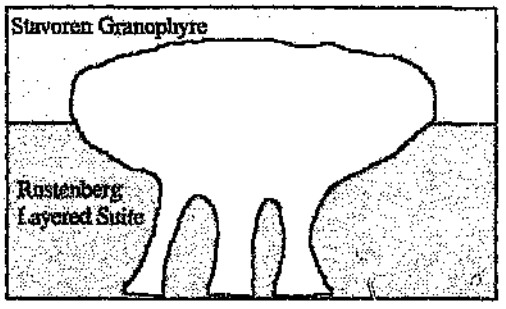
- Local occurrences of hydrothermal tourmaline veins and spheroids, similar to those of the Sn-W-Cu deposits of Cornwall (south-east England) (London and Manning, 1995), have been recognised in the Bushveld granites. In both cases, the interaction of boron-rich, magmatically derived fluids, and Fe-Mg-rich, connate fluids is thought to have resulted in localised precipitation of tourmaline

The model proposed by Kleemann (1985) (see Chapter 2) for the evolution of the Bushveld granites has been modified in Figure 8.1. The first two steps of the model are essentially the same as Kleemann's (1985) model. After emplacement of the magma, the margins of the pluton cooled rapidly and crystallised a fine-grained equivalent of the Nebo Granite. The central portions of the pluton cooled more slowly, promoting the development of large perthite and quartz crystals which are typical of the Nebo Granite. Volatile enrichment of the residual melt took place and intense hydrothermal alteration of Nebo Granite resulted in the development of the coarse-grained Klipkloof Granite.

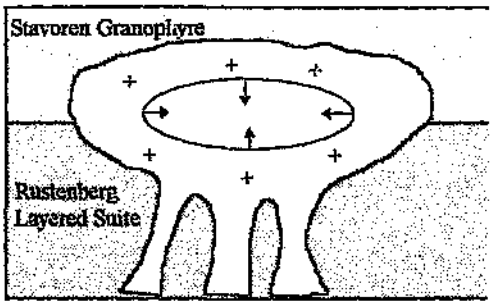
Tensional fracturing of the pluton created conduits along which external connate and meteoric fluids where channelled into the pluton. These fractures are the sites of hydrothermal alteration, such as sericitisation, albitisation and hematitisation, and in parts of the Bushveld Complex, are related to polymetallic mineralisation. Thus, the introduction of hydrothermal fluids along these fractures, served to concentrate and localise ore-forming components.

In addition to the gradual volatile enrichment of the crystallising magma, the introduction of external fluids along fractures promoted water saturation of the magma, and the consequent crystallisation of subsolvus granites. Two generations of subsolvus, fine-grained Klipkloof Granite, which were derived from the more differentiated, water saturated melt, were intruded as dykes and sills into the crystallised to partially crystallised Nebo Granite. In places where the Nebo Granite was not completely solidified, the transsolvus Porphyritic Klipkloof Granite was formed.

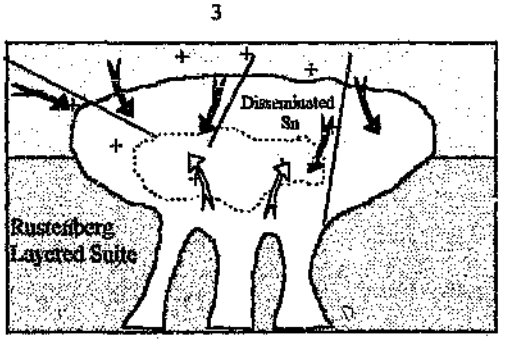
The mixing of the magmatic fluids and the connate fluids caused the precipitation of the sulphide assemblage. Initially, the connate fluid component was minor, but as the magmatic fluid component in the system waned, the connate component became more dominant, and the salinity of the fluids increased, coinciding with the precipitation of the sulphide assemblage. At this point, the introduction of cool, unsaline meteoric water (blue arrows on Figure 8.1) into the system took place, diluting the remaining metal-charged mixture of magmatic and connate fluid (pink arrows on Figure 8.1), and causing precipitation of the fluorite-hematite assemblage at lower temperatures.



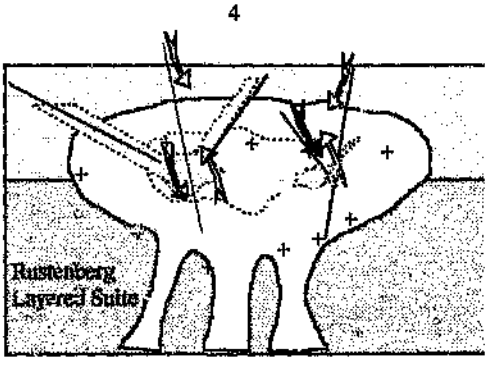
Intrusion of Nebo granite magma and formation of intrusion breccia.



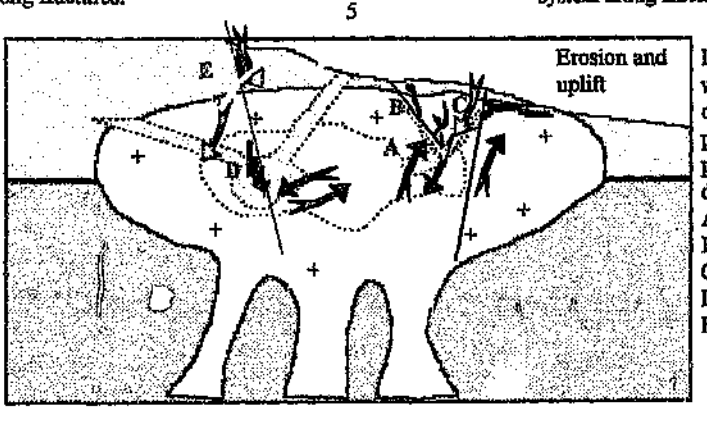
Crystallisation of fine-grained, hypersolvus Nebo granite along margins of pluton, and coarser-grained Nebo granite towards the centre of the pluton.



Disseminated Sn mineralisation forms as a result of fractional crystallisation. Late-stage volatile-rich rest liquids (yellow arrows) interact with connate fluids (red arrows) which are channelled into pluton along fractures.



Subsolvus granites form in water-saturated portions of the pluton and late-stage aplite dykes (Fine-grained Klipkloof granite) are intruded into the Nebo Granite. Meteoric water (blue arrows) enters the system along fractures.



Decending meteoric water mixed with the combined magmatic-connate fluid (pink arrows), precipitating the second and third phases of mineralisation in different settings.
A Zaaiplaats.
B Grass Valley
C Spoedwel
D Albert
E Stavoren

Figure 8.1 Proposed model for the evolution of the Bushveld granite and associated mineralisation

The hypothesis proposed for mineralisation in the granites of the eastern lobe of the Bushveld Complex is shown in Figure 8.2, with the results of this study superimposed. The high temperature fluids recognised by Ollila (1981) and Pollard *et al.* (1991) were not encountered in this study, since the disseminated tin assemblage was not well developed at any of the deposits chosen for analysis. Since the mineralisation was vein-related, the bulk of sample material post-dated that phase when high temperature fluids were circulating. Fluid inclusions from samples of the host granites immediately adjacent to the mineral deposits had been subject to stresses associated with fracturing, and this may explain why none of the high temperature fluids were preserved in these samples. The primary fluid inclusions were probably destroyed during fracturing of the crystal, and refilled by secondary fluid generations, or sealed by subsequent quartz growth.

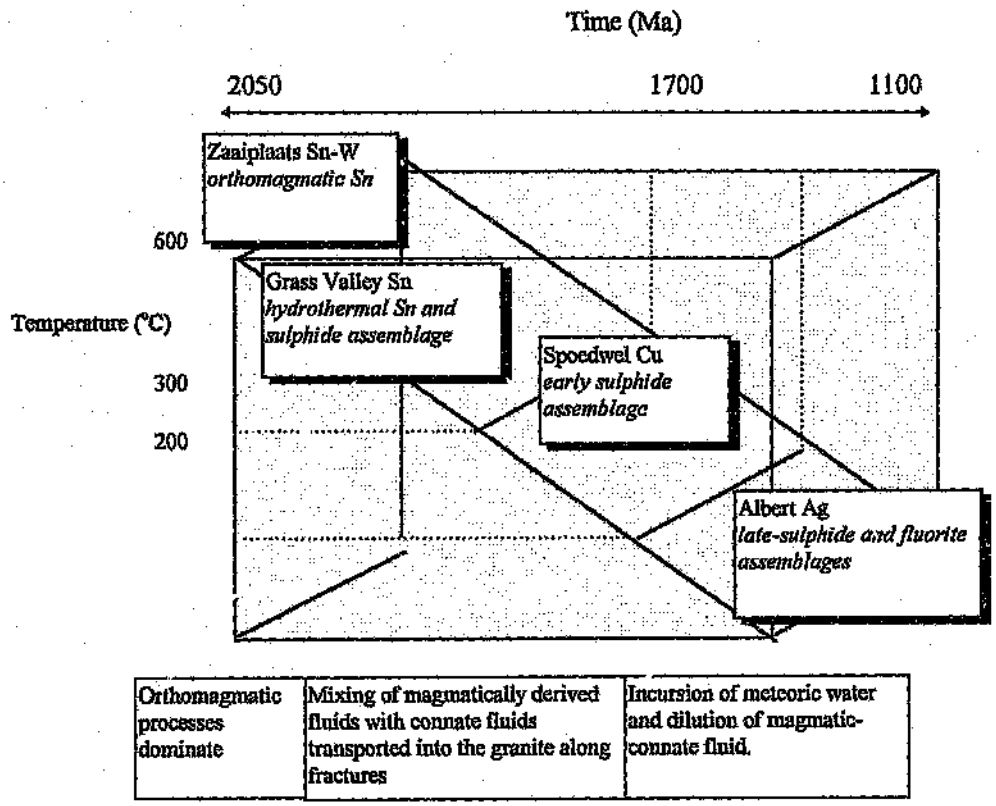


Figure 8.2 Diagrammatic representation of the hypothesis proposed for mineralisation in the granites of the eastern lobe of the Bushveld Complex with additional information obtained during this study superimposed.

The period of time from emplacement of the magma, through the various stages of granite crystallisation, and three phases of mineralisation was determined by radiogenic isotopic studies to have spanned approximately 1000 m.y. From the time of emplacement of the Nebo Granite magma at 2054 Ma (Walraven, 1993), the radiogenic isotopic systems were exposed to disturbances caused by hydrothermal activity between 1600 Ma and 1700 Ma, as well as at 400 Ma (Robb *et al.*, 1994).

Ages for the closure of lead isotopic systems vary. At Zaaiplaats in the northern part of the complex, internal exchange of Pb ceased after 1100 Ma (McNaughton *et al.*, 1991), but at Albert Silver Mine in the south, ages of a disturbance between 400 Ma and 500 Ma were obtained (Robb *et al.*, 1994). These very late isotopic disturbances were not related to mineralising events, but rather to the hydration and oxidation of earlier formed Fe- and Cu-bearing minerals.

The fluids associated with these major disturbances in radiogenic isotopic systems have been recognised. The fluids trapped in hydrothermal minerals associated with the fracture-related, replacement-type mineralisation at Albert, Spoedwel and Grass Valley corroborate the hypothesis that circulation of evolving hydrothermal fluids was active from at least 1700 Ma to 400Ma, while the pluton cooled from 600°C to less than 100°C. The fluids associated with Stage 2 (the sulphide assemblage) and Stage 3 (hematite-fluorite assemblage) may be correlated with the disturbances between 1700Ma and 1100Ma, while low temperature (less than 100°C) fluids post-dating the major episodes of mineralisation correlate with the disturbances between 500Ma and 400Ma.

The characteristics of the fluid inclusions, in conjunction with the petrographic, isotopic and geochemical evidence, all point towards fluid mixing as an important mechanism controlling the nature of the granites, as well as the localisation of mineralisation in the eastern lobe of the Bushveld Complex.

REFERENCES

Anderson, A.J., Clark, A.H., Ma, X., Palmer, G.R., MacArthur, J.D. and Roedder, E. (1989). Proton-Induced X-Ray and Gamma-Ray Emission Analysis of Unopened Fluid Inclusions. *Econ. Geol.* 84:924-939.

Barnes, H.L. (Ed.). (1967). Geochemistry of Hydrothermal Ore Deposits. J. Wiley and Sons. New York. p 798.

Bodnar, R.J. and Beane, R.E. (1980). Temporal and spatial variations in hydrothermal fluid characteristics during vein filling in pre-ore cover overlying deeply buried porphyry copper type mineralization at Red Mountain, Arizona. *Econ. Geol.* 75: 876-893.

Boyle, R. (1672). Essay about the origin and virtues of gems. William Godbid, London, p 185.

Brown, P.E. (1989). Flincor: A microcomputer program for the reduction and investigation of fluid-inclusion data. *Amer. Mineral.* 74:1390-1393.

Brown, P.E. and Lamb, W.M. (1989). P-V-T properties of fluids in the system $H_2O \pm CO_2 \pm NaCl$: New graphical presentation and implications for fluid inclusion studies. *Geochim.Cosmochim. Acta* 53: 1209-1221.

Cathelineau, M. and Nieva, D. (1985). A chlorite solid solution geothermometer. The Los Azufres (Mexico) geothermal system. *Contrib. Mineral Petrol.* 91: 235-244.

Cawthorn, R.G. and Walraven, F. (1997). The Bushveld Complex- a time to fill and a time to cool. *International symposium on plumes, plates and mineralisation 1997. Abstracts.* University of Pretoria. (compiled by C.J. Hatton).

Coetzee, J. and Twist, D. (1989). Disseminated tin mineralization in the roof of the Bushveld granite pluton at the Zaaiplaats Mine, with implications for the genesis of magmatic hydrothermal tin systems. *Econ. Geol.* 84: 1817-1884.

Coertze, F.J., Burger, A.J., Walraven, F., Marlow, A.G. and McCaskie, D.R. (1978). Field relations and age determinations in the Bushveld Complex. *Geol. Soc. S. Africa Trans.* 81: 1-11.

Cousins, C.A. (1959). The structure of the mafic portion of the Bushveld Igneous Complex. *Geol. Soc. S. Africa Trans.* 62: 179-189.

Champion, A.T. (1970). The Mineralogy and Related Geology of the Albert Silver Mine. Unpublished MSc dissertation. Univ. Natal, Durban.

Cheney, E.S. and Twist, D. (1991). The conformable emplacement of the Bushveld mafic rocks along a regional unconformity in the Transvaal succession of South Africa. *Precambrian Research.* 52: 115-132.

Clayton, R.N., O'Neil, J.R. and Mayeda, T.K. (1972) Oxygen isotope exchange between quartz and water. *J. Geophys. Res.* 77: 3057-3067.

Clayton, R.N., Goldsmith, J.R. and Mayeda, T.K. (1989) Oxygen isotope fractionation in quartz, albite, anorthite, and calcite. *Geochim. Cosmochim. Acta* 53: 725-733.

Clynne, M.A. and Potter, R.W. II (1977). Freezing point depressions of synthetic brines (abstr.) *Geol. Soc. Am. Abstr. Programs* 9: 250, 289.

Craig, H., Boato, G., and White, D.E. (1956). Isotopic geochemistry of thermal waters. Proc. Conf. Nuclear Processes in Geol. Settings. *Second Natl. Acad. Sci. Natl. Res. Council publ.* 400: 29.

Craig, H. (1963). The isotopic geochemistry of water and carbon in geothermal areas. In: Nuclear Geology on Geothermal Areas. E Tongiori (Ed.). Consiglio Nazionale della Richereche Laboratorio de Geologica Nucleare, Spoleto, Pisa, 17-53.

Creaser, R.A. (1989). The geology and petrology of Middle Proterozoic felsic magmatism of the Stuart Shelf, South Australia Ph.D. Thesis, La Trobe University. Melbourne., Vic (unpubl.).

Creaser, R.A. and Cooper J.A. (1993). U-Pb geochronology of Middle Proterozoic felsic magmatism surrounding the Olympic Dam Cu-U-Au-Ag and Moonta Cu-Au-Ag deposits, South Australia. *Econ. Geol.* **88**: 186-197.

Criss, R.E., Ekren, E.B. and Hardyman, R.F. (1984). Casto ring zone: A 4 500km^2 fossil hydrothermal system in the Challis volcanic field, central Idaho. *Geol.* **12**: 331-334.

Criss, R.E. and Taylor, H.P. Jr. (1986). Meteoric-hydrothermal systems. *Reviews in Mineralogy* **16**:373-424.

Crocker, I.T. (1979). Metallogenic aspects of the Bushveld granites: Fluorite, tin and associated rare metal-carbonate mineralization. *Spec. Publ. Geol. Soc. S. Afr.* **5**: 295.

Crocker, I.T. (1985). Volcanogenic fluorite-hematite and associated pyroclastic rock suite at Vergenoeg, Bushveld Complex. *Econ. Geol.* **80**:1181-1200.

De Bruiyn, H. (1980). The geology of the acid phase of the Bushveld Complex, north of Pretoria - a geochemical/statistical approach. Unpub. Ph. D thesis, University of the Orange Free State. p 175.

DuBessy, J., Audeoud, D. Wilkin, R. and Kosztoanyi (1982). The use of the Raman microprobe MOLE in the determination of the electrolytes dissolved in the aqueous phase of fluid inclusions. *Chem. Geol.* **37**: 137-150.

Dubessy, J., Geisler, D., Kosztolanyi, C. and Vernet, M. (1983) The determination of sulphate in fluid inclusions using the M.O.L.E. Raman microprobe. Application to a Keuper halite and geochemical consequences. *Geochim. Cosmochim. Acta* **47**: 1-10.

Dubessy, J., Poty, B. and Ramboz, C. (1989). Advances in C-O-H-N-S fluid geochemistry based on micro-Raman spectrometric analysis of fluid inclusions. *Eur. J. Mineral.* 1:517-534.

Dubessy, J., Boiron, M.C., Moisette, A, Monnin, C., and Sretenskaya, N. (1992). Determinations of water hydrates and pH in fluid inclusions by micro-Raman spectrometry. *Eur. J. Mineral.* 4: 885-894.

Eriksson, P.G., Scweitzer, J.K., Bosch, P.J.A., Schreiber, U.M., van Deventer, J.L., and Hatton, C.J. (1993). The Transvaal Sequence: an overview. *J. Afr. Earth Sci.* 16: 25-51.

Fabre, D and Couty, R. (1986). Investigation on the density effects in the Raman Spectrum of methane up to 3,000 bar. Application to the determination of pressure in fluid inclusions trapped in minerals. *C.R. Acad. Sc. Paris, t. 303, Serie II, n° 14.*

Faurie, J.N. and von Gruenewaldt, G. (1979). Zaaiplaats project: Pretoria, Univ. *Pretoria Inst. Geol. Research Bushveld Complex, Ann. Rept.* 1978:11-15.

Frick, A. (1993). Spoedwel Copper Mine (Pty) Ltd. Unpublished report.

Giggenbach, W.F. (1986). The use of gas chemistry in delineating the origin of fluid discharges over the Taupo Volcanic Zone: A review. *Proc. Intl. Volcanol. Congress, New Zealand* 5: 47-50.

Goldstein, R.H. and T.J. Reynolds. (1994). Systematics of fluid inclusions in diagenetic minerals. SEPM short Course 31. USA.

Graney, J.R. and Kesler, S.E. (1995). Factors affecting gas analysis of inclusion fluid by quadrupole mass spectrometry. *Geochim. Cosmochim. Acta* 59: 3977-3986.

Gribble, C.D. and Hall, A.J. (1992). Optical mineralogy: *Principles and Practice.* London. UCL Press. p 302.

Guilbert, J.M. and Park, C.F. Jnr. (1986). The Geology of Ore Deposits. W.H. Freeman and Company. United States of America. p 985.

Hall, W.E., Friedman, I. and Nash, J.T. (1974). Fluid inclusion and light stable isotope study of the Climax molybdenum deposits, Colorado. *Econ. Geol.* 69: 884-901.

Haynes, D.G., Cross, K.C., Bills, R.T. and Reed, M.H. (1995). Olympic Dam Ore Genesis: A fluid-Mixing Model. *Econ. Geol.* 90: 281-307.

Heinrich, C.A., Ryan, C.G., Mernagh, T.P., Eadington, P.J. (1992). Segregation of Ore Metals between Magmatic Brine and Vapour: A Fluid Inclusion Study Using PIXE Microanalysis. *Econ. Geol.* 87: 1566-1583.

Horn, E.E. (1983). Analysis of fluid inclusions with the Heidelberg proton microprobe. 6th Symposium European Current Research on Fluid Inclusions 6th Orleans France Apr. 6-8 Abstracts p. 76.

Horn, E.E. and Traxel, K. (1985). Fluid inclusion investigations with the proton microprobe (PIXE). Symposium European Current Research on Fluid Inclusions. 8th Univ. Gottingen 10-12 April. Abstracts p 76.

Horn, E.E. and Traxel, K. (1987). Investigations of individual fluid inclusions with the Heidelberg proton microprobe - a non-destructive analytical method. *Chem. Geol.* 61: 29-35.

Hunter, D.R. (1976). Some enigmas of the Bushveld Complex. *Econ. Geol* 71: 229-248.

Jenkin, G.R.T., Linklater, C. and Fallick A.E. (1991) Modeling of mineral $\delta^{18}O$ values in an igneous aureole: Closed-system model predicts apparent open-system $\delta^{18}O$ values. *Geol.* 19: 1185-1188.

Johnson, J.P. and Cross, K.C. (1995). U-Pb Geochronological Constraints on the Genesis of the Olympic Dam Cu-U-Au-Ag Deposit, South Australia. *Econ. Geol.* **90**: 1046-1063.

Johnson, J.P. and McCullogh, M.T. (1995). Sources of mineralising fluids for the Olympic Dam deposit (South Australia): Sm-Nd isotopic constraints. *Chem. Geol.* **121**: 177-199.

Jones, H.D. and Kesler, S.E. (1992). Fluid inclusion gas chemistry in east Tennessee Mississippi Valley-type districts: Evidence for immiscibility and implications for depositional mechanisms. *Geochim.Cosmochim. Acta* **56**: 137-154.

Karner, F.R. and Bertram, D.L. (1972). Modal variation in granitic units of the White Mountain plutonic-volcanic series, New Hampshire. *24th Int. Geol. Congr.*, Sect 2, 164-170.

Kazahaya, K. and Matsuo, S. (1986). D/H and 18O/16O fractionations in NaCl aqueous solution-vapor systems at elevated temperatures (abstr.) *Terra Cognitia.* **6**:262.

Kleemann, G. (1985). The Geochemistry and Petrology of the Roof Rocks of the Bushveld Complex East of Groblersdal. Unpublished MSc dissertation Univ. Pretoria.

Kleemann, G.J. and Twist, D. (1989). The Compositionally-zoned Sheet-like Granite Pluton of the Bushveld Complex. Evidence Bearing on the Nature of A-type magmatism. *J. Petrology* **30**(6):1383-1414.

Kruger, F.J. (1994). The Sr-isotopic stratigraphy of the western Bushveld Complex. *S. Afr. J. Geol.* **97** (4): 393-398.

Lee, C.A. and Sharpe, M.R. (1986). The structural setting of the Bushveld Complex - an assessment aided by LANDSAT imagery. In: Anhaeusser, C.R. and Maske, S. (Eds.) Mineral Deposits of Southern Africa Vols I and II. *Geol. Soc. S. Afr.* 1031-1038.

Leube, A., and Stumpfel, E. F. (1963) The Rooiberg and Leeuwpoort Tin Mines, Transvaal, South Africa. *Econ. Geol.* **58**: 391-418, 527-557.

London, D. and Manning, D.A.C (1995). Chemical Variation and Significance of Tourmaline from Southwest England. *Econ. Geol.* **90**: 495-519.

Lowenstern, J.B., Mahood, G.A., Rivers, M.L. and Sutton, R.S. (1992). Evidence for Extreme Partitioning of Copper into a Magmatic Volatile Phase. *Rept. Geol. Surv. Japan*, No. 279:97.

Martin, R.F. and Bonin, B. (1976). Water and magma genesis: The association hypersolvus granite-subsolvus granite. *Canadian Mineralogist* **14**: 228-237.

Matsuhisa, Y., Goldsmith, J.R. and Clayton, R.N. (1979) Oxygen isotope fractionation in the system quartz-albite-anorthite-water. *Geochim. Cosmochim. Acta* **43**: 1131-1140.

Matthews, A. and Beckinsale, R.D. (1979) Oxygen isotope equilibration systematics between quartz and water. *Amer. Miner.* **64**: 232-240.

McMillan, P.F. and Hofmeister, A.M. (1988). Infrared and Raman Spectroscopy. *Reviews in Mineralogy* **18**: 99-160.

McNaughton, N.J., Pollard, P.J., Groves, D.I. and Taylor, R.G. (1993). A Long-Lived Hydrothermal System in Bushveld Granites at the Zaaiplaats Tin Mine: Lead Isotope Evidence. *Econ. Geol.* **88**: 27-43.

Meyer, C. and Hemley, J.J. (1967). *Wall Rock Alteration.* In: Geochemistry of Hydrothermal Ore Deposits. Hubert Lloyd Barnes (Ed.). J.Wiley and Sons. New York. 166-232.

Molengraaf, G.A.F. (1901). Geologie de la Republique Sud-Africaine du Transvaal. *Bull. Soc. Geol. Fr.* 4: 13-92.

Mullis, J., Dubessy, J., Poty, B. and O'Neil, J. (1994) Fluid regimes during late stages of a continental collision: Physical, chemical, and stable isotope measurements of fluid inclusions in fissure quartz from a geotraverse through the Central Alps, Switzerland. *Geochim. Cosmochim. Acta* 58: 2239-2267.

Murphy P.J. and Roberts, S. (1996). Melting and nucleation behaviour of clathrates in multivolatile fluid inclusions: evidence of thermodynamic disequilibrium. *Chem. Geol.* 135:1-20.

Norman, D.I. and Musgrave J.A. (1992). N2-Ar-He compositions in fluid inclusions: Indicators of fluid source. *Geochim. Cosmochim. Acta* 58: 1119-1131.

Ohmoto, H. (1986). Stable isotope geochemistry of ore deposits. *Reviews in Mineralogy* 16: 491-560.

Ohmoto, H. and Rye, R.O. (1970). The Bluebell mine, British Columbia. I. Mineralogy, paragenesis, fluid inclusions and the isotopes of hydrogen, oxygen and carbon. *Econ. Geol.* 65: 417-437.

Ollila, J.T. (1981). A Fluid inclusion and mineralogical study of tin deposits and rocks associated with the Bushveld Complex at the Zaaiplaats, Union and Rooiberg tin mines in the central Transvaal, South Africa. Unpublished PhD thesis. Rand Afrikaans Univ. p 257.

O'Neil, J.R. and Clayton, R.N. (1964). Oxygen isotope geothermometry. *Isotopic and Cosmic Chemistry.* H. Craig, S. Miller and G. Wasserburg. (Eds.). North Holland, Amsterdam, 157-168.

Parsons, I. (1978). Feldspars and fluids in cooling plutons. *Miner. Magazine* **42**: 1-12.

Pasteris, J.D., Wopenka, B. and Seitz, J.C. (1988). Practical aspects of quantitative Laser Raman Microprobe Spectroscopy for the study of fluid inclusions. *Geochim. Cosmochim. Acta. 52*:979-988.

Pasteris, J.D. (1996). The Laser Raman Microprobe as a Tool for the Economic Geologist. Applications of Microanalytical techniques to understanding mineralizing Processes. Oct. 25-27.

Phillips, W. (1875). The rocks of the mining districts of Cornwall and their relation to metalliferous deposits. *Geol. Soc. London Quart. J.* **31**: 319-345.

Plumlee G.S., Goldhaber, M.B. and Rowan, E.L. (1995). The Potential Role of Magmatic gases in the Genesis of Illinois-Kentucky Fluorspar Deposits: Implications from Chemical Reaction Path Modeling. *Econ. Geol.* **90**: 999-1011.

Pollard, P.J., Taylor, R.G., Taylor, R.P. and Groves, D.I. (1991). Petrographic and Geochemical Evolution of Pervasively Altered Bushveld Granites at the Zaaiplaats Tin Mine. *Econ. Geol.* **86**:1401-1433.

Pollard, P.J., Andrew, A.S. and Taylor, R.G. (1991). Fluid inclusion and Stable Isotope Evidence for Interaction between Granites and Magmatic Hydrothermal Fluids during Formation of Disseminated and Pipestyle Mineralization at the Zaaiplaats Tin Mine. *Econ. Geol.* **86**:121-141.

Potter, II, R.W. (1977). Pressure corrections for fluid inclusions homogenisation temperatures based on volumetric properties of the system NaCl-H_2O. *U.S. Geol. J. Res.* **5**: 603-607.

Reynolds, T.J. (1991). Workshop on application of fluid inclusions to minerals exploration and to research on ore deposit genesis. Course notes. EGRU/Dept. of Geology. University of the Witwatersrand.

Robb, L.J., Robb, V.M. and Walraven, F. (1994). The Albert Silver Mine revisited: Towards a model for polymetallic mineralization in granites of the Bushveld Complex, South Africa. *Explor.Mining Geol.* Vol. 3, No. 3 : 247-262.

Roedder, E. (1990). Fluid inclusion analysis Prologue and epilogue. *Geochim. Cosmochim.Acta.* **54**: 495-507.

Roedder, E. (1984). Fluid Inclusions. *Reviews in Mineralogy* **12.** p 644.

Ryan, C.G., Cousens, D.R., Heinrich, C.A., Griffin, W.L., Sie, S.H. and Mernagh, T.P. (1991). Quantitative PIXE microanalysis of fluid inclusions based on a layered yield model. *Nucl. Instr. and Meth.* **B54**:292.

Ryan, C.G., Heinrich, C.A. and Mernagh, T.P. (1993). PIXE microanalysis of fluid inclusions and its application to study ore metal segregation between magmatic brine and vapour. *Nucl. Instr. and Meth.* **B77**:463-471.

Ryan, C.G., Heinrich, C..A., van Achterbergh, E., Ballhaus, C., and Mernagh, T.P. (1995) Microanalysis of ore-forming fluids using the scanning proton microprobe. *Nucl. Instr. and Meth.* **B104**: 182-190.

Rye, R.O. and O'Neil, J.R. (1968).The ^{18}O content of water in primary fluid inclusions from Providencia , north central Mexico. *Econ. Geol.* **63**: 232-238.

Saggerson, E.P. and Turner, L.M. (1982). General comments on the identification of chlorites in thin sections. *Mineralogical Magazine* December **46**: 469-473.

Scoggins, A.J. (1991). Kwandebele: A regional appraisal of the base metal potential of the Bushveld granites. *STK Mineral Development Division. LIB REF No*: 2958.

Seitz, J.C., Pasteris, J.D. and Wopenka, B. (1987). Characterization of CO_2-CH_4-H_2O fluid inclusions by microthermometry and laser Raman microprobe spectroscopy: inferences for clathrate and fluid equilibria. *Geochimica et Cosmochimica Acta.* **51**: 1651-1664.

Sheppard, T.J., Rankin, A.H. and Alderton, D.H.M. (1985). A Practical Guide to Fluid Inclusion Studies. Blackie. London. 10-11.

Sheppard, T.J. (1986). Characterization and isotopic variations in natural waters. *Reviews in Mineralogy* **16**: 165-184.

Sheppard, T.J. and Charef, A. (1986). Eau organic: caracterisation isotopique et evidence de son role dans le gisement Pb-Zn de Fedj-el-Adoum, Tunisie. *C. R. Acad. Sci. Paris. T. 302, serie II* n°. 19 1189-1192.

Sheppard , S.M.F. and Taylor, H.P. Jr. (1974). Hydrogen and oxygen isotope evidence for the origins of water in the Boulder batholith and the Butte ore deposits, Montana. *Econ. Geol.* **69**: 926-946.

Smits, G. (1980). A mineralogical study of the Rooibokkop-Boschhoek copper deposit in the Marble Hall area. *National Institute for Metallurgy* Report No. 2057 pp65.

Sohnge, P.G. (1944) The structure, ore genesis, and minerals sequence of the cassiterite deposits in the Zaaiplaats Tin Mine, Potgietersrust, District, Transvaal. *Trans. Geol. Soc. S. Afr.* **47**: 157-182.

Sorby, H.C. (1858). On the microscopic structure of crystals, indicating the origin of minerals and rocks. *Geol. Soc. London Quart. J.* **14**: (1) 453-500.

South African Committee for Stratigraphy (SACS) (1980). Stratigraphy of South Africa. Part 1: *South Africa Geol. Survey Handbook* **8**, p 690.

Strauss, C.A. and Truter, F.C. (1944). The Bushveld Granites of the Zaaiplaats Tin mining area. *Trans. Geol. Soc. S. Afr.* **47**: 47-75.

Strauss, C.A. (1954). The geology and mineral deposits of the Potgietersrus Tin-fields. *South Africa Geol. Survey Mem.* **46** p 252.

Taylor B.E. and O'Neil J.R. (1977).Stable isotope studies of metasomatic skarns and associated metamorphic and igneous rocks. Osgood Mountains, Nevada. *Contrib. Mineral. Petrol.* **63**:1-49.

Tuttle, O.F. and Bowen, N.L. (1958). Origin of granite in the light of experimental studies in the system Na $AlSi_3O_8$-$KAlSi_3O_8$-SiO_2-H_2O. *Geol. Soc. Amer. Mem.* **74**.

Twist, D. (1985). Geochemical evolution of the Rooiberg silicic lavas in the Loskop dam area, southeastern Bushveld. *Econ. Geol.* **80**: 1153-1165.

van den Kerkhof (1990). Isochoric phase diagrams in the systems CO_2-CH_4 and CO_2-N_2: Application to fluid inclusions. *Geochim. Cosmochim. Acta* **54**: 621-629.

Vellutini, P. (1975). Sur la structur du massif du granit rouge de Porto (Corse du Nord-ouest). *C.R. Acad. Sci. Paris,* **280**, ser. D, 913-916.

Vennemann, T.W. and O'Neil, J.R. (1993). A simple and inexpensive method of hydrogen isotope and water analyses of minerals and rocks based on zinc reagent. *Chem. Geol. (Isotope Geoscience section)* **103**:227-234.

Voet, H.W. (1981). Summary of exploration activities 1885-1980. Int. Rep. Anglo American Corp. Ltd. p 14.

Von Gruenewaldt, G. (1973). The main and upper zones in the Bushveld Complex in the Rossenkal area, eastern Transvaal. *Geol. Soc. S. Afr. Trans.* **76**: 53-61.

Von Gruenewaldt, G. (1979). A review of some recent concepts of the Bushveld Complex, with particular reference to the sulfide mineralization. *Canadian Mineralogist.* **17**: 233-256.

Von Gruenewaldt, G., Sharpe, M.R. and Hatton, C.J. (1985). The Bushveld Complex: Introduction and Review. *Econ. Geol.* **80**: 803-812.

Wagner, P.A. (1921). The Mutue Fides-Stavoren Tin Fields. *Geol. Surv. S. Afr.* No. 16. p 191.

Walraven, F. (1981). The Klipkloof Granite of the Bushveld Complex- an example of systematic radiogenic ^{87}Sr loss. *Ann. Geol. Surv. S. Afr.* **15**: 49-53.

Walraven, F. (1985). Genetic aspects of the granophyric rocks of the Bushveld Complex. *Econ. Geol.* **80**: 1166-1180.

Walraven, F. (1987). Geochronological and isotopic studies of Bushveld Complex rocks from the Fairfield borehole at Moloto, northwest of Pretoria. *S. Afr. J. of Geol.* **90**: 352-360.

Walraven, F. (1990). A chronostratigraphic framework for the north-central Kaapvaal craton, the Bushveld Complex and the Vredefort structure. *Tectonophysics* **171**: 23-48.

Walraven, F. and Hattingh, E. (1993). Geochronology of the Nebo Granite, Bushveld complex. *S. Afr. J. Geol.* **96**: 31-41.

Walraven, F. and Martini, J. (in press). Zircon age determinations of the Oak Tree Formation, Chuniespoort Group, Transvaal Sequence: implications for Transvaal-Griqualand West basin correlations. *S. Afr. J. Geol.*

Walraven, F. (1997). Geochronology of the Rooiberg Group, Transvaal Supergroup, South Africa. *Economic Geology Research Unit Information Circular* No. 316.

Walraven, F., Beukes, N.J. and Retief, E.A. (in press). 2.64 Ga zircons from the Vryberg Formation, Griqualand West: implications for the age of the Transvaal Supergroup and accumulation rates in carbonate/iron formation successions. *Precambrian Reasearch.*

Zartman, R.E. and Marvin, R.F. (1971). Radiometric age (Late Ordovician) of the Quincy, Cape Ann, and Peabody granites from eastern Massachusetts. *Geol. Soc. Amer. Bull.* 82:937-958.

Zirkel, F. (1870). Mikromineralogische Mittheilungen. N Jahrb. Mineral., Geol., Palaont. 801-832.

APPENDIX

TABLE OF POLISHED THIN SECTION DESCRIPTIONS FROM GRASS VALLEY TIN MINE.

SECTION NO.	GRAIN SIZE (MM)	GANGUE MINERALS	ORE MINERAL PARAGENETIC SEQUENCE	COMMENTS
MF1		quartz, biotite, K-feldspar, albite, perthite, zircon		Granophyre. Graphic intergrowths of quartz and hematitised perthite.
MF2		quartz, perthite, albite, K-feldspar, biotite		Coarse-grained granophyre.
MF3a		K-feldspar, albite, quartz, sericite, muscovite	hematite stringers	White hand specimen. No hematitisation. Muscovite rosettes, sericitic alteration, and hematite patches associated with monazite.
MF3b	0.5-1	quartz, sericite, muscovite, fluorite	chalcopyrite, tetrahedrite/tennantite, sphalerite	White/pale green hand specimen. Intense sericitisation. Dark purple fluorite vein associated with sulphides. Growth zonation observed in fluorite. Fluorite postdates the sulphides.
MF5	>2	quartz, muscovite	pyrite	Large muscovite rosettes.
MF6		chlorite, quartz, albite, perthite, biotite		Granophyre.
MF7a	>2	biotite, chlorite, quartz, albite, perthite, sericite	hematite, monazite	Medium- to coarse-grained white with dark patches. Perthite is highly albitised. Hematite and biotite occur in dark patches. Albitised hypersolvus granite.

TABLE OF POLISHED THIN SECTION DESCRIPTIONS FROM GRASS VALLEY TIN MINE.

SECTION NO.	GRAIN SIZE (MM)	GANGUE MINERALS	ORE MINERAL PARAGENETIC SEQUENCE	COMMENTS
MF7b	>2	perthite, quartz, microcline, biotite	? tourmaline	medium- to coarse-grained, albitised perthite with dark patches.
MF8				Pale-pink granophyre.
MF9a	.5	perthite, biotite, albite		Pegmatoidal Perthite with biotite patches. Minor albite patches.
MF9b	0 5	quartz, perthite, albite (primary and secondary), chlorite, biotite, sericite	hematite	Albitisation of perthite. Feldspars appear zoned. Albite and perthite crystals have secondary growth rims.
MF10	0.5	fluorite, quartz, albite, perthite, K-feldspar, sericite, biotite	monazite, zircon, hematite	Red, fine-grained, porphyritic granite. Interstitial fluorite. Discrete albite grains. Hematitised perthite, as well as discrete fresh K-feldspar. Zircons with 2 visible growth zones. Hematite- fluorite association in blebs.
MF11	>2	quartz, muscovite, perthite, fluorite, muscovite, albite	hematite stringers, monazite	Fusion and albitisation. Interstitial fluorite. Euhedral albite crystals associated with fluorite. Transsolvus granite.
MF12a	0.5	quartz, sericite	monazite	Altered hypersolvus granite with no albite/albitisation. Only muscovitisation.
MF12b	>0.5	quartz, sericite	hematite, monazite	Intense sericitisation. Patch of hematite.

TABLE OF POLISHED THIN SECTION DESCRIPTIONS FROM GRASS VALLEY TIN MINE.

SECTION NO.	GRAIN SIZE (MM)	GANGUE MINERALS	ORE MINERAL PARAGENETIC SEQUENCE	COMMENTS
MF12c		muscovite, quartz	hematite	Fine-grained, pale green host. Three quartz pulses. Massive quartz and muscovite intergrown. Hematite pseudomorphs after muscovite present.
MF1	0.5	quartz, sericite, perthite, albite, muscovite		Euhedral quartz. Feldspars sericitised, albitised and hematitised. Patches of hematite. No primary grains of albite.
Mf2	1-2	quartz, perthite, albite, sericite, muscovite, K-feldspar		Sericitisation and albitisation. Multiple quartz phases. Possible introduction of K-feldspar with later quartz pulses.
MF3	0.5-1	quartz, perthite, muscovite, sericite		Muscovite and sericite occur as stringers around quartz and perthite. Cryptocrystalline quartz in patches. No albitisation. Hematite not liberated from perthite lattice.
MF4		quartz, sericite, muscovite rosettes		Intense sericitisation. No feldspars remain. Quartz edges resorbed.
GV01		perthite, quartz, muscovite, chalcedony	hematite	Brecciated, medium-grained red, hypersolvus granite cut by veins filled with 1) chalcedony 2) transparent quartz 3) hematite. Intense hematite of K-feldspar. No albitisation. Hematite precipitation associated with transparent quartz and postdates chalcedony deposition.

TABLE OF POLISHED THIN SECTION DESCRIPTIONS FROM GRASS VALLEY TIN MINE.

SAMPLE NO.	GANGUE	ORE MINERAL PARAGENETIC SEQUENCE	COMMENTS
GV02	quartz, calcite	cassiterite, galena, sphalerite chalcopyrite, chalcocite	Pegmatitic. Euhedral quartz overgrown by milkier quartz and then hematite aggregates. 8 quartz pulses. Calcite is late stage in-fill after milky-limonite-stained quartz. Cassiterite and calcite are intergrown in central portions. Galena, sphalerite, chalcopyrite, postdate early euhedral quartz.
GV04	quartz, muscovite,	hematite, pyrite, sphalerite	Pegmatoidal quartz associated with muscovite, quartz, hematite and pyrite aggregates.
GV05	quartz vein	hematite	Quartz vein with multiple quartz growth stages. Hosted by medium-grained hematitised granite. quartz 1 - white chalecedony quartz 2 - cream chalcedony quartz 3- transparent ,small euhedral crystals quartz 4- transparent, large euhedral crystals quartz 5- milky, packed with inclusions on the rims. Quartz 6- transparent quartz, euhedral small quartz 7- milky white with haematite spheroids on crystal surface. Quartz 8- massive in-fill.
GV06	perthite, quartz, muscovite	hematite, goethite	Quartz is interstitial to perthite. Muscovite occurs locally filling entire interstitial cavities. Localized hematite patches.
GV07a	albite		Granophyre. Hosts quartz vein (GV07b).
GV07b	quartz		Multiple quartz pulses (>8) . Last pulse capped by hematite.
GV08	quartz, albite, perthite, fluorite, epidote	hematite	Albitisation extensive. Areas near fluorite blebs are more albitised. Fluorite postdates epidote. Hypersolvus granite.
GV09	chalcedony muscovite	hematite	Patchy deep red medium-grained granite. Quartz veinlets. Bleached wall rock. No albitisation associated with bleaching. Argillitisation associated with chalcedony. No alteration of wall rock adjacent to chalcedony veins.
GV10	quartz, perthite, muscovite sericite	hematite	Bleached with hematite patches. No primary albite.
GV12	quartz perthite, sericite, albite, muscovite		Hypersolvus granite. Deep red hand specimen. 3 quartz pulses evident.

TABLE OF POLISHED SECTION DESCRIPTIONS FROM ALBERT SILVER MINE.

SECTION NO.	ORE MINERAL PARAGENETIC SEQUENCE	COMMENTS
RP1.16	pyrite, sphalerite, galena	0.1-0.5mm euhedral/ subhedral pyrite. Disseminated specks (>01mm)magnetite. Massive chlorite, disseminated sulphides.
RP1.17	pyrite, (magnetite)	Disseminated pyrite (0.1-0.5mm)- fractured. Small specks of magnetite. Chlorite zone.
RP2.18	magnetite?	Small disseminated specks (0.1mm). Granite host (quartz, hematitised feldspar).
RP2.25	arsenopyrite, pyrite, sphalerite, chalcopyrite	Milky-white quartz and smoky-gray quartz. Arsenopyrite unfractured, pyrite fractured. Chalcopyrite and sphalerite fill fractures in pyrite.
RP2.25	pyrite, galena, sphalerite, chalcopyrite	quartz with multiple growth stages- bottroidal.
RP2.8A	galena , hematite	Chlorite zone with quartz vein (milky-white) bearing sulphides.
RP3.12c	pyrite, hematite, leucoxene, zircon	Black with some sulphide specks and quartz crystals. Pyrite (0.2mm) euhedral/subhedral, hematite occurs as rosettes.
RP4.9	pyrite, galena, bornite, chalcopyrite, hematite,	Hematitised fine-grained granite with milky quartz vein bearing sulphides.
A15 11c	pyrite, hematite	Chain of linked euhedral pyrite grains in vein (3mm). Small disseminated hematite specks in host granite.
A18	hematite	Massive hematite zone.
A30	chalcopyrite, bornite, chalcocite, hematite,	Bornite altered to chalcocite. Chalcopyrite almost totally replaced.
A31	bornite, chalcocite, hematite	Well defined paragenesis seen in this section.
A32	hematite	Massive hematite cross-cut by quartz veins.
A33	hematite	Massive hematite in gangue.
A34	hematite, goethite	Massive haematite with goethite veinlets.
A35	hematite, goethite	Hematite occurs in rosettes, flakes and anhedral masses. Goethite veinlets present.
AS5.5	hematite	Massive hematite.
AS8.5	hematite	Massive hematite.
As15.3	pyrite, tetrahedrite/tennantite, chalcopyrite, bornite, digenite, hematite	Needles of hematite project form bottroidal structures. Postdate pyrite/chalcopyrite.
AS15.4	bornite, chalcocite, digenite, tetrahedrite/tennantite, hematite, fluorite	Disseminated specks associated with fluorite.
AS17 (10b)	arsenopyrite, pyrite, chalcopyrite, hematite, pitchblende	Euhedral pyrite disseminated and as veinlets. Veinlets of chalcopyrite in fractured arsenopyrite. Fine-grained granitic host.

TABLE OF POLISHED SECTION DESCRIPTIONS FROM ALBERT SILVER MINE (CONTINUED)

AS17.12a	pyrite, sphalerite, chalcopyrite	Veinlets lined with pyrite and sphalerite, and central portions filled with chalcopyrite.
AS19(16a)	pyrite, arsenopyrite, galena, sphalerite, chalcopyrite, haematite, magnetite	
AS25 (8h)	pyrite, chalcopyrite, haematite	quartz veins.
AS17.17b	pyrite, arsenopyrite, galena, tetrahedrite/tennantite, chalcopyrite, magnetite	Magnetite and chalcopyrite appear to have precipitated together.

TABLE OF POLISHED THIN SECTION DESCRIPTIONS FROM ALBERT.

SECTION NO.	GRAIN SIZE (MM)	GANGUE MINERALS	ORE MINERAL PARAGENETIC SEQUENCE	COMMENTS
A1	≥1	quartz, sericite, muscovite	hematite, monazite	Quartz in sericite matrix. Hematite associated with muscovite - in stringers.
R53	>1	quartz, sericite, muscovite	monazite, limonite, hematite	As above.
R53 (A5)		quartz, muscovite, sericite	hematite veinlets,	Quartz massive with undulous extinction. Muscovite and sericite along grain boundaries. 2 quartz generations: fine-grained aggregates (0.1mm) filling spaces between coarser material.
A6		As A5 but more hematite and fracturing of quartz grains.		
A7		quartz	hematite	Quartz fractured and filled by hematite.
A9	>2	albite, microcline, biotite, sericite, quartz		Porphyritc granite. Patch perthite. Microcline twinning. Partial hematitisation of feldspar. Biotite interstitial.
AS8.9	0.1-0.3	quartz, sericite, albite, green chlorite, biotite		Hematitised perthite, sericitisation of albite, No fresh feldspars.

TABLE OF POLISHED THIN SECTION DESCRIPTIONS FROM ALBERT.

SECTION NO.	GRAIN SIZE (MM)	GANGUE MINERALS	ORE MINERAL PARAGENETIC SEQUENCE	COMMENTS
A11	>1	quartz, green/brown chlorite, biotite, muscovite, sericite, albite	monazite	Hematitised perthite with white patches (albitisation). Veins filled with sericite cut across patch perthite phenocrysts. Transsolvus granite.
A12	0.1-0.3	quartz, sericite, albite, biotite		Partial sericitisation. Sericitsation occurs in central portions of feldspars, suggesting a secondary episode of feldspar growth.
A13	.2	Sericite, quartz, biotite, muscovite	hematite veinlets	Intense sericitisation of quartz and feldspars.
A14		quartz, muscovite	hematite	Two quartz generations: coarse-grained and cryptocrystalline. Occurs as veins in hematite.
A15	0.3	quartz, sericite, muscovite		Two quartz generations.
A17 M78/765	2-5	green chlorite, quartz, muscovite, sericite		Fine-grained green chlorite. Sericite and chlorite intergrown. Extreme alteration.
A18	massive	quartz	bornite, chalcocite, digenite, hematite, sphalerite	Paragenetic sequence uncertain
A19 M78/765	>0.5	quartz, sericite	hematite	Fine-grained. Extreme sericitisation.
A21		quartz, sericite		Quartz highly fractured/shattered.
A23	0.3	quartz, sericite		Fractured quartz with undulous extinction.
A24 M78/765		green chlorite, sericite, muscovite, quartz	pyrite, bornite, chalcocite, hematite, covellite,	Fine-grained. Cryptocrystalline quartz cross-cut by 3rd quartz generation.
A25	massive	quartz, chalcedony	pyrite, bornite, chalcocite, digenite, hematite	Two quartz generations.
A30		quartz, chalcedony	bornite, chalcocite, magnetite, hematite	Massive hematite zone. Bottroidal growth structures.
A31		quartz	magnetite, hematite	Disseminated.

TABLE OF POLISHED THIN SECTION DESCRIPTIONS FROM ALBERT.

SECTION NO.	GRAIN SIZE (MM)	GANGUE MINERALS	ORE MINERAL PARAGENETIC SEQUENCE	COMMENTS
RPIC R53		quartz, sericite, very deep green chlorite, lime-green muscovite	pyrite	Chlorite associated with pyrite. Multiple quartz growth stages marked by fluid inclusions. Disseminated pyrite.
C4 RP1		quartz, sericite, muscovite, green chlorite	pyrite, chalcopyrite, ?sphalerite	Possibly multiple pyrite growth stages. Chlorite associated with pyrite. Sulphides associated with quartz vein.
RP1d	1	quartz, sericite, ?siderite	hematite needles, chalcopyrite, pyrite veinlets, molybdenum veinlets, cassiterite	Feldspar completely sericitised. Disseminated sulphides. Paragenesis unclear.
RP1f	0.3	quartz, sericite, green chlorite, muscovite		Fe staining in quartz fractures. Chlorite in veinlets.
RP1g	>-0.3	quartz, chlorite sericite,		Abundant sericite.
RP1h		quartz, chalcedony	pyrite	Cross-cut by secondary quartz vein.
RP1I	0.3	quartz, sericite, muscovite	hematite	Graded contact between hematitised and unhematitised host. Sericite more abundant where less hematite occurs. Corroded quartz.
RP1j		sericite, chlorite, muscovite, quartz		Intergrown. Remnant quartz.
RP1k		chlorite, sericite, muscovite (blackened)		Chlorite is more abundant than sericite.

TABLE OF POLISHED THIN SECTION DESCRIPTIONS FROM ALBERT.

SECTION NO.	GRAIN SIZE (MM)	GANGUE MINERALS	ORE MINERAL PARAGENETIC SEQUENCE	COMMENTS
AS9.1	2-4	perthite, sericite, albite, green chlorite, biotite, fluorite		Interlocking albite grains. Minor hematitised perthite surrounded by albite.
AS9.2	2-4	quartz, sericite, biotite		Sericitised equivalent of AS9.1. No hematitisation.
AS9.4	>0.5	quartz, albite, sericite, K-feldspar, muscovite	hematite, magnetite	Porphyritic. Phenocrysts of quartz and perthite. Hematite rims and stringers occur. Muscovite with black specks (magnetite).
NL1a North lode	>0.5	quartz, albite, biotite, K-feldspar, zircon, sericite		Fine-grained gray porphyritic granite. Sericitsation of albite. K-feldspar with weak hematite schillers. Subsolvus matrix. Large perthite phenocrysts. Transsolvus granite.
NL1b North lode	>0.5	K-feldspar, albite, quartz, biotite, sericite	hematite	Fine-grained porphyritic granite. Perthite in subsolvus matrix, i.e. transsolvus.
NL1c	0.3-0.5	K-feldspar, albite, quartz, biotite, sericite, zircon	hematite	Fine-grained porphyritic granite. Phenocrysts zoned. Tartan-twinned microcline. Zoned albite with unaltered rim and, sericitised core. Sericitisation of quartz and feldspars. 2 quartz pulses, first embayed, second fresh.

TABLE OF POLISHED THIN SECTION DESCRIPTIONS FROM ALBERT.

SECTION NO.	GRAIN SIZE (MM)	GANGUE MINERALS	ORE MINERAL PARAGENETIC SEQUENCE	COMMENTS
NL2		quartz, chalcedony	hematite	Massive hematite ore.
NL3		quartz	hematite	Milky-quartz surrounded by bottroidal hematite.
G1	>5	quartz, K-feldspar, biotite, albite,		Coarse-grained granite. Perthite hematitised, albite unhematitised. Albite has secondary growth rims. Central portions sericitised.
D1	>5	chlorite, sericite, quartz	hematite	Completely altered.
F1	0.5	chlorite, sericite, quartz, albite,	hematite	Fine-grained porphyritic granite, sericitised, hematitised and chloritised. Transsolvus granite.
OD1		quartz	(chalcopyrite), covellite, hematite	Hematitised breccia. Evidence for hematite/covellite relationship.
OD2		quartz	hematite	Massive hematite vein material.
OD3		quartz, olive-green chlorite,	arsenopyrite, tetrahedrite/tennantite, chalcopyrite, bornite, chalcocite	Massive ore.
OD4		quartz, chalcedony	tetrahedrite/tennantite, chalcopyrite, covellite, hematite	Sample banded: chalcopyrite then chalcopyrite /hematite, then hematite.
OD5		quartz	galena, arsenopyrite, hematite	Vein quartz with hematite needles. Galena fills interstitial spaces in quartz.

TABLE OF POLISHED THIN SECTION DESCRIPTIONS FROM ALBERT.

SECTION NO.	GRAIN SIZE (MM)	GANGUE MINERALS	ORE MINERAL PARAGENETIC SEQUENCE	COMMENTS
W/A	0.5	quartz, albite, biotite, perthite, sericite, K-feldspar, chlorite		Transsolvus granite. Biotite altered to chlorite.
W/B		perthite,quartz, albite, biotite, sericite, K-feldspar		Medium-grade transsolvus granite grading into fine-grained subsolvus material.
W/C	>5	quartz, biotite, albite, K-feldspar, chlorite		Coarse-grained subsolvus granite.
W2	2	quartz, sericite chlorite	hematite	Medium-grained altered granite with localized patches of hematite. No feldspars remain.
W3		quartz, sericite		Medium- to coarse-grained granite. Highly sericitised.
W4	0.5	quartz, chalcedony, sericite	hematite	Silicified granite. Vein of hematite intergrown with chalcedony.
W5	0.5	quartz, green chlorite, perthite, ±albite, sericite	hematite	Fine-grained pink granite. High perthite component. Albite and other K-feldspars rare. Hypersolvus granite.
AS13.1	0.3	quartz, green chlorite, sericite, perthite, biotite		Sericitisation of zoned albite (rapakivi?).
AS13.2		quartz, albite, sericite, chlorite, K-feldspar, biotite, chalcedony	cassiterite?	Fine-grained porphyritic, transsolvus granite. Chlorite veinlets and chloritisation of feldspars. Phenocrysts of patch perthite.

TABLE OF POLISHED THIN SECTION DESCRIPTIONS FROM ALBERT.

SECTION NO.	GRAIN SIZE (MM)	GANGUE MINERALS	ORE MINERAL PARAGENETIC SEQUENCE	COMMENTS
AS13.5	0.3	quartz, sericite, green chlorite, perthite	hematite	Highly sericitised, fine-grained granite. Only minor residual perthite remains unsericitised.
AS13.62	0.3	biotite, chlorite, quartz, sericite, K-feldspar, albite, perthite		Biotite altering to chlorite. Fresh K-feldspar partially sericitised. Hematitised perthite and zone albite crystals. Transsolvus granite.
AS25.2	0.5-2	quartz, albite, sericite, K-feldspar, biotite, chlorite		There appears to be more albite, as secondary growth and as patches in perthite. Sericitised cores suggest sericitisation occurred before albitisation.
AS25.5a	0.3	quartz, sericite, green chlorite		Fine-grained pale green. Quartz and perthite phenocrysts, Intense sericitisation of transsolvus granite.
AS25.5b	0.3	quartz, sericite, biotite, chlorite		Fine-grained pale green host. Quartz grains have absorbed boundaries.
AS25.5c		quartz, sericite, chlorite, muscovite		pale green. Muscovite rosettes.
AS25.6a	0.3	quartz, chlorite, perthite, biotite	hematite	Completely altered.

TABLE OF POLISHED THIN SECTION DESCRIPTIONS FROM ALBERT.

SECTION NO.	GRAIN SIZE (MM)	GANGUE MINERALS	ORE MINERAL PARAGENETIC SEQUENCE	COMMENTS
AS25.6b	0.3	quartz, sericite		Intense sericitisation.
AS25.6c	0.3	quartz, sericite, biotite, chlorite, perthite		Residual patches of hematitised perthite showing the beginnings of sericitisation. Therefore, hematitisation predates sericitisation.
AS25.7	0.3	quartz, sericite, chlorite, muscovite, biotite		Biotite replaced by sericite?
AS25.8b	0.3	quartz, chalcedony, sericite, chlorite		Swarm of quartz veins cutting across fine-grained pale-green host. Quartz veins are cryptocrystalline.
AS25.8g		chalcedony, chlorite		
AS25.9		quartz, sericite, muscovite, chlorite, biotite		Muscovite replaces biotite.
As25. 10f		chalcedony, chlorite	arsenopyrite	arsenopyrite in vein
As25.10g		quartz, green chlorite, muscovite, sericite	pyrite, arsenopyrite, galena, chalcopyrite	Quartz veins in fine-grained host. Chlorite rosettes surround quartz and sulphides.
AS25.11	0.3	quartz, perthite, sericite, chlorite, albite		Transsolvus granite. Secondary albite present.
AS25.13	0.3-0.5	quartz, sericite, chlorite, biotite	chalcopyrite, hematite	Fine-grained green host. No feldspars left. A patch with biotite, hematite and chalcopyrite. No biotite elsewhere.
AS16.1	0.5	perthite, albite, sericite, quartz, green chlorite	hematite	Pink porphyritic granite. Medium - grained. Discrete feldspars still visible, partially to completely sericitised.

TABLE OF POLISHED THIN SECTION DESCRIPTIONS FROM ALBERT.

SECTION NO.	GRAIN SIZE (MM)	GANGUE MINERALS	ORE MINERAL PARAGENETIC SEQUENCE	COMMENTS
AS16.2		quartz, perthite, chlorite, fluorite		Angular perthite and quartz fragments. Fluorite and chlorite, as well as breccia fragments, cemented by quartz. Chlorite vein.
AS16.3A	0.3 (fine)	quartz, K-feldspar, sericite, biotite, chlorite		Sharp boundary between fine- and coarse-grained pink granite. Faint hematitisation of perthite. Interlocking crystals. Coarse crystals overgrow border crystals of fine grained material. No erosional boundary. Crystals form interlocking boundary.
	1 (coarse)	quartz, perthite, albite, sericite, K-feldspar, biotite		
As16.4	0.3	quartz, sericite, muscovite, K-feldspar, albite	hematite	K-feldspar is not sericitised.
AS16.5		quartz, perthite, sericite		Coarse-grained. Sericite occurs along fractures. Chalcedony vein runs parallel to sericite veins.
AS16.6a	3-5	albite, quartz, K-feldspar, chlorite, biotite	monazite associated with biotite	Coarse-grained. Quartz overgrows zoned euhedral albite crystals. Sericitised cores.
AS8.3		quartz	hematite	Massive quartz with hematite veinlets. Multiple quartz growth in bottroidal shape. Hematite lines veins with needles projecting inwards, overgrown by cryptocrystalline quartz and then normal quartz.
AS8.7a	0.3	quartz, sericite, muscovite	hematite	Sericitised fine-grained host. Sericite has hematite specks.

TABLE OF POLISHED THIN SECTION DESCRIPTIONS FROM ALBERT.

SECTION NO.	GRAIN SIZE (MM)	GANGUE MINERALS	ORE MINERAL PARAGENETIC SEQUENCE	COMMENTS
AS8.4a		quartz	hematite	Massive quartz. Streaky undulous extinction of quartz grains. Hematite specks rim some early formed euhedral crystals.
AS8.4a		quartz	hematite	As above. Hematite veins cutting through cockscomb quartz with multiple growth stages
AS8.6	0.3	quartz, sericite	hematite	Deep red, patchy, fine-grained material. No feldspars left.
AS8.7	0.3	quartz, sericite, muscovite	hematite	Fine-grained pale green host. Hematite veinlets and rims.
AS8.8	0.3	quartz, sericite, biotite, chlorite	hematite	Fine-grained green host.
AS14.1b		quartz, sericite, muscovite, green chlorite	galena, tetrahedrite /tennantite, sphalerite, chalcopyrite	Fine-grained pale-green host with sulphide specks. Chalcedony veinlets. Sulphide patch associated with massive green chlorite.
AS14.2		quartz, sericite, biotite, chlorite, perthite	hematite, zircon/monazite	Medium-grained porphyritic transsolvus granite.
AS14.3		quartz, sericite, green chlorite, biotite, muscovite		Coarse-grained. Biotite altering to chlorite. Quartz veinlets. Muscovite intergrown with chlorite.
AS14.4b		quartz, sericite, green chlorite, chalcedony, muscovite	zircon	Silicification intense.
AS14.5		quartz, sericite, chlorite	sphalerite, hematite	Coarse-grained, pale green host. Sericite and chlorite intergrown.
AS14.7	0.5	quartz, sericite, muscovite	hematite	Fine-grained porphyritic granite. Phenocrysts altered to quartz and sericite.

TABLE OF POLISHED THIN SECTION DESCRIPTIONS FROM UNMINERALISED RED EPISYENITE AT SPOEDWEL.

SECTION NO.	GRAIN SIZE (MM)	GANGUE MINERALS	ORE MINERAL PARAGENETIC SEQUENCE	COMMENTS
SD58	<2	perthite, zircon, quartz, muscovite, chlorite		Partially fused, hypersolvus granite.
SE04	<2	perthite, albite, quartz, muscovite	hematite	Albitisation of perthite, hematite stringers and rims, partial fusion.
SD59A	<2	perthite, zircon, quartz, muscovite	pyrite, chalcopyrite, chalcocite	Hypersolvus granite.
SE01	<2	perthite, albite, zircon, quartz, muscovite, chlorite	chalcopyrite, (±leucoxene)	Partial fusion, hypersolvus granite.
SE02	>2	perthite, muscovite, chlorite	cassiterite, chalcopyrite	Extreme fusion.
SE03	≥2	perthite, albite, quartz		Albitisation, no fusion, hypersolvus granite.
SD72	≥2	perthite, quartz, chlorite	cassiterite, chalcopyrite	Extreme fusion.
SD31	≥2	perthite, quartz, muscovite, K-feldspar	cassiterite, leucoxene	Transsolvus granite.

TABLE OF POLISHED THIN SECTIONS FROM THE SULPHIDE-EPISYENITE CONTACT AT SPEEDWEL.

SECTION NO.	GRAIN SIZE (MM)	GANGUE MINERALS	ORE MINERAL PARAGENETIC SEQUENCE	COMMENTS
CB06	≥2	perthite, chlorite, K-feldspar, quartz, muscovite, albite	chalcopyrite	Fused transsolvus granite with chalcopyrite veins and albitisation.
SF04	≥2	perthite, muscovite, albite, K-feldspar, quartz	cassiterite, pyrite, chalcopyrite, bornite, covellite	Transsolvus granite.
SC10	≥2	perthite, quartz, chlorite, muscovite	cassiterite, pyrite, chalcopyrite, covellite	Sharp contact, fusion, and albitisation.
PT01	≥2	perthite, muscovite, K-feldspar, albite, quartz	pyrite, chalcopyrite, chalcocite	Partial fusion, transsolvus, and albitisation.
SF22	≥2	perthite, quartz, muscovite, K-feldspar, sericite	pyrite, chalcopyrite, covellite	Albitised transsolvus granite.
PB06	>2	perthite, muscovite, quartz, albite, K-feldspar	arsenopyrite, cassiterite, sphalerite, chalcopyrite, covellite	Transsolvus at hypersolvus-subsolvus granite contact.
SF34	≥2	perthite, K-feldspar, albite, muscovite, quartz	arsenopyrite, cassiterite, sphalerite, chalcopyrite, covellite	Fused transsolvus granite.
SF03	≥2	perthite, quartz, albite, sericite, K-feldspar	pyrite, sphalerite, chalcopyrite	Massive chalcopyrite at hypersolvus /subsolvus granite contact. Albitised transsolvus granite.
SF25		perthite, quartz, muscovite, sericite, albite, K-feldspar	arsenopyrite, chalcopyrite	Transsolvus granite.
PP08	≥2	perthite, muscovite, quartz, K-feldspar, albite	pyrite, chalcopyrite, covellite	Transsolvus granite.

TABLE OF POLISHED THIN SECTION DESCRIPTIONS FROM SPOEDWEL WITH DISSEMINATED MINERALISATION.

SECTION NO.	GRAIN SIZE (MM)	GANGUE MINERALS	ORE MINERAL PARAGENETIC SEQUENCE	COMMENTS
SC06	>>2	perthite, quartz, chlorite, K-feldspar	pyrite, sphalerite, chalcopyrite	Hypersolvus granite with coarse-grained sulphides (>>2mm).
FOP14	>>2	perthite, quartz, chlorite	arsenopyrite, pyrite, cassiterite, sphalerite, chalcopyrite	Extreme fusion of hypersolvus granite with coarse-grained sulphides.
SC04	1	perthite, muscovite, quartz, K-feldspar, albite, fluorite	pyrite, chalcopyrite	Fused transsolvus granite.
SD61	>>2	perthite, quartz, muscovite,	cassiterite, zircon, pyrite, chalcopyrite, covellite	Partial fusion of hypersolvus granite.
SD04	>>2	perthite, quartz, chlorite, muscovite	pyrite, cassiterite, sphalerite, chalcopyrite, covellite	Fused hypersolvus granite.
SD46	>>2	perthite, quartz, muscovite, fluorite, sericite,	pyrite, chalcopyrite, chalcocite, covellite	Hypersolvus granite.
SD50	≥2	perthite, chlorite (olive-green and grass-green), fluorite, muscovite, sericite	pyrite, chalcopyrite, covellite	chalcopyrite>>pyrite Hypersolvus granite with minor albitisation.
SF26	≥2	perthite, K-feldspar, muscovite, sericite, q[illegible]	pyrite, chalcopyrite, covellite	Fused hypersolvus granite.
SC02	≥2	n[illegible]vite, green chlorite, quartz, sericite, albite	cassiterite, sphalerite, chalcopyrite, covellite	Fused hypersolvus granite.
SW21	≥2	perthite, quartz, muscovite, sericite	pyrite, chalcopyrite, bornite, chalcocite, covellite	Fused hypersolvus granite. Two veins: 1) muscovite and chalcopyrite 2)quartz
SD62	≥2	perthite, muscovite, albite, green ch[illegible]e	pyrite, cassiterite, chalcopyrite, covellite	Partial fusion. Vein of subsolvus granite in hypersolvus host.
SD64	>>2	perthite, albite, green chlorite, muscovite, quartz, K-feldspar, sericite	pyrite, chalcopyrite	Fusion of transsolvus granite.

TABLE OF POLISHED THIN SECTION DESCRIPTIONS FROM SPOEDWEL WITH DISSEMINATED MINERALISATION (CONTINUED).

SECTION NO.	GRAIN SIZE (MM)	GANGUE MINERALS	ORE MINERAL PARAGENETIC SEQUENCE	COMMENTS
SD34	>> 2	perthite, fluorite, quartz, muscovite, K-feldspar, sericite, albite	pyrite, chalcopyrite	Fusion and albitisation at transsolvus-hypersolvus contact.
SW02	>2	perthite, quartz, albite, muscovite, green chlorite	zircon, chalcopyrite	Subsolvus granite.
SD49	>2	perthite, quartz, K-feldspar, muscovite, sericite,	pyrite, chalcopyrite, chalcocite, digenite	Subsolvus material starts crystallizing with pyrite.
SD29B	>1	perthite, green chlorite, monazite, quartz		Very fine-grained, extreme fusion, no albitisation, only hypersolvus material present.
SA06		Perthite, brown chlorite, quartz, muscovite, albite, K-feldspar, sericite	zircon, cassiterite, sphene (leucoxene), pyrite	Disseminated mineralisation at subsolvus/hypersolvus contact. Albitisation of perthite.
SD38	1	perthite, muscovite, albite, K-feldspar, quartz	pyrite, chalcopyrite, covellite	Albitisation of fused perthite, minor subsolvus granite and disseminated sulphides.
SA01	>1	quartz, muscovite, sericite, albite, K-feldspar,	monazite, cassiterite, leucoxene, chalcopyrite, covellite	Partial albitisation, and extreme fusion of host. Disseminated chalcopyrite. Sericitisation near contact with subsolvus granite.
SA09	≥1	sericite, fluorite, muscovite, brown chlorite	cassiterite, pyrite, chalcopyrite, bornite, chalcocite, covellite	Fine-grained subsolvus granite.
PP03	1	perthite, albite (X2), sericite, muscovite	goethite, chalcopyrite, covellite	Extreme fusion and albitisation.
SD59B	>1	muscovite, quartz, green chlorite associated with quartz vein	goethite, chalcopyrite, bornite, chalcocite	Fusion, local albitisation, and silicification associated with quartz vein.
SE05	1	perthite, quartz, K-feldspar, muscovite, fluorite, albite (X2), sericite	cassiterite, hematite,	Albitisation of perthite in transsolvus granite. Subsolvus material associated with fluorite and sulphides.

TABLE OF POLISHED THIN SECTION DESCRIPTIONS FROM THE MASSIVE SULPHIDE ZONE AT SPOEDWEL.

SECTION NO.	GRAIN SIZE (MM)	GANGUE MINERALS	ORE MINERAL PARAGENETIC SEQUENCE	COMMENTS
SP23		albite, K-feldspar, quartz, muscovite,	massive pyrite, sphalerite, chalcopyrite	No perthite. Subsolvus granite.
SF24		muscovite, albite, K-feldspar	huge pyrite grains, chalcopyrite massive	Subsolvus material embayed by sulphides.
SF08		albite, muscovite, quartz, K-feldspar	arsenopyrite, chalcopyrite, galena, tetrahedrite/tennantite , sphalerite	Sphalerite surrounds pyrite and chalcopyrite. Predominantly albite matrix. Note chalcopyrite precedes galena and sphalerite.
CB50		perthite, albite, muscovite, sericite, K-feldspar	monazite, arsenopyrite, pyrite, sphalerite, chalcopyrite	Pyrite overgrowth on albitised perthite grains.
SF20		perthite, quartz, sericite, muscovite, albite, K-feldspar	pyrite, chalcopyrite, covellite	Small perthite specks in subsolvus matrix.
CB11		K-feldspar., quartz, albite, muscovite, sericite	arsenopyrite, pyrite, chalcopyrite	Albite, K-feldspar, and quartz of subsolvus material found within pyrite grains.
SF05		quartz, albite, muscovite, K-feldspar	pyrite, chalcopyrite	Massive sulphide, minor gangue component.
SF?'		quartz, sericite	pyrite, chalcopyrite, covellite	Massive chalcopyrite. No feldspers present.
PB20		quartz, muscovite,	cassiterite, monazite, pyrite, chalcopyrite, covellite,	Large pyrite grains surrounded by massive chalcopyrite. Large crystals of monazite.
SF25B		(perthite), muscovite, albite, quartz, K-feldspar	pyrite, chalcopyrite, covellite, monazite	Transsolvus granite.
SD43		quartz, muscovite, albite, sericite, K-feldspar	pyrite, chalcopyrite, zircon	Subsolvus granite.
SD45A	>2	Chlorite, quartz	pyrite, chalcopyrite	Pyrite and chalcopyrite in chlorite matrix. Quartz embayed by chlorite.
SF28	>2	K-feldspar, quartz, muscovite, albite	arsenopyrite, pyrite, chalcopyrite, covellite	Subsolvus matrix.

TABLE OF POLISHED THIN SECTION DESCRIPTIONS FROM THE MASSIVE SULPHIDE ZONE AT SPOEDWEL (CONTINUED).

SECTION NO.	GRAIN SIZE (MM)	GANGUE MINERALS	ORE MINERAL PARAGENETIC SEQUENCE	COMMENTS
SD63	>2	quartz, muscovite, albite, K-feldspar, green chlorite	pyrite, chalcopyrite, covellite	Subsolvus matrix.
SD09	1	albite, K-feldspar, quartz, muscovite	cassiterite, pyrite, chalcopyrite, covellite	Subsolvus matrix.
SD25		quartz, muscovite, albite, K-feldspar, green chlorite	chalcopyrite, covellite	Subsolvus matrix.
SD49B	1	green chlorite, quartz	pyrite, chalcopyrite, covellite, zircon	Chlorite matrix.
PB02		albite, quartz, muscovite, fluorite, sericite, residual perthite, green chlorite, (K-feldspar)	Arsenopyrite, galena, chalcopyrite, covellite magnetite	Well zoned quartz inside chalcopyrite masses. Albite highly sericitised. Fluorite precipitation occurred before chalcopyrite. Veins of magnetite lined by covellite within chalcopyrite.
SD26		perthite, muscovite, albite, green chlorite, quartz, sericite, K-feldspar	pyrite, chalcopyrite, covellite	Pronounced albitisation of perthite.
SW01		Green chlorite, albite, muscovite, sericite, quartz, K-feldspar	leucoxene, pyrite, arsenopyrite, chalcopyrite, monazite, covellite	Subsolvus granite.
SF30		quartz, albite, muscovite, sericite, K-feldspar, green chlorite	zircon, pyrite, galena, sphalerite	Albite is sericitised and chloritised. Subsolvus granite.
SD45B	>2	green chlorite, quartz	zircon pyrite, chalcopyrite,	Chlorite matrix containing zircons with alteration haloes.
SD45A	2	green chlorite, quartz	pyrite, chalcopyrite	Chlorite matrix.
SF36	>1	albite, quartz, K-feldspar, muscovite, green chlorite	pyrite, galena, sphalerite	Subsolvus granite.
SF33	>1	albite, quartz, K-feldspar, muscovite,	pyrite, galena, chalcopyrite, sphalerite	Subsolvus granite. Questionable paragenesis.

TABLE OF POLISHED THIN SECTION DESCRIPTIONS FROM THE MASSIVE SULPHIDE ZONE AT SPOEDWEL (CONTINUED).

SECTION NO	GRAIN SIZE (MM)	GANGUE MINERALS	ORE MINERAL PARAGENETIC SEQUENCE	COMMENTS
SF31	>1	albite, quartz, K-feldspar, muscovite, green chlorite	galena, sphalerite only	Subsolvus granite.
SD55A		quartz veinlets, chlorite	pyrite, sphalerite, magnetite	Chlorite matrix. Vugs lined by small quartz crystals. Magnetite in veins.
SD70		green chlorite, quartz,	chalcopyrite, chalcocite, bornite, magnetite? Limonite, zircon	Chlorite matrix with quartz veins and vugs. Quartz is coarse-grained in vugs and fine-grained in veins.
SD73	>2	sericite, muscovite, green chlorite, K-feldspar, albite	pyrite only	Extreme sericitisation of original subsolvus host.
SD27		quartz, green chlorite, very fine grained quartz (chaledony?), sericite	pyrite, sphalerite, chalcocite, chalcopyrite, covellite, magnetite	Questionable paragenesis. Chlorite matrix.
WS01		green chlorite, quartz	chalcopyrite veinlets, bornite veinlets in chalcopyrite veinlets, chalcocite rims on chalcopyrite, monazite in quartz veins, zircon	Chlorite matrix. Euhedral perthite crystal outlines still visible.

TABLE OF POLISHED THIN SECTION DESCRIPTION OF MISCELLANEOUS SAMPLES FROM SPOEDWEL.

SECTION NO.	GRAIN SIZE (MM)	GANGUE MINERALS	ORE MINERAL PARAGENETIC SEQUENCE	COMMENTS
FG01	0.1-0.5	(perthite?), quartz, green chlorite, albite, biotite		Small scale graphic intergrowths. Granophyric texture.
FG03	0.5-1	biotite, albite, haematised feldspar (K-feldspar)	zircon	As above.
SD05	>>2	perthite, green chlorite, quartz	monazite, pyrite, chalcopyrite	Transition between heavily and partially chloritised hypersolvus material.
SC09	2	perthite, green chlorite, sericite, quartz	monazite, pyrite, chalcopyrite, bornite, chalcocite	Fused hypersolvus granite.
SC08		perthite, muscovite, quartz, green chlorite, albite	zircon, pyrite, sphalerite, chalcopyrite	Massive muscovite zone at contact between fused hypersolvus material and subsolvus material.
SD71		perthite, quartz, green chlorite	monazite only	Massive quartz invasion of chlorite matrix.
SF38		albite, green chlorite, muscovite, quartz, K-feldspar	pyrite, galena only	Chloritised subsolvus granite.

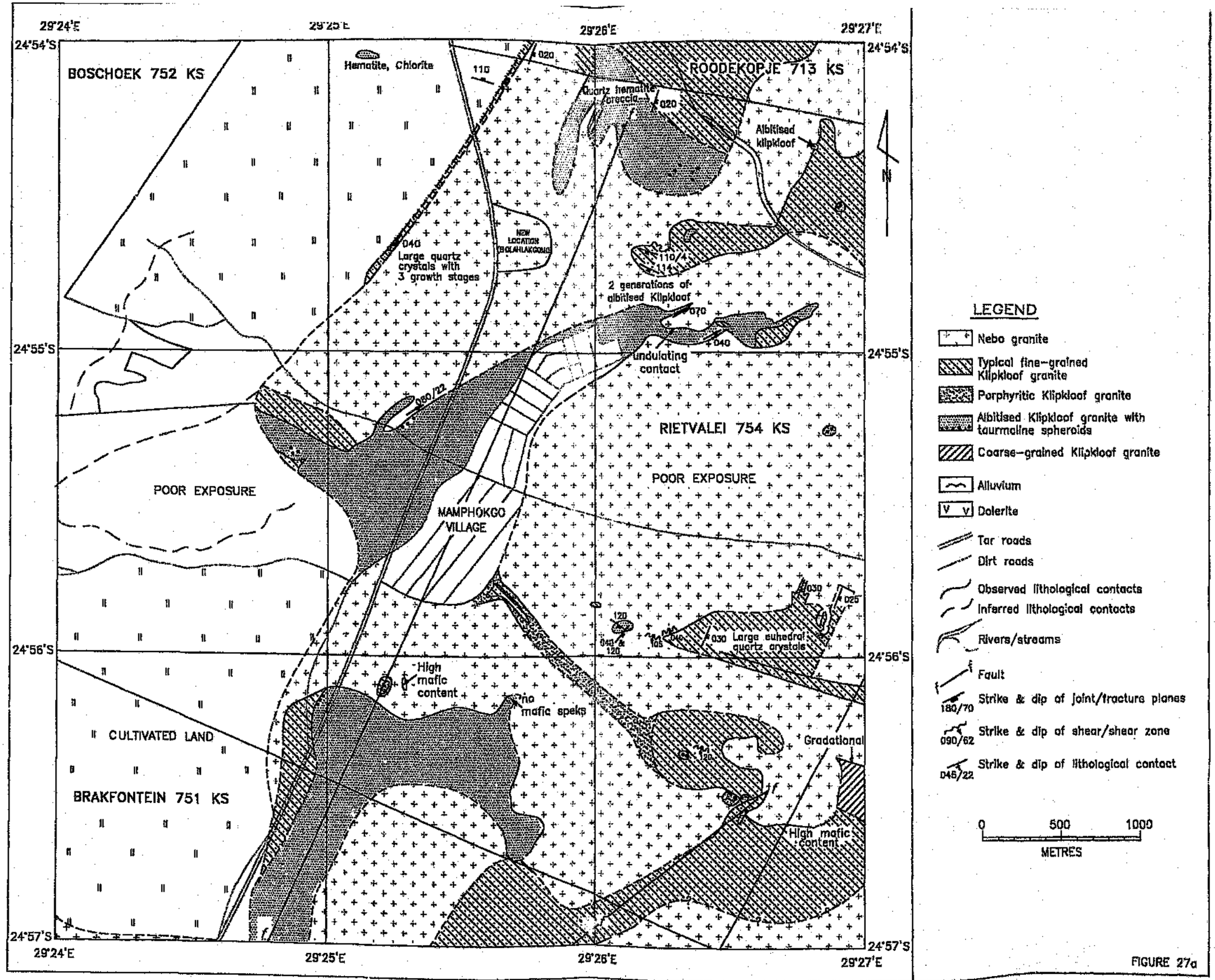

29°24'E
29°25'E
29°26'E
29°27'E
24°54'S
24°55'S
24°56'S
24°57'S
BOSCHOEK 752 KS
ROODEKOPJE 713 KS
RIETVALEI 754 KS
BRAKFONTEIN 751 KS
Hematite, Chlorite
Quartz hematite breccia
Albitised klipkloof
2 generations of albitised Klipkloof
Large quartz crystals with 3 growth stages
NEW LOCATION (MOLAHLAKGONG)
undulating contact
POOR EXPOSURE
MAMPHOKGO VILLAGE
CULTIVATED LAND
High mafic content
no mafic speks
Gradational
Large euhedral quartz crystals
N
LEGEND
Nebo granite
Typical fine-grained Klipkloof granite
Porphyritic Klipkloof granite
Albitised Klipkloof granite with tourmaline spheroids
Coarse-grained Klipkloof granite
Alluvium
Dolerite
Tar roads
Dirt roads
Observed lithological contacts
Inferred lithological contacts
Rivers/streams
Fault
180/70 Strike & dip of joint/fracture planes
090/62 Strike & dip of shear/shear zone
045/22 Strike & dip of lithological contact
0
500
1000
METRES

FIGURE 27a

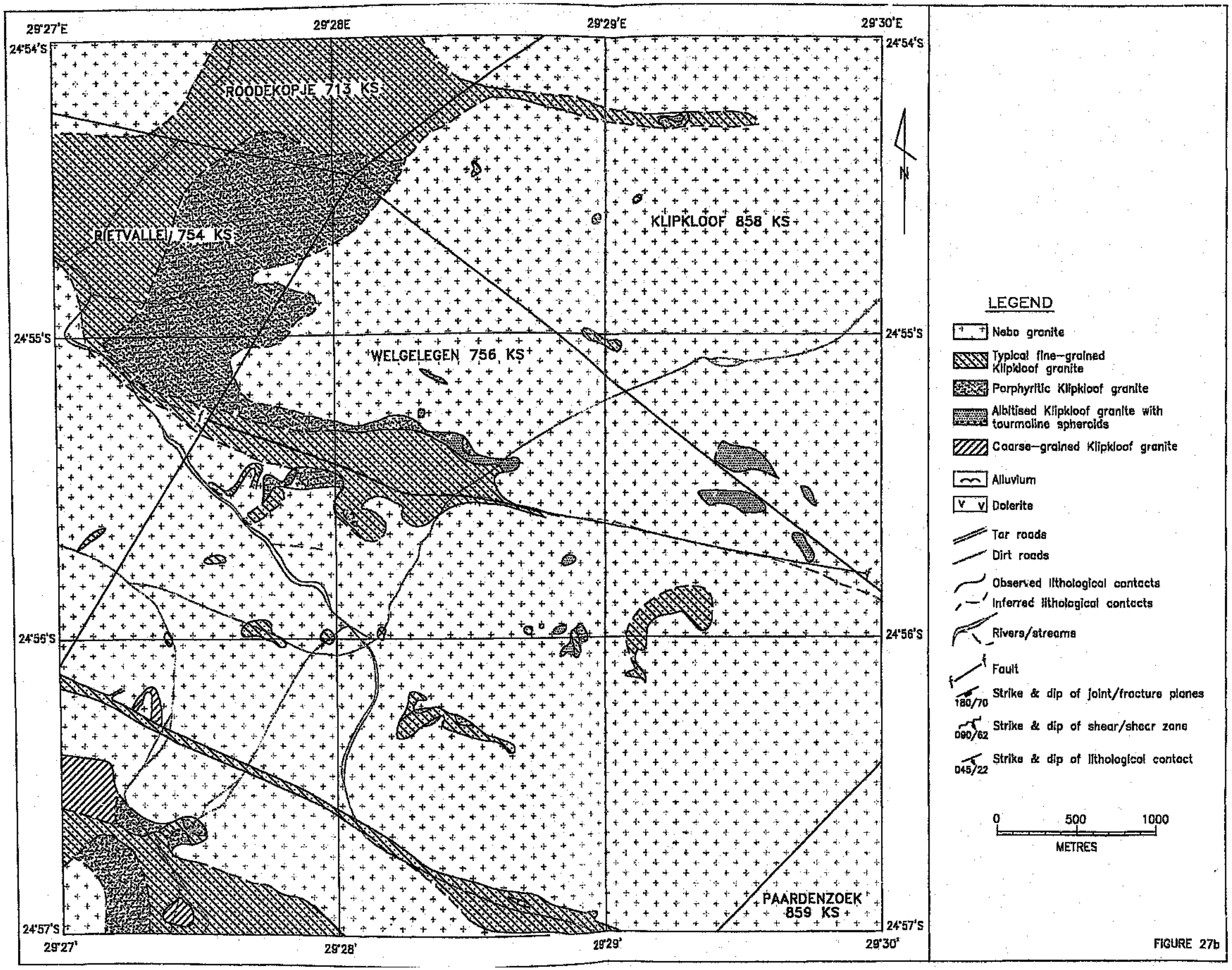

29°27'E
29°28E
29°29'E
29°30'E
24°54'S
24°55'S
24°56'S
24°57'S
ROODEKOPJE 713 KS
RIETVALLEI 754 KS
KLIPKLOOF 858 KS
WELGELEGEN 756 KS
PAARDENZOEK 859 KS
N
LEGEND
Nebo granite
Typical fine-grained Klipkloof granite
Porphyritic Klipkloof granite
Albitised Klipkloof granite with tourmaline spheroids
Coarse-grained Klipkloof granite
Alluvium
Dolerite
Tar roads
Dirt roads
Observed lithological contacts
Inferred lithological contacts
Rivers/streams
Fault
180/70 Strike & dip of joint/fracture planes
090/62 Strike & dip of shear/shear zone
045/22 Strike & dip of lithological contact
0
500
1000
METRES

FIGURE 27b

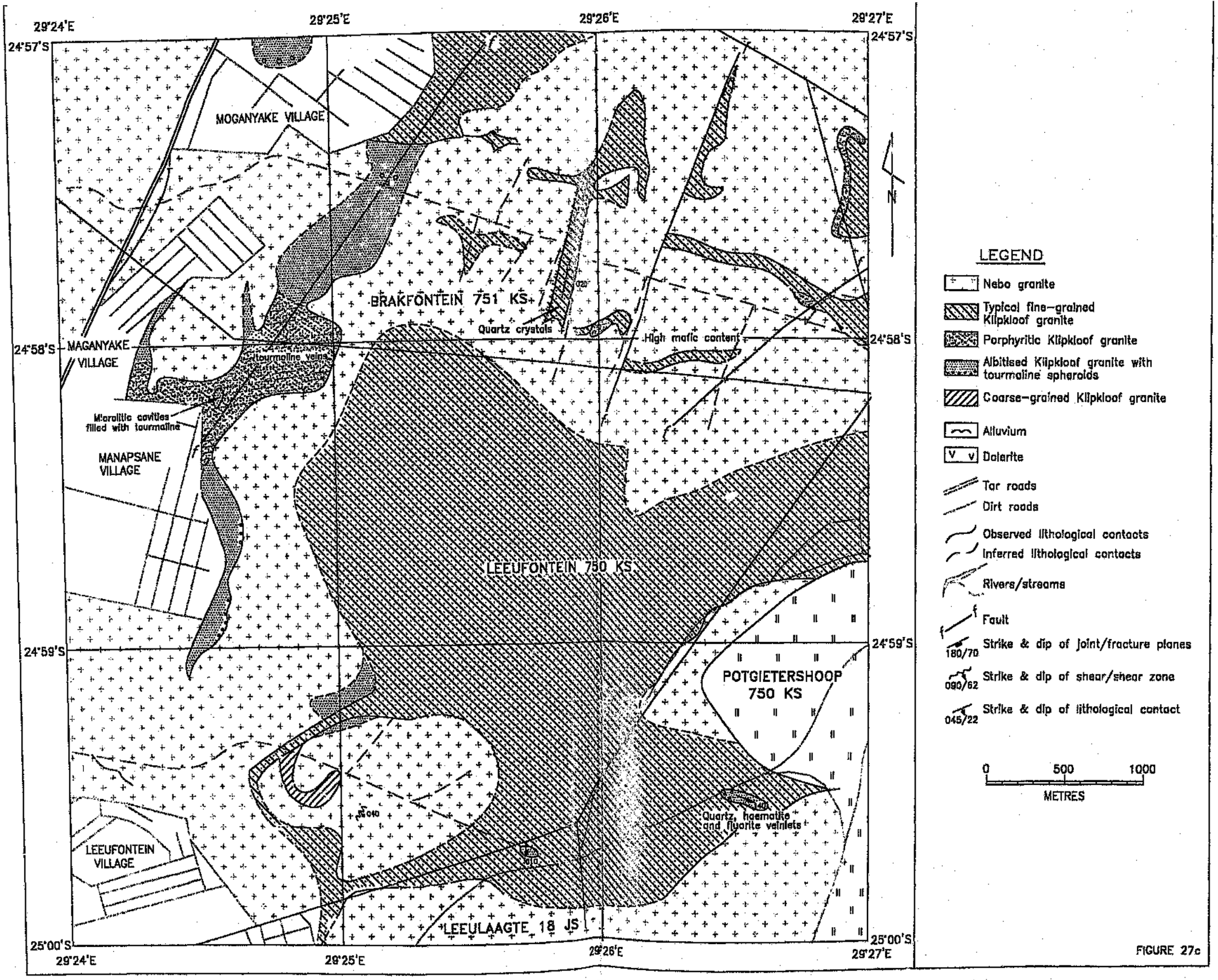

29°24'E
29°25'E
29°26'E
29°27'E
24°57'S
24°58'S
24°59'S
25°00'S
MOGANYAKE VILLAGE
MAGANYAKE VILLAGE
MANAPSANE VILLAGE
LEEUFONTEIN VILLAGE
BRAKFONTEIN 751 KS
LEEUFONTEIN 750 KS
POTGIETERSHOOP 750 KS
LEEULAAGTE 18 JS
Quartz crystals
High mafic content
Tourmaline veins
Miarolitic cavities filled with tourmaline
Quartz, haematite and fluorite veinlets
N
LEGEND
Nebo granite
Typical fine-grained Klipkloof granite
Porphyritic Klipkloof granite
Albitised Klipkloof granite with tourmaline spheroids
Coarse-grained Klipkloof granite
Alluvium
Dolerite
Tar roads
Dirt roads
Observed lithological contacts
Inferred lithological contacts
Rivers/streams
Fault
180/70 Strike & dip of joint/fracture planes
090/62 Strike & dip of shear/shear zone
045/22 Strike & dip of lithological contact
0
500
1000
METRES

FIGURE 27c

29°27'E 29°28'E 29°29'E 29°30'E

24°57'S

24°58'S

24°59'S

25°00'S

PAARDENZOEK VILLAGE

WELGELEGEN

WELGELEGEN 756 KS

Interstitial fluorite

fusion
–hematite patches–
–Chlorite–

quartz veins (025°)

large biotite specks

poor exposure

020
080 2 shear directions

090

034

DIKGALOPENG VILLAGE

HARTEBEESTFONTEIN 20 JS

POTGIETERSHOOP 750 KS

Cultivated Land

N

LEGEND

- Nebo granite
- Typical fine–grained Klipkloof granite
- Porphyritic Klipkloof granite
- Albitised Klipkloof granite with tourmaline spheroids
- Coarse–grained Klipkloof granite
- Alluvium
- Dolerite
- Tar roads
- Dirt roads
- Observed lithological contacts
- Inferred lithological contacts
- Rivers/streams
- Fault
- 180/70 Strike & dip of joint/fracture planes
- 090/62 Strike & dip of shear/shear zone
- 045/22 Strike & dip of lithological contact

0 500 1000
METRES

FIGURE 27d

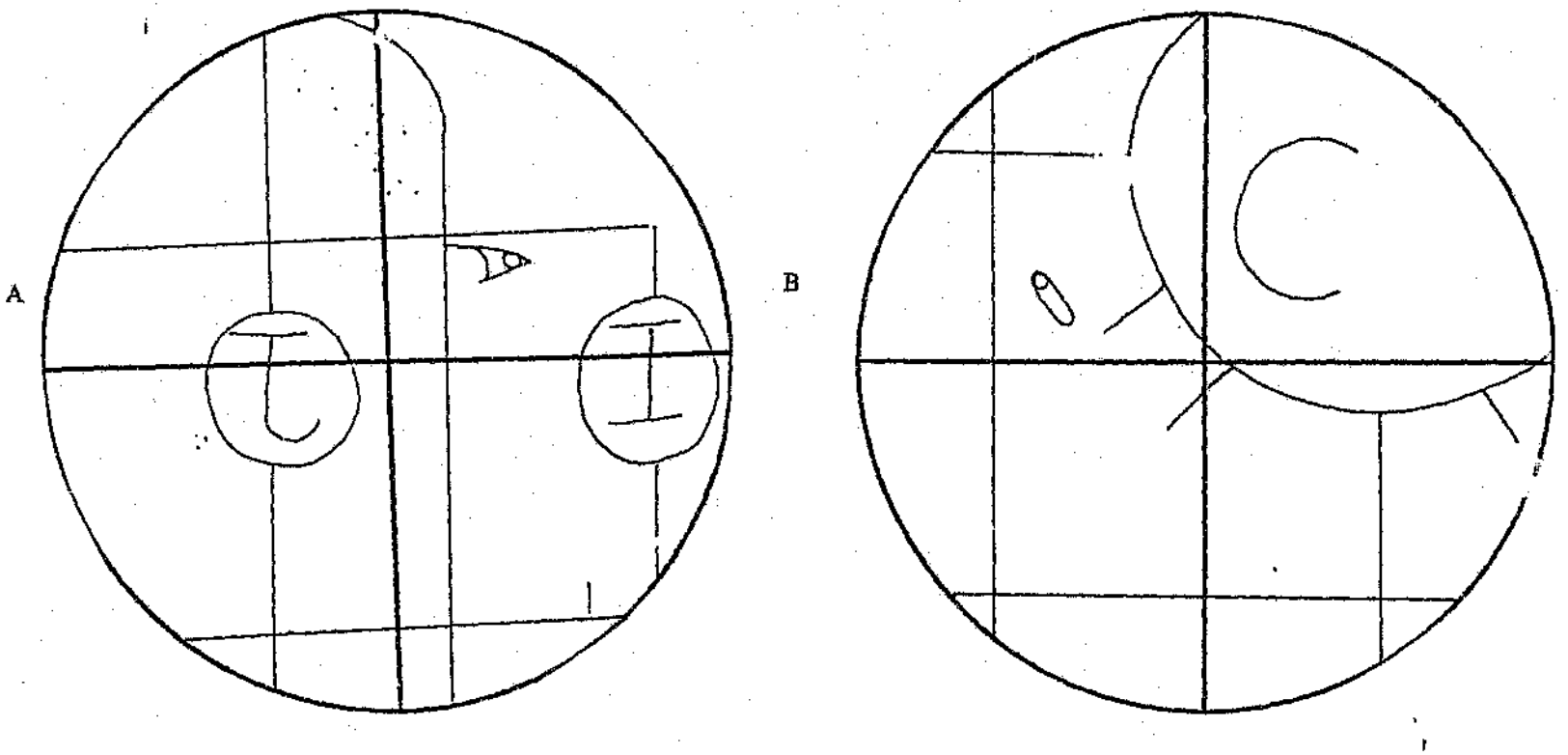


Figure 5.42 A) Synthetic NaCl fluid inclusion
B) Synthetic KCl fluid inclusion



DEPOSIT: Grass Valley
SAMPLE : GV02
Field 2

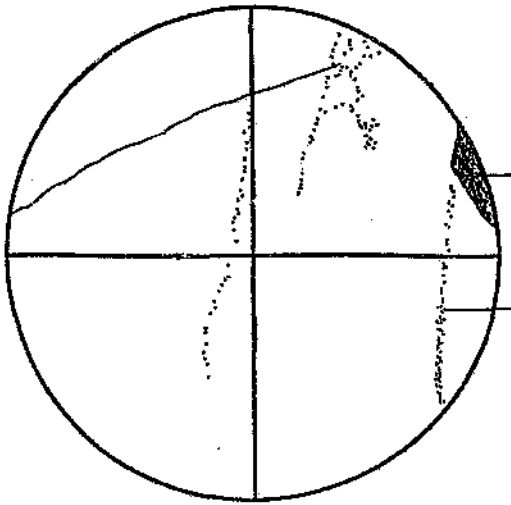
Cassiterite

Calcite

Quartz

Magnification: X40

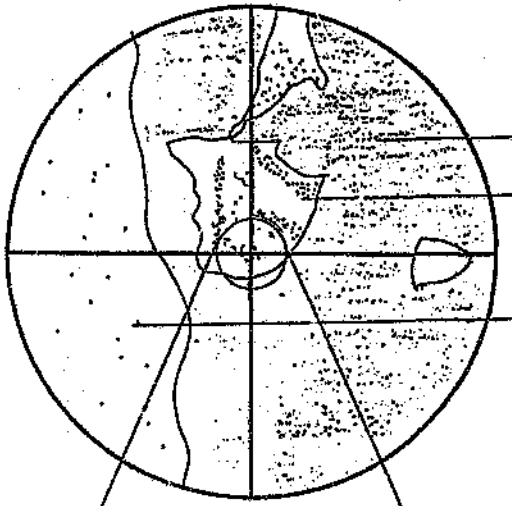
Field 3



Cassiterite

Secondary trails of fluid inclusions in quartz

Magnification: X40



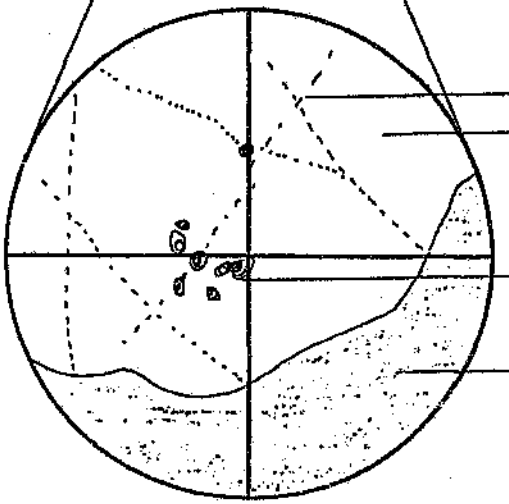
DEPOSIT: Grass Valley
SAMPLE : GV01
Field 3

F (perthite)

Fl. ..clusions in quartz

Chalcedony

Magnification: X 40



Secondary fluid inclusion trails

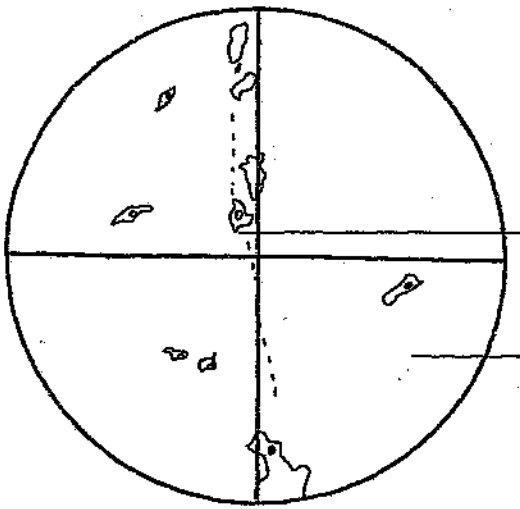
Quartz

CO_2-rich fluid inclusions

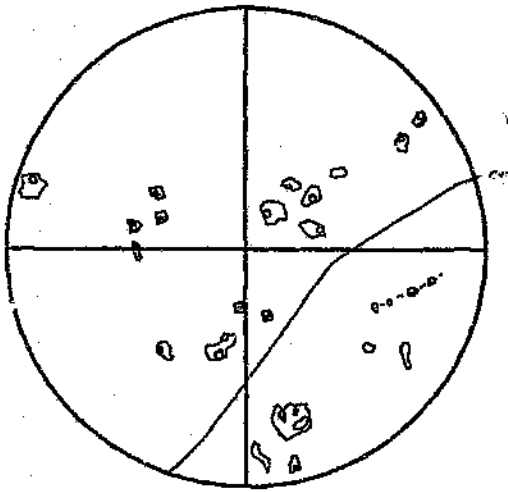
Perthite

Magnification: X 200

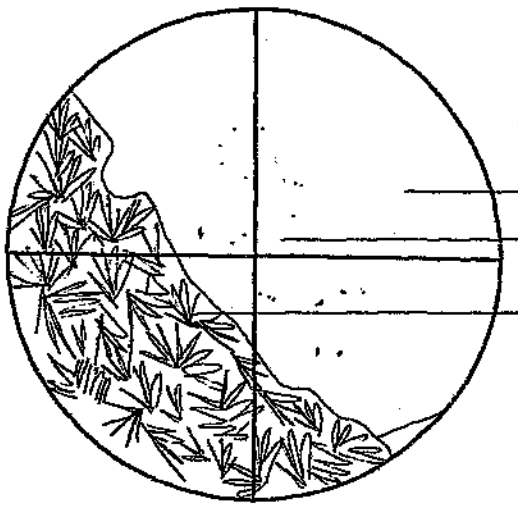
DEPOSIT: Grass Valley
SAMPLE : GV04
Field 1



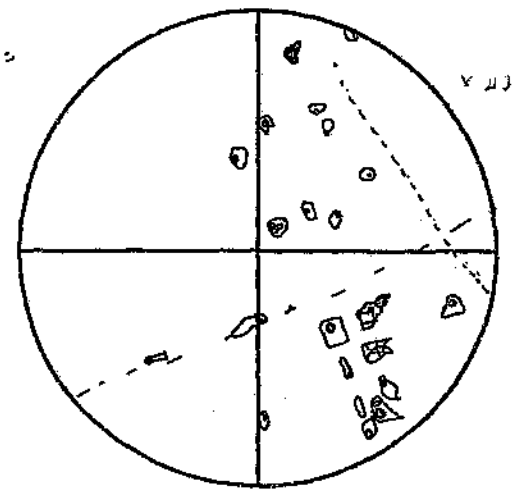
Magnification: X400



Field 2



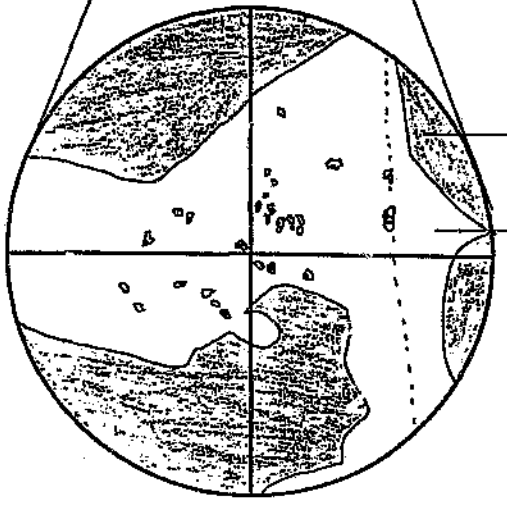
Magnification: X40



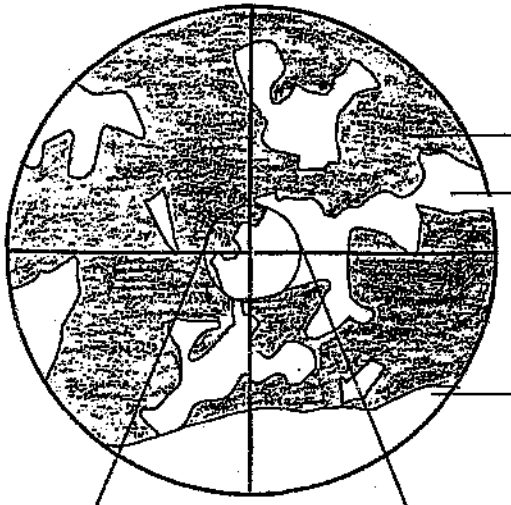


DEPOSIT: Grass Valley
SAMPLE : GV07
Field 1

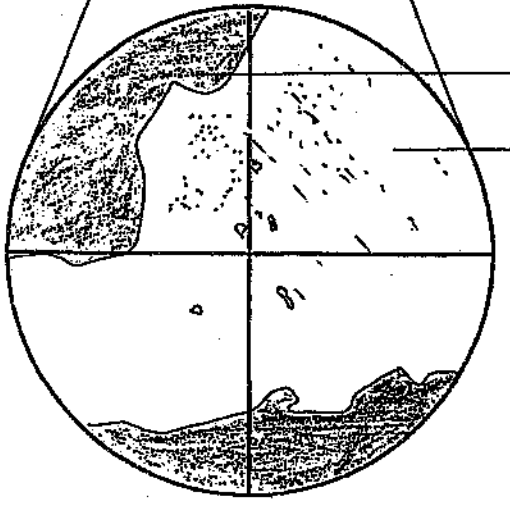
Magnification: X40



Magnification: X200



DEPOSIT: Grass Valley
SAMPLE : GV07
Field 2



Magnification: X200

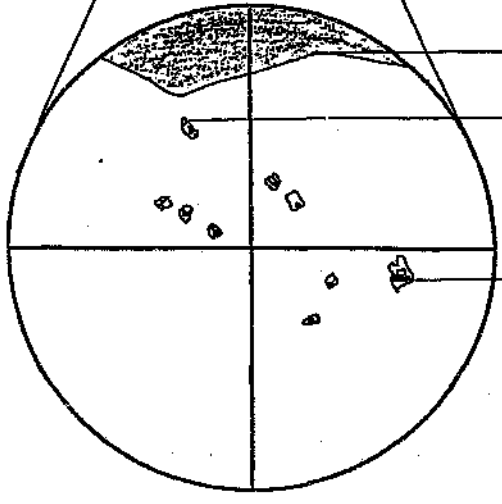


DEPOSIT: Grass Valley
SAMPLE : GV09
Field 3

Perthite

Growth zones in quartz

Magnification: X40

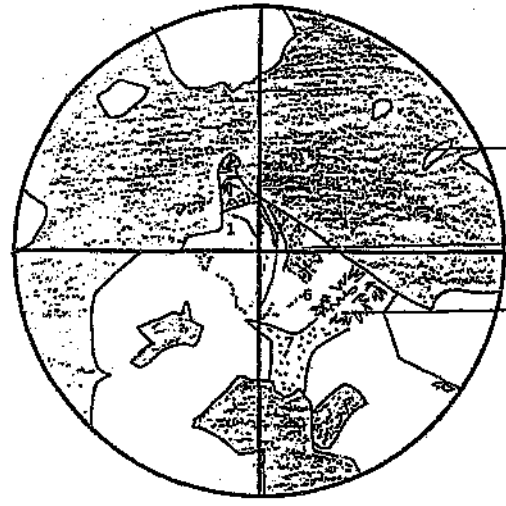


Perthite

Haematite crystal in fluid inclusion

Opaque solid in fluid inclusion

Magnification: X400



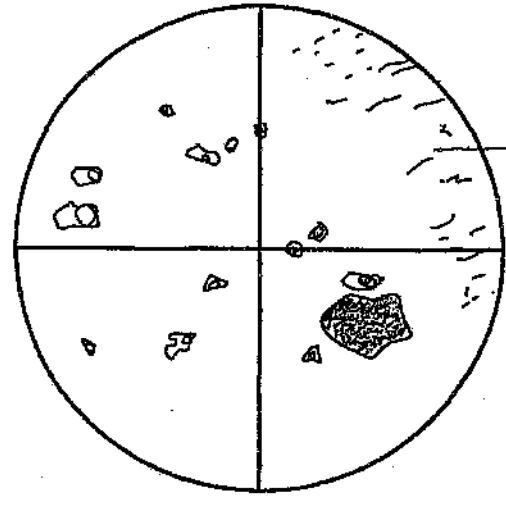
DEPOSIT: Grass Valley
SAMPLE : GV12
Field 1

Perthite

Multiple growth zones in quartz

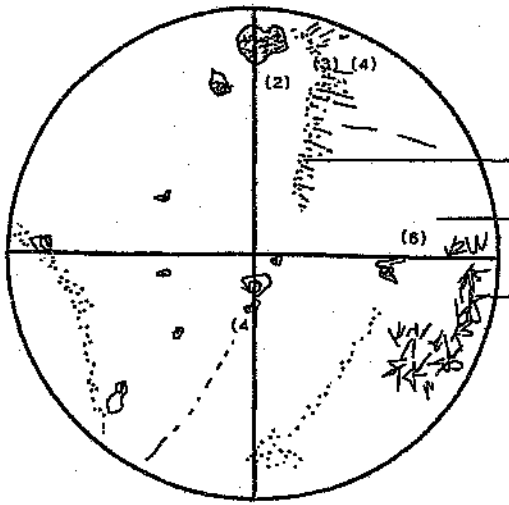
Muscovite

Magnification: X40



Growth zone in quartz outlined by fluid inclusions

Magnification: X400



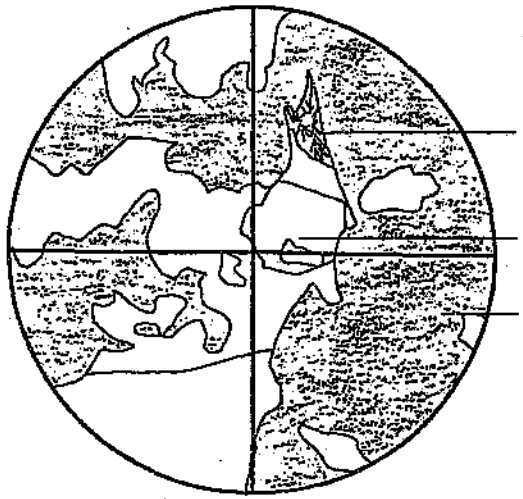
DEPOSIT: Grass Valley
SAMPLE : GV12
Field 1b

Growth zones in quartz (2 3, 4 & 6)

Quartz

Muscovite

Magnification: X200



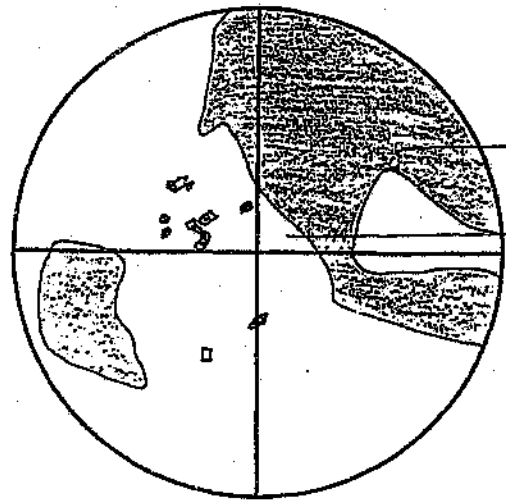
Field 2

Chlorite

Quartz

Perthite

Magnification: X40

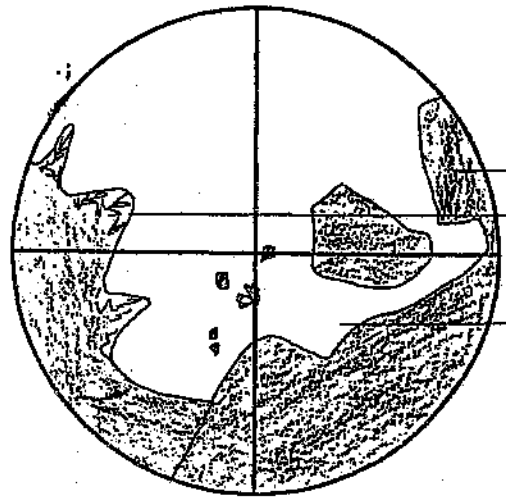


DEPOSIT: Grass Valley
SAMPLE : GV12
Field 2

Perthite

Quartz

Magnification: X200



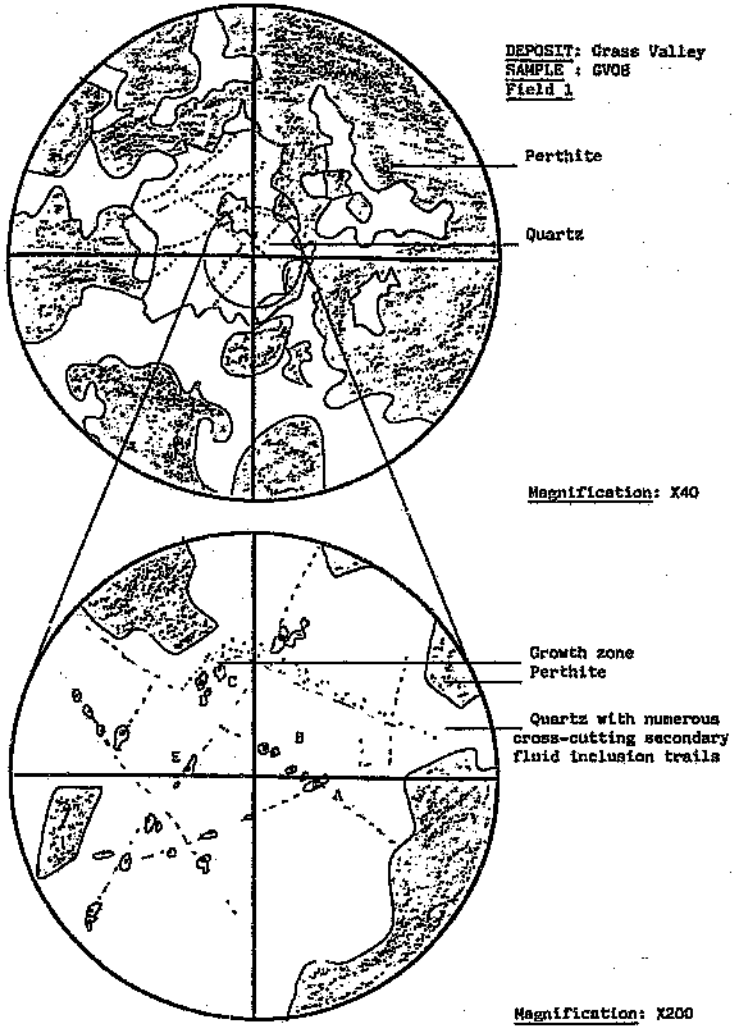
Field 3

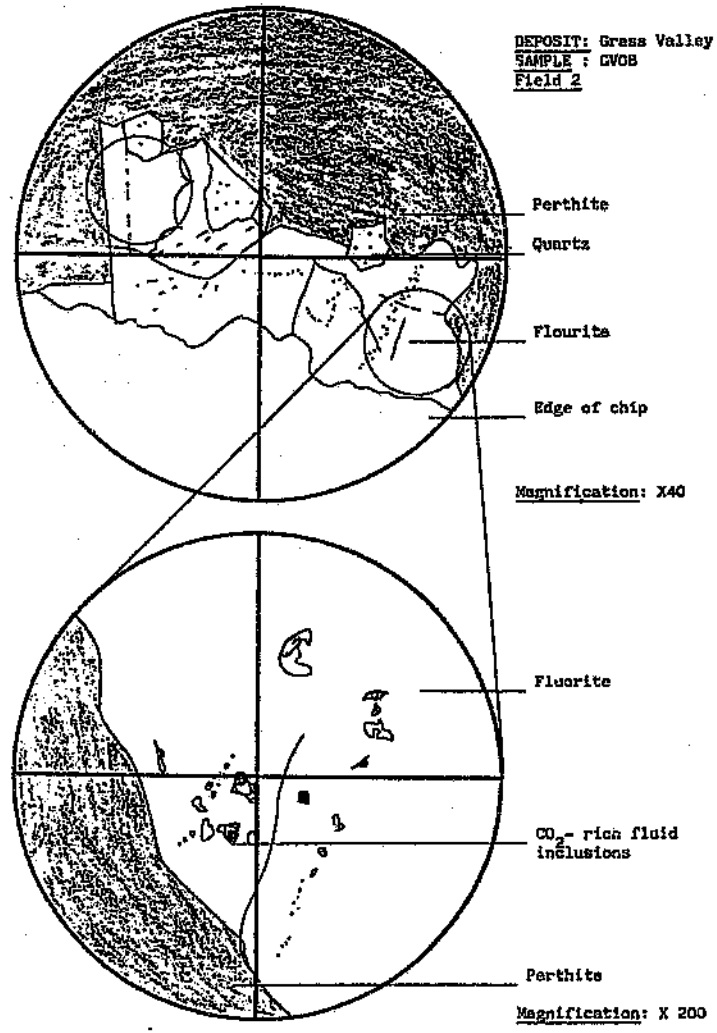
Perthite

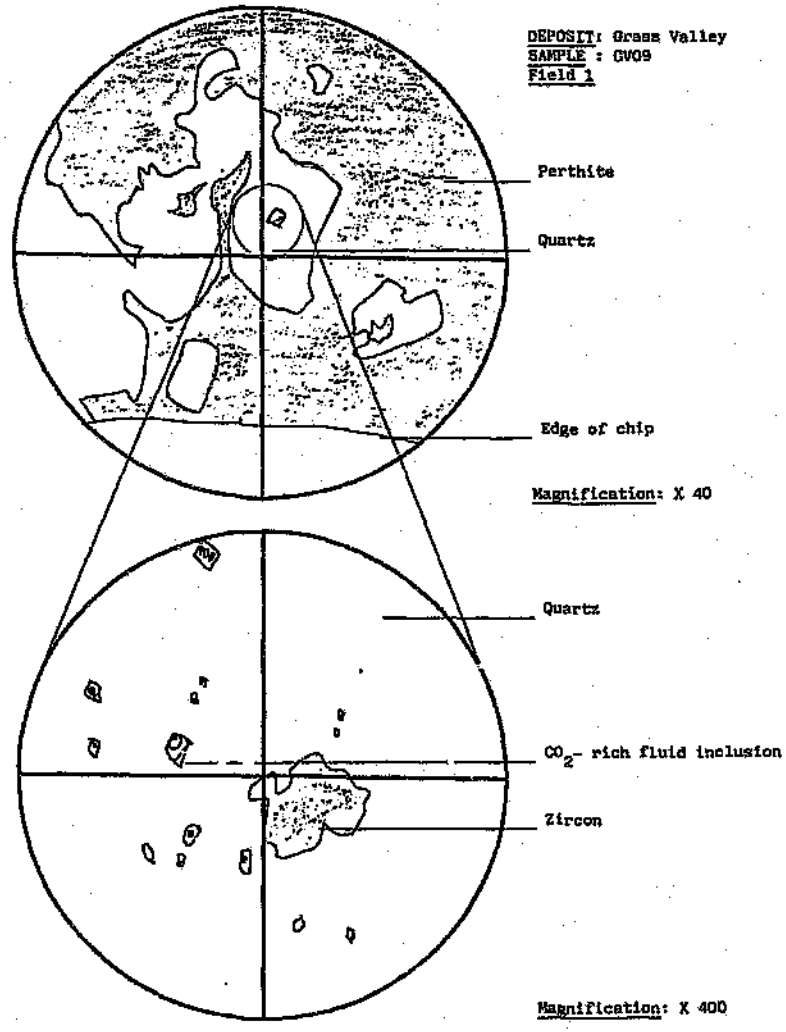
Chlorite

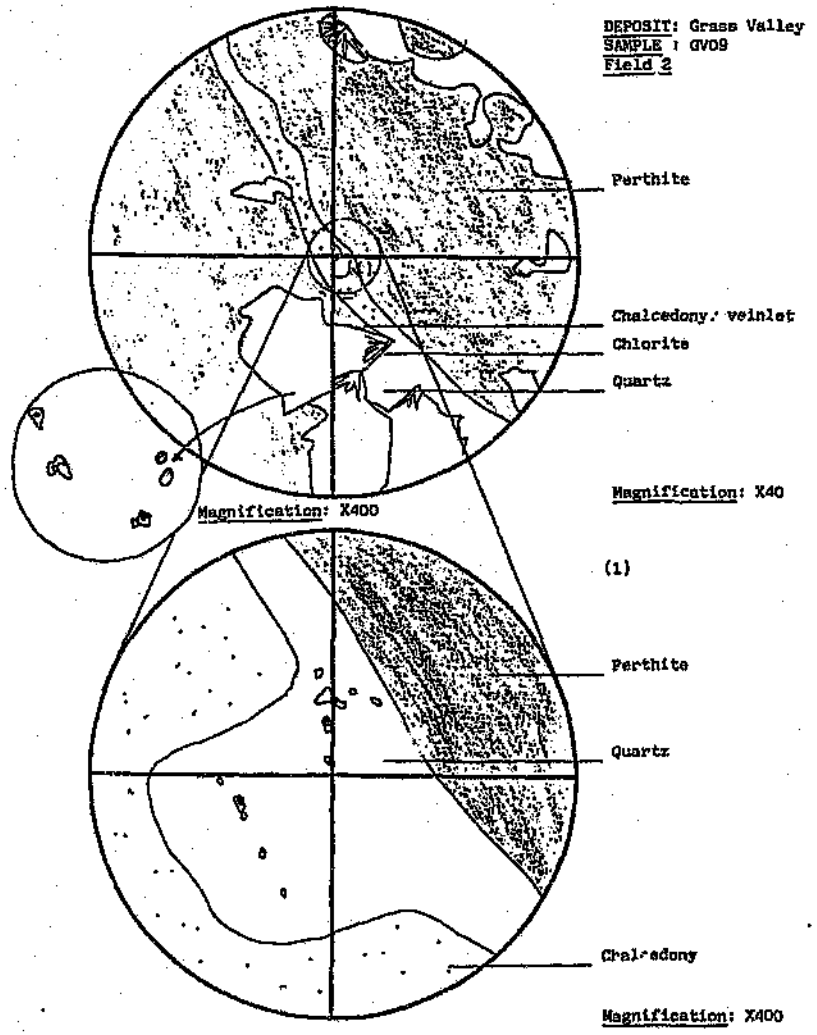
Quartz

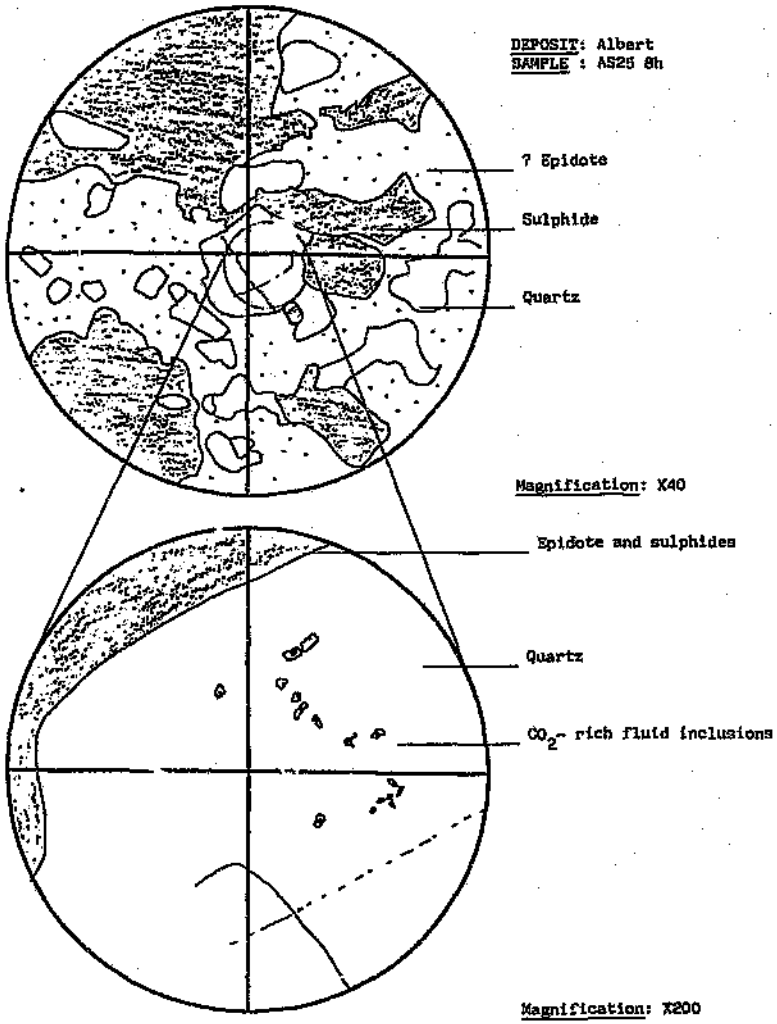
Magnification: X200

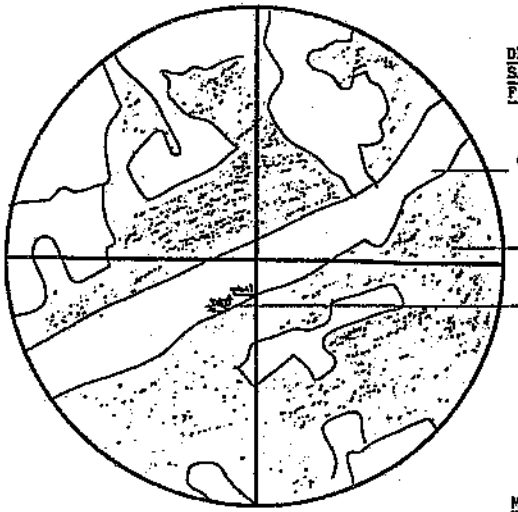

DEPOSIT: Grass Valley
SAMPLE : GV08
Field 1
Perthite
Quartz
Magnification: X40
Growth zone
Perthite
Quartz with numerous cross-cutting secondary fluid inclusion trails
Magnification: X200


DEPOSIT: Grass Valley
SAMPLE : GV08
Field 2
Perthite
Quartz
Flourite
Edge of chip
Magnification: X40
Fluorite
CO_2- rich fluid inclusions
Perthite
Magnification: X 200


DEPOSIT: Grass Valley
SAMPLE : GV09
Field 1
Perthite
Quartz
Edge of chip
Magnification: X 40
Quartz
CO_2- rich fluid inclusion
Zircon
Magnification: X 400

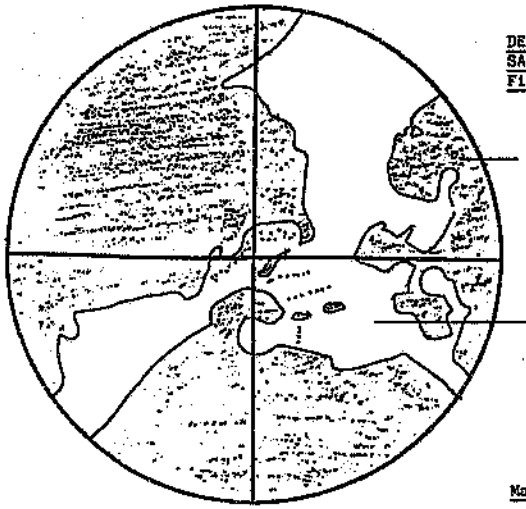

DEPOSIT: Grass Valley
SAMPLE : GV09
Field 2
Perthite
Chalcedony veinlet
Chlorite
Quartz
Magnification: X40
Magnification: X400
(1)
Perthite
Quartz
Chalcedony
Magnification: X400


DEPOSIT: Albert
SAMPLE : AS25 8h
? Epidote
Sulphide
Quartz
Magnification: X40
Epidote and sulphides
Quartz
CO_2- rich fluid inclusions
Magnification: X200



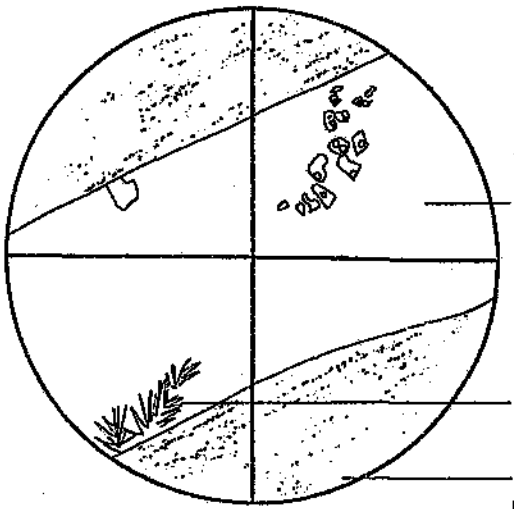
DEPOSIT: Spoedwel
SAMPLE : SP6
Field 1

Magnification: X40

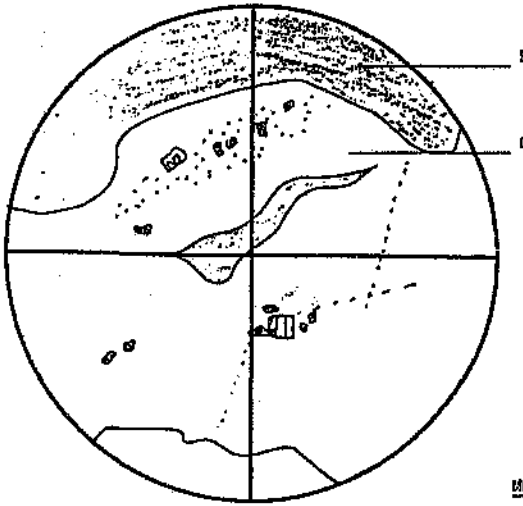


DEPOSIT: Spoedwel
SAMPLE : SP6
Field 2

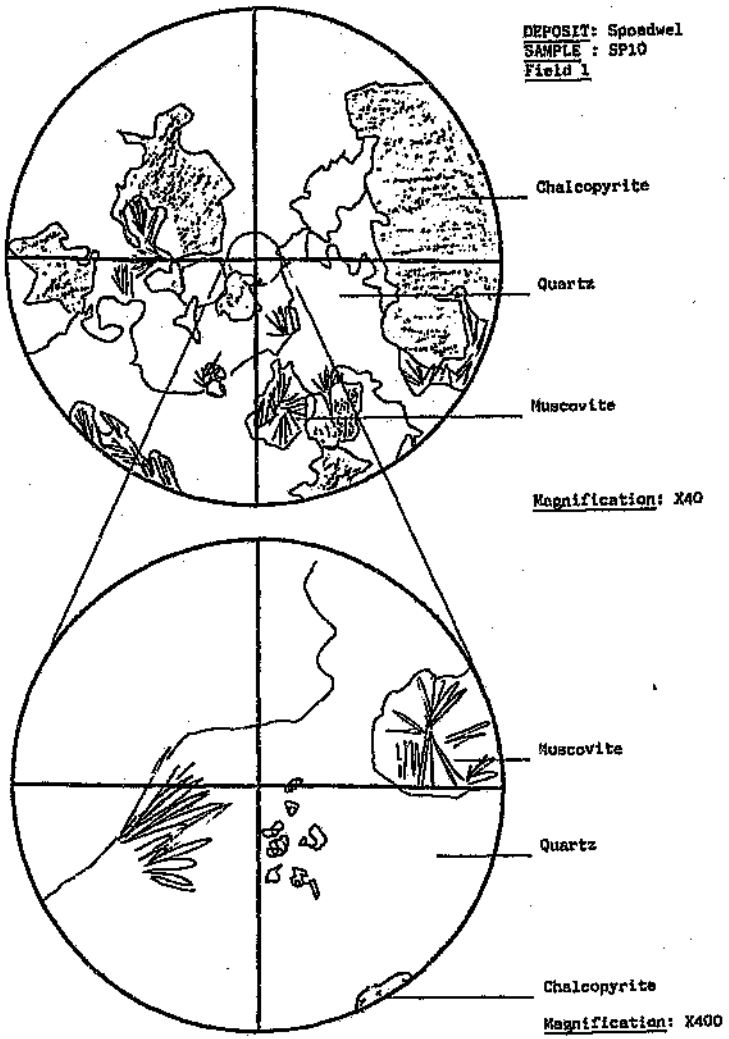
Magnification: X40

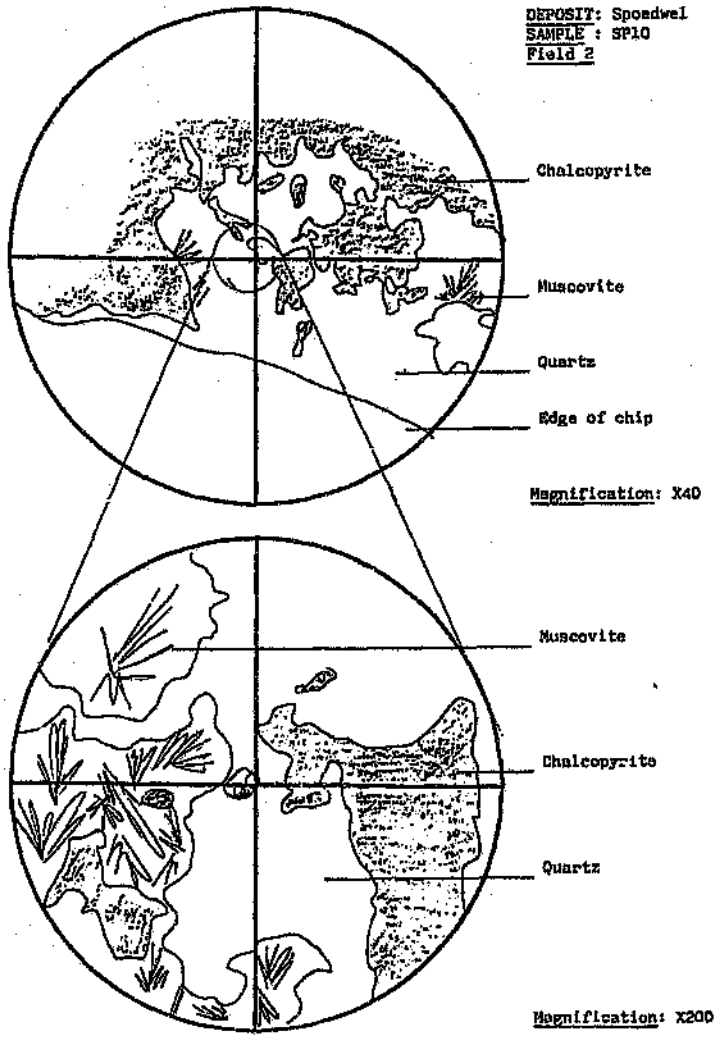


Magnification: X200



Magnification: X200

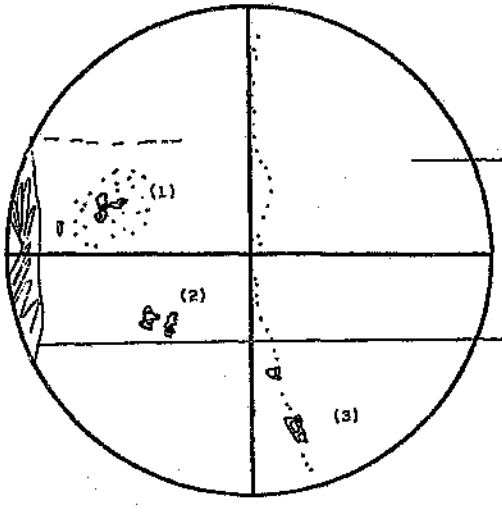

DEPOSIT: Spoadwel
SAMPLE : SP10
Field 1
Chalcopyrite
Quartz
Muscovite
Magnification: X40
Muscovite
Quartz
Chalcopyrite
Magnification: X400


DEPOSIT: Spoadwel
SAMPLE : SP10
Field 2
Chalcopyrite
Muscovite
Quartz
Edge of chip
Magnification: X40
Muscovite
Chalcopyrite
Quartz
Magnification: X200

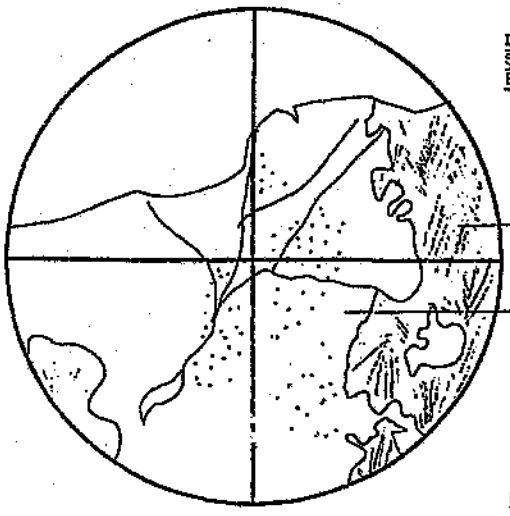


DEPOSIT: Spoedwal
SAMPLE : SP11
Field 1

Magnification: X40

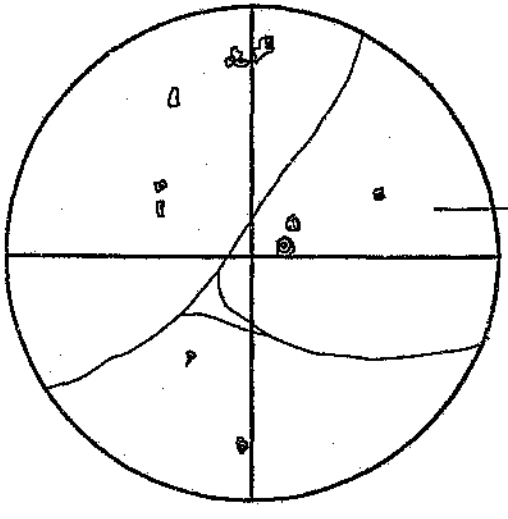


Magnification: X200



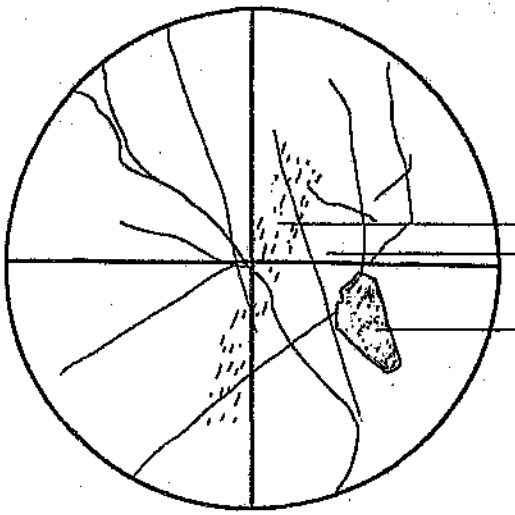
DEPOSIT: Spoedwal
SAMPLE : SP11
Field 2

Magnification: X40



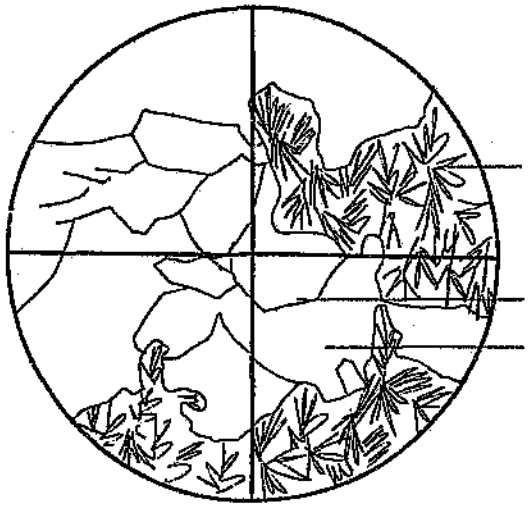
Magnification: X400

DEPOSIT: Spoedwel
SAMPLE : SP13
Field 1



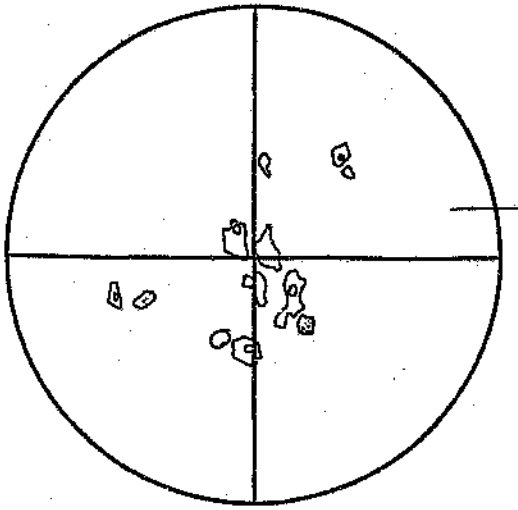
Magnification: X40

FIELD 2



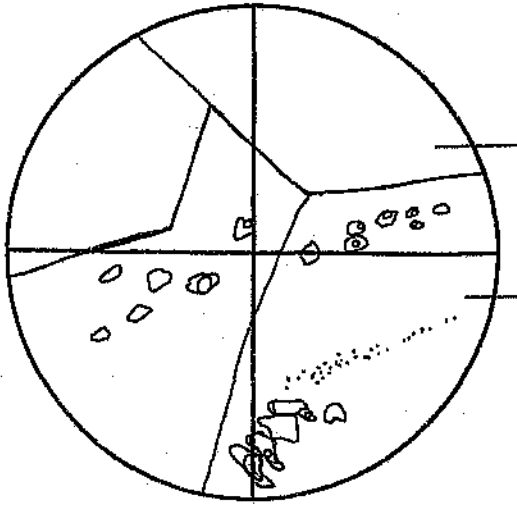
Magnification: X40

DEPOSIT: Spoedwel
SAMPLE: SP13
Field 2a

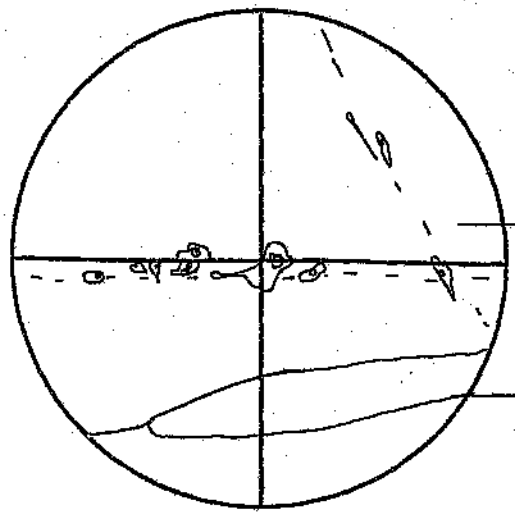


Magnification: X 400

Field 2b

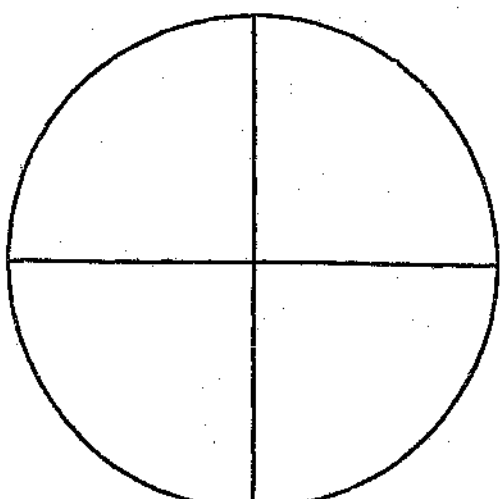


Magnification: X400



DEPOSIT: Spoedwel
SAMPLE : SP13
Field 3

Magnification: X200



SAMPLE NO.	INCLUSION	ORIGIN	Tfreeze	Te	Intermediate melting events			T final melting	Th	Th CO2	Tfinal melting CO2
GV01	TRAIL A	S	-38.5					-5.5			
FIELD 1	B	S						-4.7			
	TRAIL A	S	-47	-41				2			
	B	S	-47					-5.1			
	TRAIL (X20)	S	-42					2.1			
	A	S	-36					-1.5			
	B	S	-43					-1.5			
	CO2 TRAIL 1	S								27.7	-57.4
		S								28.3	-57.4
		S								22.5	-57.4
		S								23.1	-57.4
	CO2 TRAIL 2	S								22.8	-57.4
		S								26.8	-57.4
		S								27.8	-57.4
		S								27.7	-57.4
		S								26.5	-57.4
		S								23.1	-57.4
FIELD 2	CO2 TRAIL 3 A	S								24.9	-57.4
	B	S								27.4	-57.4
	CO2 TRAIL 3 A	S								27.3	-57.4
	D	S	-97.9							26.2	-57.4
	E	S								26.2	-57.4
	F	S								26.7	-57.4
	G	S								26.7	-57.4
	CO2 TRAIL 4 H	S								26.2	-57.4
FIELD 3	CO2 TRAIL 1	S	-96.4							25.9	-57.8
	2	S	-98.9							25.3	-57.8
	3	S								25.3	-57.8
	4	S								24.7	-57.8
	5	S								25.4	-57.8
	6	S		-53	-48	-35	-10.1			25.2	-57.8
	TRAIL A	S						16.1			-57.8
	B	S						16.1			
	M		-96.4							26.1	-57.6
	C							-1			

SAMPLE NO.	INCLUSION	ORIGIN	Tfreeze	Te	Intermediate melting events			T final melting	Th	Th CO2	Tfinal melting CO2
	D							0			
GV02	A		-80.2	-48	-38	-22.3			141		
FIELD 1	B		-71								
	C		-71								
	D		-71								
	E		-71								
	F		-71								
	G		-59.5						152		
	H		-54					-16.9	149		
	I		-54					-16.9	160		
	A	S	-7[illegible]	-46	-36	-23.9		-7.7			
	B	S	-40.6					-15.1			
	C	S	-74					-7			
	E	S	-48					-14.9			
CHIP 2	TRAIL A	S	-66	-50	-39	-23		-14	133		
	B	S	-64					-14	134		
	C	S	-64					-14			
	TRAIL D	S	-80	-52	-31	-22.5		-6.8			
	ZONE 1 A	P	-35					-4.2	143		
	C	P	-49	-44	-19				167		
	D	P	-36					-4	143		
	E	P	-45					-2.4	134		
	ZONE 2 (X50)	P	-46	-43				-0.4	194		
	CO2 TRAIL A	S	-98							29.9	-57.4
	(X20)B	S	-92							29.9	-57.4
	D	S								29.9	-57.4
	E		-96					7.5	>205		
QUARTZ 3											
	A	P								29.9	-57.4
	B	P		-50	-37	-27	-24				
	C	P		-50	-37	-27	-24	-9.5			
	D	P								29.2	
	ZONE (X100)	P	-34					-0.7			

SAMPLE NO.	INCLUSION	ORIGIN	Tfreeze	Te	Intermediate melting events			T final melting	Th	Th CO2	Tfinal melting CO2
	ZONE 1A	P						-4			
	B	P							233		
	E	P						-5.5			
	F	P						-6.7	214		
	G	P						-0.5	217		
	D	P						0.4			
GV04	A	S	-35.2	-33	-23			-1.5	108		
FIELD 1	B	S	-35.2	-33	-23			-2.1	127		
	C	S	-35.2	-33	-23			-2.1	127		
	A	S	-38.7	-33	-23			-1	99		
	B	S	-35.7	-33	-23			-1			
	D	S		-33	-23			0.6			
	X	S	-39.9	-33	-23			-1.7	99		
	B	S	-40	-33	-23			-2.8	128		
	C	S	-39	-33	-23			-1.5	83		
GV05	CO2 TRAIL (X15)	S	-96							27.1	-57.4
FIELD 2	CO2 TRAIL (X15)	S	-96							25.4	-57.4
FLUORITE	A	S	-96					10.1		24.9	-57.4
	C	S	-55	-45	-36			-8.9			
	D	S	-52	-45	-36						
	E	S	-49	-45	-36			-4.3			
	X	S	-44	-33	-22			-14.9			
FIELD 1	CO2 TRAIL A	S	-96					7.3		30	-57.1
QUARTZ	CO2 TRAIL B	S	-95							28.4	
	C	P	-42		-38			-17			
	D	P	-42			-24		-5			
	E	P						-4			
	ZONE (X100)	P	-40	-37				-17			
VEIN QUARTZ											
FIELD 1	D	P	-49	-27				-7.9	101		
QUARTZ 4	E	P	-46						101		
	F	P	-52					-6.8	101		

SAMPLE NO.	INCLUSION	ORIGIN	Tfreeze	Te	Intermediate melting events			T final melting	Th	Th CO2	Tfinal melting CO2
	A		-46					-8.7	101		
	B		-45					-8.6	101		
	C							-7.3	101		
FIELD 2											
QUARTZ 6,7 & 8	A		-95.3							29.8	-57
	C									30	-57
CHIP 3											
QUARTZ 7	A	P								27.4	
	B	P	-44	-39				-7			
	C	P						-7	148		
	D	P						-7			
	E	P						-1.5	195		
	F	P						-6.5			
GV06											
FIELD 2 (1)	CO2 TRAIL A	S								29.3	
	B	S								28.3	
	C	S								28.9	
	D	S	-95.9					8.4	>200	28.4	-57.4
FIELD 2 (2)	ZONE (X30)	P	-45	-35.6				-22.9	175		
		P						-19.7			
	(X8)	P	-52.9	-39	-33			-15.3	113		
GV10	A	-53	-49	-42	22			-17	157		
	C									25.3	
	D							-18			
	E	-55								180	
	F							-1.1			
	1,2,3	P		-34.6	-30	-25		13.3			

SAMPLE NO.	INCLUSION	ORIGIN	Tfreeze	Te	INTERMEDIATE MELTING EVE			Tfinal melting	Th	ThCO2
SP3	1	P	-46		-36			0.8	n/a	
fluorite	2	P	-46		-36			-12	n/a	
	3	P	-46		-36			-4.6	187	
	4	P	-46		-36			?	180	
	X		-52		-37	-23	-15	-13.7	?	
	Y		-59		-33	-16		-12	190	
	A			-46					205	
	B	P		-42					259	
SP3(.)	X11	S	-42					-0.5	114	
fluorite								-0.5	270	
								-0.5	237	
								-0.5	243	
								-0.5	255	
SP3	X10	S	-55	-44	-37	-30	-15.9	-8.6	123	
			-59	-44	-37	-30	-15.9	-9.5	124	
			-48	-44	-37	-30	-15.9	-8.7	128	
SP3	X6	S	-40	-37				-0.6	n/a	
SP3	A (X250)	?	-61.5	-42				-13.2	128	
	B		-61.5	-42				-13	127	
	C		-61.5	-42				-13.1	128	
			[-65;-54]	-42				-13.2	[137;150]	
SP3	X100	P	-49	-40	-23.8	-19	-6.9	-4.3	150	
SP3	6							-4.7		
	5							-1.2		
	2							-0.4		
	B							-3.8		
	N		-42					-2.9		
			-70.1	-47	-43	-20			146	
SP3	X200	?	-43		-20			-1.2	129	
SP3								-0.2	220	
	A	P	-37	-40				-3.1	[189;205]	
	B	P	-49	-40				-4.6	[189;205]	
	C	P	-49	-40				-13.2	[189;205]	
	D	P	?					-3	?	
	C	P	-51					-4.5	147	
	D	P	-51					?	230	

SAMPLE NO.	INCLUSION	ORIGIN	Tfreeze	Te	INTERMEDIATE MELTING EVE			Tfinal melting	Th	ThCO2
SP3	1		-45	-36				-8.4		
	2		-38		-23			-4.3		
	3		-43		-23			-4.3		
SP3	X50	S	-49	-35				[-3.9;-2.5]	[174;220]	
SP2(1)		P	-69	-43.5				-27	167.5	
	1 TO 8	P	-67	-35				-23	184	
SP2(1)	1,2,3	P	-59					-34	22.8	
SP2(1)	3		-57	-44						
SP2(1)	4		-56.3	-50				-27		
SP2(1)	A	P							147	
	B	P		-45	-32.9			[-19;-23]	191	
	C	P	-57	-47	-32.9			[-19;-23]		
	D	P	-51.9	-45	-32.9	-28		[-19;-23]		
	E	P	-57	-47				-19.9	216	
SP2(1)		P	-83	-40				-11.9		
		P	-57	-40				-22.7		
		P	-53	-42				-26	143	
		PS	-65	-47				-23	161	
		PS	-63	-47				-23	156	
		PS	-70	-47				-23		
SP2(4)	A	P	-72	-53	-44	-35		0.1	164	
	B	P	-46			-22		-10.2	240	
	C	P	-51			-22		-6.2	175	
	D	P	-72			-44			125	
	E	P	-89	-67		-49	-38	?-38	164	
	A	S	-44	-53		-35	-6.9	-6.9	106	
	B	S	-44					0		
	1	P	-72.8					-10.1		
	2	P	-74.4							
SP1	A	P		-52	-47	-31.7		3	161	
	B	P	-83	-58				-34	155	
	C	P	-77					-31	155	
	1	S	-83	-54				1	173	
	4	S	-77						159	
	5	P	-81	-52				-30	149	

SAMPLE NO.	INCLUSION	ORIGIN	Tfreeze	Te	INTERMEDIATE MELTING EVE	Tfinal melting	Th	ThCO2
	6	P				-28	173	
SP2(3)			-42	>-48		-7.4		
QZ						0		
			-42			0		
			-39			3		
			-39			10		
			-42.4			-9		
			-42.4			-4.1		
			-64	>-36		-4.1		
	X6		-64			-7.2		
SP2(3)	1	P	-48	-39		0		
	2	P	-48	-39		0		
	3	P	-46	-49		0		
	4	P	-29			-2		
	5	P				-4		
	X100	S				[0;3]		
	X6	S	-68			-38	93	
	E	S	-39			1.7	111.5	
	F	S	-37.7			1.8	139	
L1	1,2,3	S	?	?				
	1	P	?					
	2	P	?	-39		0.3		
	3	P		?		0.3		
	4,5	P	-40					
	1	?P	-71			0.3		
	2	?P	-71			5		
	3	?P	-71					
	4	?P	-71	-50		-14.4		
SP7 (il)	1	P	-40	<-28		-5	225	
	2	P	-40	<-28		-5	206	
	3	P	-40	<-28		-5	206	
	4	P	-40	<-28		-5	190	
	5	P	-40	<-28		-5		
	A	PS	-52	<-23		0	288	
	C	PS	-52	<-23			272	

SAMPLE NO.	INCLUSION	ORIGIN	Tfreeze	Te	INTERMEDIATE MELTING EVE			Tfinal melting	Th	ThCO2
SP7 (I)	b	P	-52					-5.1	228	
	x									
	1		-52							
	2			-34						
	3			-34						
	4			-34				-7.9	173	
	5								190	
	7							-9.8	228	
SP7 (2)	A		-85							
	B		-85	-52.2						
	C		-85	-52.2						
	D		-85							
	A	S	-39					-3.6	86	
	B	S	-49					-3.6	197	
	X								125	
	Y								219	
	Z	P							174	
L1	1	P	-44		-30					
	2,3	P	-44		-23			-5.5	216	
	4	P	-44					-10.4	200	
	1		-51	-35				-4.9	200	
	2							-5.6	219	
	1			-30.1	-20			-5.6	219	
	2							-4.1	216	
	3	P	-54	-35	-21			-6.5	162	
	4	P	-49	-35	-29	-9.1		-6.5	148	
	5	PS							182	
	6	PS							182	
	7	PS							182	
SP7(I)	A	S		-44	-21			-9.9		
	1	S	-47	-44	-31			-10.2		
	2	S		-52				-0.9		

SAMPLE NO.	INCLUSION	ORIGIN	Tfreeze	Te	INTERMEDIATE MELTING EVE			Tfinal melting	Th	ThCO2
SP2	N		-57	-39	-33			-13.8		
	A	P	-79		-33				170	
	B	P	-79	-39				-0.8		
	C	P	-79		-29			-0.8		
	D	P	-65					-33	178	
	X		-31	-24				-22	378.5	
	Y		-87					-31	255.8	
	N		-63						310	
	Z		-76						240	
	1		-76					0		
	2		-76							
L1	A	P	-35	-29	-17.8			0.2	193	
	B	P	-35	-29				0.2	193	
	1		-35	-29				0.3	<205	
	2		-35	-29				0.3	<205	
	3		-35	-29				0.3	187	
	A		-42	-22	-29.4			0.3	179	
	X		-32					0.3	160	
	D		-32	-17				0.3		
	1	P	-43					0.3	174	
	2	P	-43					-4.9	194	
	3	S	-43					-4.9	189.6	
	1								213	
	2		-42.4					0.3	191	
	1	P	-50	<-29				0.3	214	
	2	P	-50	<-29				-5	244	
	3								203	
	4								220	
SP2	4		-76	-39	-31	-10		5.7		
	1	P	-87	-45	-35	-30		5.6	126	
	A	P	-65	-30.3				-14.1	220	
	B	P	-65	-30.3				-15.8	220	
	C	P	-74	-38	-28	-22		-9	217	
	A	S	-71		-24	-18		-18		
	B	P	-58		-23.4				232	
	C	P	-65		-29.7	-22.1		-12.8	222	

SAMPLE NO.	INCLUSION	ORIGIN	Tfreeze	Te	INTERMEDIATE MELTING EVE			Tfinal melting	Th	ThCO2
SP2	1,2,3	S	-64	-30.3	-24	-9				
	A		-67	-45	-38	-29		9.4		
	B		-59	-38.8	-28	-23		7.6		
	C		-63	-36	-24	-21.5		10.2		
	A		-57	-39	-33	-23.3				
	N			-27	-16.6			-13.8		
	A		-65	-39	-33	-23.9				
	B		-65	-39		-23.9		-0.8		
	C		-65	-39	-29	-23.9		-0.8		
SP3	A	P	-56.7	-39	-28	-11		-4.5		
	B	P	-56.7	-39	-28	-24		-9.3		
	C	P	-56	-39				-9.9		
	1	P	-56	-39				-8.7		
	2	P	-56	-39				-8.4		
	3	P	-59	-39				-8.4		
	A	P	-52	-30	-21	-12.2		-7.3	152	
	B	P	-52	-34	-21			-7.8	163	
	C	P	-52	-34	-21			-5.8		
	D	P	-52	-34	-21			-2.2		
	E	P	-52	-34	-21			-2.8		
	X	S	-70	-53	-43	-33		-16	149	
	A	S	-64	-53	-43	-33		-16	123	
	B	S	-67	-53	-43	-33		-16.2	136	
	C	P	-48	-41		-30.3		-1	149.8	
	D	P	-48	-41	-30.5	-13		-1	136	
	E	P			-30.5	-13		-1	158	
	F	P						-1	168	
	Y	P							409	
SP3 (lli)	1 (X32)	P	-53	-40				-10		
	2	P	-48	-38				-9	97	
	3	P	-87	-43						
	A		-46	-21				-9.2	158	
	B		-42					0.1		
	C		-42					0.1		
	5	S	-59	-30	-21			-10		

SAMPLE NO.	INCLUSION	ORIGIN	Tfreeze	Te	INTERMEDIATE MELTING EVENTS			Tfinal melting	Th	ThCO2
GC600	A	S	-67	-51	-35	-24		-3.7	165	
CHIP 1	B	S		-48	-35	-24		1.7	200.9	
	D	S	-68	-50	-37				165	
	E	S	-64						165	
	X	P	-38	-29				-1.2	200	
CHIP 2	A	P	-45	-36	-12.8			-2.7	186	
	B,C,D	P							176	
	E	P	-67	-47	-28			9	163.8	
CHIP 3	1								164	
	2								163.2	
	A		-40					-3.9		
	B		-40					-3.9		
	N								162	
	A		-59					?-40		
	B		-59					?-41		
	A		-48	-34	-24			-22.2		
	B,C		-48	-34	-24			-22.2		
CHIP 2C	C		-71	59				-37.9		
	A		-71	-59	-27	-16	-3	4.3		
	D		-71	-59						
	B		-71	-59				-38		
	1,2,3		-69	-50				-26		
	A,B,		-69	-50				-24.2		
	B		-83	-51	-35	-5.9		3	142	
	A		-65	-51	-35	-25	-7.6	2.2	142	

SAMPLE NO.	INCLUSION	ORIGIN	Tfreeze	Te	INTERMEDIATE MELTING EVENTS			Tfinal melting	Th	ThCO2
CHIP 2D	1,2,3	S	-59					-29	155	
	X,Y,Z	S						-37.9	128	
	1,2	S						5		
	Z	S						-33.3		
	A	P	-72	-54	-24.6			6	126	
	B	P	-72	-54	-24.6			0.1	126	
	C	P	-72	-54	-24.6			-12.3	127	
	C	P	-72	-54	-24.6					
	D,E	P	-72	-54	-24.6					
	1,2,3,4	S	-78	-54	-33			-25.9	123	
	5	S	-63.4	-50				8	142	
	A	S	-78	-50.9	-26.8			-26.8	165	
	B	S							165	
	1	P							235	
	2	P			-33	-1.1		-1.1	276	
	3	P							75	
	4	P						-1	231	
	A,B,C	P		-45	-30	-20.8			164	
GC40c	N,A,B	S						?-46	98	
	C,X	S		-52				-42	98	
	M	S	-88					-42	125	
	X	S						-42		
	A	S	-59.5	-43	-35	-22	-12.3	-5.3	<100	
	TRAIL (X250)	S	-54					-3.3	<101	
	1,2	S	-54					-4.7	<102	
	C	S	-54					-8	<103	
	4	S	-54					-2.2	<104	
	A,B	P	-71	-53				?		
	C	P	-71	-53				?		
	D	P	-71	-53				?		
	E	P	-71	-53				?		
	F	P	-71	-53				-42		
	G	P	-71	-53				-34	116	
	H	P	-71	-53					135	
	I	P	-71	-53					140	

SAMPLE NO.	INCLUSION	ORIGIN	Tfreeze	Te	INTERMEDIATE MELTING EVENTS			Tfinal melting	Th	ThCO2
ZNS	ZONE 1	P	-47	-39.1	-27			-12	188	
SPHALERITE	ZONE 2	P	-50	-32				-10	200-215	
SAMPLE NO.	INCLUSION	ORIGIN	Tfreeze	Te	INTERMEDIATE MELTING EVENTS			Tfinal melting	Th	ThCO2
HBQ	A	P	-52	-31	-22			-10.4	206.1	
QUARTZ	B	P	-33	-21	-6.4			0.1	201.6	
	X	P							172	
	A	P	-62	-43	-38			-2.4	212	
	B	P	-33	-37	-34			-1.6	198	
	C	P	-33	-37					208	
	D	P	-33	-37	-34			-1.6	212	
	E	P	-33	-37	-34			-21	212	
	F	P	-33	-43	-34			-7.9	204	
HBQ (2)	1			-30				2.2		
	2			-30				-20.5	132	
	3			-30				-20.5		
	4			-30				-22		
	5			-30				-21		
	6			-30				-7.8		
	X			-30				-11	207	
	1							0.1	97.5	
	2								218	
	3								149	
	4							-15	137	
	5		-46	-35				-21.5	137	
	7		-46	-35				0.1	218	
	A		-48	-46				-3.7	244	
	B		-48	-29				-22.4		
	C,D		-48						248	
	1		-62					-16.9		
	2		-62					-15.1	195	
	3		-62	-45					243	
	4		-69	-40				-21.6		
	5		-69					-20.6		

SAMPLE NO.	INCLUSION	ORIGIN	Tfreeze	Te	INTERMEDIATE MELTING EVENTS			Tfinal melting	Th	ThCO2
HB1 (4)	TRAIL (X25)	S							221-225	
	TRAIL (X25)	S							246.5	
	A	S							233	
	TRAIL (X100)	S						-8.1	205	
	B	S						-7	212	
	TRAIL (X5)	S						-7.9	227	
	A	S		-48	-24.5			-1.9	231.1	
	B	S	-73					-19.1	151	
	C	S	-73					-19.1	151	
	X (X 2)	S						-0.4	207	
	TRAIL (X200)	S	-56	-43	-31	-20		-6.4		
	A	S	-46					-2.1	208	
	B	S	-52					-7.9	191	
	C	S	-52					-5.5	154	
	D,E	S						-8.2	204	
	TRAIL(X50)	S						-8	224	
HB1 (5)	TRAIL (X4)	S							168	
	TRAIL (X3)	S							214	
	A	S							184	
	TRAIL (X50)	S							210	
	A	S							236	
	B	S							183	
	C	S							183	
	D,E	S							231	
	TRAIL (X20)	S							203-216	
	TRAIL (X10)	S							215	
	TRAIL (X25)	S							165	
	A							-1.6	186	
	B							0	165	
	C							-1.5	165	
	D							-0.5	189	
	E							-0.4	197	
	F							0.4		

SAMPLE NO.	INCLUSION	ORIGIN	Tfreeze	Te	INTERMEDIATE MELTING EVENTS			Tfinal melting	Th	ThCO2
HB1	6	S		-42	-33	-19		-1.8		
	8	S		-30				-1.7		
	1	P	-59	-48	-20	-8.5		0.9		27
	A	P	-69	-41	-33	-15		0.1		
	B	P						-6.4		
	C	P								
	D	P						-12		
	E	P						-7.2		
	1	S			-16	-10.2		0.1	193	
	2	S	-57					0.7		
	3	S	-57						171	
	A	S						0.7	209	
	B	S						0.4		
	C	S						0.5	203	
HB1 (II)	X				-11	-1.2		0.6		
	A				-19	-8.1	-1.1	1.6	221	
	B				-12	-4.8	-1.8		197	
	C							-1.1		
	D							-15.6		
	X	PS	-70	-53.9	-49	-37	-21.7			
HB1 (3)	1			-47	-34.6	-19.8		0.6		
	2		-61					-12.5		
	3		-62					-4.6		
	1		-40					0		
	2		-38					0		
	3		-30.6					0.1		
	A		-79	-51				-39		
	B		-83	-51	-45			-39		
	1							-7.9		
	2							-7.9		

SAMPLE NO.	INCLUSION	ORIGIN	Tfreeze	Te	INTERMEDIATE MELTING EVENTS			Tfinal melting	Th	
HB1	1	P	-110		-29.6	-23		-15		
	2	P	-65		-39	-26.4	-10.5	-4	175	
	3	P	-65	-48	-33	-26.1		-28.8		
	4	P	-65	-48		-24				
	1	S	-90	-45	-26			-15		
	2	S		-45	-36	-26	-21	-19.4		
	3	S		-45						
	4	S		-45	-26	-21				
	5(x3)		-93	-45	-21	-8		-4.2	175	
HB1 (I)	1	P		-31	-7.3	-2.3		0.1	141.6	
	2	P				-2.3		0.1	161	
	3	P		-31				0.1	244	
	4	P							180	
	1	P	-56	-43				-18		
	2	P	-54	-30	-23	-14.4		-4.2		
	3	P						-24		
	X	S	-54	-31	-24	-14	-6.2	-4		
	Y	S	-54	-31				-4		
HB1(I)	M		-70	-37				-4.4		
	N		-54	-34				-11		
HB1 (II)	A	P	-58	-51	-35	-26	-8.4	-6	241	
	B	P	-88	-51		-22		-15	241.3	
	D	P	-75	-50	-37	-18	-13	-7.2		
	E	P		-54	-32	-28	-24	-16		
	F	P				-8		-2.8		
HB1	A1	S	-75						70.4	
	A2	S	-75	>-38	-20					
	A3	S	-75	>-38	-20			-4.4	173	
	B(X3)	S	-75	-41	-20			-8.6	202	
	A	S		-23	-9			-0.5		
	B	S		-23	-9			-0.6		
	C	S						0.1		
	D	S						0.1		
	2	S								
	5	S		-48	-21	-6				

SAMPLE NO.	INCLUSION	ORIGIN	Tfreeze	Te	Intermediate melting events			Tfinal melting	Th
	5	S	-52	-42	-28	-21		-15	137
	6	S	-52	-42	-28	-21		-8.3	161
RP11 11A	A	?						-22.3	168
	B	?						12	143
RP11 11A	1	?		>-46	-37	-24		12.5	96.4
	2	?		-44				9.2	
	3	?		-44				-9	
	4	?							131
	5	?						-0.5	135
RP11 11A	1	S							143
	2	S						-11.4	114.3171
RP1 11A	A	P		-50	-31				114
	B	P		-50	-31			-11.2	115
	C	P		-50	-31			-6.4	154
		S	-50	?		-25	-19.5	-6.3	
RP1 11	A	S	-42		-33			-7.5	200
Field 1	F	S	-42					-6.5	207
Vein 1	G	S	-64		-56	-35		-1.8	
								3	
RP1 11	A (X500)	P	-44					-1	161
Field 2	B	P	-39					-7.3	
	C	P	-47					-5.3	165
RP1 11		P	-40					-0.4	122
field 3 a		P	-40					-3.1	109
		P		-40				-3.1	109
field 3b		P		-42	-30			-5.9	130
								-5	140

SAMPLE NO.	INCLUSION	ORIGIN	Tfreeze	Te	Intermediate melting events			Tfinal melting	Th
RP11 11A	1	?	-51	-42	-30	-23	-18	-12	
	2	?	[-51;-58]	-42	-30	-23	-18	-11.8	
	3	?	[-51;-58]	-42	-30	-23	-18	-17	121
	4	?	[-51;-58]	-42	-30	-23	-18	-15	127
	5	?	[-51;-58]	-42	-30	-23	-18	-8.2	128
	6	?	[-51;-58]	-42	-30	-23	-18	-5.5	<128
	1	?						-0.3	
	2	?						-3	
	3	?						-2	99
	4	?						-6.5	139
RP11 11A	1	P	-54.5	-50	-44	-33	-22	-8.9	214
FIELD 1	2	P	-53	-50				-17.3	169
	3	P	-53	-50				-13.9	154
	4	P		-50				-1.8	
	B	S	-65	-50	-36	-29		6.6	126
	A	S	-68	-46				11.7	128
	C	S	-69	-46				10.4	128
	3	S	[-51;-64]					13	147
	4 (X100)	S	[-51;-64]	-40				-3.6	
		S		-54.5	-21			-18	138
		S						-16	182
	A	S		-54	-28			13.4	
	C	S						16	
RP11 11A	1	S	-69	>-36	-36	25		-22.3	159
	A	P	-53					-21	
	B	P	-44	-52	-36	-27	-20	-7.4	
	C	P	-82					7.9	
	X	P	-50	-37				-9.5	
	E	P	-53					-8	
	G	P	-63					-11	
			-50					-6.9	
RP11 11A	1	S	-52	-42	-28	-21			121
	2	S	-52	-42	-28	-21		-12	
	3	S	-52	-42	-28	-21		-16	125
	4	S	-52	-42	-28	-21		-21	137

SAMPLE NO.	INCLUSION	ORIGIN	Tfreeze	Te	Intermediate melting events			Tfinal melting	Th
AS26 10C	1		-43	-40	25			5.1	
	2							-3.9	
	3							0.3	
	4							-0.8	
	5							-2.4	
	1		-43					1.6	
AS26 10C	2		-43					1	
FLUORITE	X10		-43					[-1.5;0]	
		S	-47	-38	-20	-12		1	
		S						-1	
CHIP1		S	[-46;-56]					-8.8	
		S	[-46;-56]					-4.2	
		S	[-46;-56]					-4	
		S	[-46;-56]					-2.8	
		S	[-46;-56]					-2.8	
		S	[-46;-56]					-1.3	
		S	[-46;-56]					-0.2	
		S	[-46;-56]					0.2	
		S	[-46;-56]						
AS26 10C	A	?P	-37	-34	-23	-18	-12	-3.5	243
CHIP 2	D		-37	-34				-1.4	140
fluorite ass	E							-3.5	
with chl &aspy	F							-2.2	145
	B								122
	X30	S	-45	-31	-22	-5.1	-2.1	-1.7	235.8
RP11 11A	A	P			-28	-24		13.9	95
vein qz ass	D	P							
withpy	F	S	-74	-45	-32			-8.1	168
	G	S						-4.3	168
								-10.3	
								-8.4	
RP11 11A		S	-76	-45	-30	-24	-23.5	-7.6	99
		S	-51	-41	-34	-24		-8.2	

SAMPLE NO.	INCLUSION	ORIGIN	Tfreeze	Te	Intermediate melting events			Tfinal melting	Th
RP2 20B	X17	S	-40	-33	-27	-21.7		-3.1	
FLUORITE		S	-40					-5.3	
		S	-40					-4.1	
	E	S	-38	-33	-30	-25.6	-20	-3.2	
	B	S	-38		-26			-13	
	A	S	-62					-5.2	
	C	S			-26				
	D	S							
	B	S	-39		-30			0	
	A	S	-48					-8.1	
RP2 20B	A	S	-50	-38	-27.1			-4.8	273
	B (X100)	S	-50	-38	-28			[-2.6;-1.7]	[71;93]
	X	S	-49	-34	-20.9	-15		-4.8	111.9
	D	P	-78	-41	-29			-8.8	116
	B	P	-78					-6.8	
	C	P	-78						
	A	P	-78					-20.5	199
		P	-83					-4.3	
RP2 20B	1		[-42;-47]	-49	-32	-24		-13.5	171
field 3	5		[-42;-47]					-5.8	
fluorite	6		[-42;-47]					-15	
	7		[-42;-47]					-12.4	
	8		[-42;-47]					-10	
	10		[-42;-47]	-50	-37	-26		-6.1	69.3
	11		[-42;-47]					-14	>262
	12		[-42;-47]					-10	>263
	13		[-42;-47]	-49	-42	-30	-24	-10.1	200
RP2 20B	1(x100)	S	-54	-52				-13.4	[70;240]
field 4	2		-54	-52				-11	[70;240]
	3		-54	-52				-11	234
	4		-54	-52				-9.8	[70;240]

SAMPLE NO.	INCLUSION	ORIGIN	Tfreeze	Te	Intermediate melting events			Tfinal melting	Th
RP2 27/9	A	S	-83	-46				-13.5	147
CHIP1	B	S	-62					-15	98.9
	A	S	-63	-59	-40	-31		-18.1	137
	E	S	-70	-59	-40	-31		-24.5	150
RP2 27/9	L	S	-62	-36	-31	-24		-12.2	
	K	S	-62	-36				-12.3	
	N	S	-63	-36				-11	
	C	S	-63	-41					108
		S	-49					1.9	
	X	S	-77	-59	-40	-31		-26	
	1	S	-77	>-41	-30	-23.8	-16		
	2	S	-77	>-42					
	Y	S	-77	>-43					
	A	S		>-40	-30				
	B	S		>-40				-10	155
		S		>-41				-10	159
		S		>-43				-3.6	
	F	S	-32	-55				14	143
	D	S		-55				-10	175
	E	S		-55				-10.2	
								9.2	225
								3	135
RP2 27/9	B		-49					-6.9	191.8
								-4.9	
	C								195
	D		-69					-7	195
								-6.5	181
	A		-49	-48.4	-46	-45	-27	-6.5	
			-51					-11	225
			-50.9	-57	-49	-41	-26	-7.3	
			-74					-18	191
				-57				-5.3	<191
RP2 27/9		S		<-44	-29				135
		S						-7.8	
		S						-6.9	

SAMPLE NO.	INCLUSION	ORIGIN	Tfreeze	Te	Intermediate melting events			Tfinal melting	Th
RP1 11A	A	?P		>-47	-32			-5	147
Vein 2	B	?P	-42	>-48	-31			0	114
	C	?P	-40	>-49	-30			-5	
	D	?P	-50	>-50	-29				156
	E	?P	-50	>-51	-28			-2	
RP1 11A	1 (X3)							-5.1	158
	2							-5.3	156
	3							-2.1	104
	4								
RP1 11A			-39	-38	-33	-16		-4.8	131
	D							-5.4	171
	B							-1.2	104
RP1 11A			-37		-36	-25		-6.4	
Vein 3			-37					-7.8	134
			-40.7					-7.6	120
								-6.2	152.9
			-43		-37	-31			119
			-38					-24	103
RP2 27A			-48.1	-46	-44	-20.7	-16.6	-4.2	
CHIP 1	1	?	-60	-52	-33	-28	-24		131
	2	P		-52				11.9	134
	3	P						12.5	133
	4	P	-66					15.3	147
	6	P						-4	76
			-75	>-50	-43	-33	-2.3	8.6	119.7
RP2 27A		S	-35	-18				4.3	
CHIP2		S	-42					2.3	128
		S	-39					-2	
		S						-2.5	158
		?						-4	
		?						4	128
		?							173
RP2 27A		S	-42	?-45				7.2	113
CHIP3		S	-40			-23		-0.4	111.6

SAMPLE NO.	INCLUSION	ORIGIN	Tfreeze	Te	INTERMEDIATE MELTIN			Tfinal melting	Th
TB01	A	S	-59	-37.5	-27	-23		-11.9	148
QUARTZ	B	S		-49.5				-22.2	>110
CHIP 1	C	S		-49.5				-17.6	
	D	S						-17	
	A	S	-65	-29				-20.9	102
	B	S	-74	-29					110
	A	S	-56	-33				-11.4	70
	B	S	-58	-33				-11.2	72
	4	S		-23	-19			6.4	136
	A	P	-62	-44.8	-25	-21		16	200
CHIP 2	1,2,3,4	S	-62	-58	-32			-16	
QUARTZ	A	S	-55.8	?-28				-13.4	122
	A	S	-61	-30	-21			-12.9	167
	B	S	-59					-12.9	85
	C	S	-57.7	-30	-21			-12.9	
	1,2			-33	-21			-10	149
	3	S	-66		-21			-14	100
CHIP 3									
TOURMALINE	A	S	-52	-44.6	-41	-31	-10	-9.7	82
	B	P						-12.7	85
QUARTZ	A	P	-62	-35				-14.3	115
	B	P						-12.7	115
CHIP 4	A	S		-47				-10	122
	C	S		-36	-24	-22		-20	86.5
	D	P		-36	-24	-22		-15.1	156
	E	P		-36	-24	-22		16.5	140
	F	P		-36	-24	-22		15.3	187
WG35									
FIELD 1	ZONE (X9)	P	?	?-50	-30	-24		?	
FIELD 2	ZONE (X9)	S		?	?	?	?	?	?
FIELD 3	TRAIL (X10)	S	-42	-35	-30	-24	-19	-5.1	
	TRAIL A	S	-73	-51	-44	-23		2.9	123
	B	S						6.1	128
	TRAIL (X7)	S	-75	-47	-21.1				71

SAMPLE NO.	INCLUSION	ORIGIN	Tfreeze	Te	INTERMEDIATE MELTIN			Tfinal melting	Th
WGA35	A	?	-80	-55	-44			-23	160
FIELD 1	B	?	-60					-23	160
	C	?	-60					-23	160
	D	?	-60					-20	78
	E	?	-60					-19	94
	F	?						-21	
	G	?						-18	
	H							5.9	135
FIELD 2	A	S	-65	-55	-43	-34	-23	-25	146
	B	S	-65					-14.2	162
	C	S	-65					-14.6	161
	D	S	-65						149
	E	S	-65					-24.7	125
	X	S	-65					-14	
	B	S						-16	143
	C	S							70
	D	S						-10.1	146
	A	S	-75	-54	-31	-24		-17.3	
	B	S	-73	-54	-31	-24		-19.4	148
	C	S	-75	-54	-31	-24		-21	164
WG03	1	S	-52	-50	-43	-36	-9.6	-6.2	
FIELD 1	2	S						-6.2	
	3	S	-46					-2	
FIELD 2	F			-51				>0	
	I			-49.5	-45	-38.5		>0	
	H							0.4	

RESULTS OF THERMAL DECREPITATION ANALYSES OF SAMPLES FROM GRASS VALLEY.

SAMPLE	T(°C) OF DECREPITATION	MASS DETECTED	COMMENTS
GV01	100-150	44 (CO_2^+ /N_2O^+)	Gradual increase of background.
		28 (N_2/$C_2H_4^+$/CO^+)	
		18 (H_2O^+)	
	170	2 (H_2)	Single inclusion burst.
	181	40 (Ar^+)	Ar reaches peak at 200°C, then starts declining rapidly.
GV02	85	44 (CO_2^+ /N_2O^+)	Gradual increase.
	118	12 (C^+)	Single inclusion burst containing methane.
		16 (O^+/CH_4^+/NH_2^+)	
		15 (CH_3^+/NH^+)	
	206	44 (CO_2^+ /N_2O^+)	Whole series of small bursts.
		28 (N_2/$C_2H_4^+$/CO^+)	
		16 (O^+/CH_4^+/NH_2^+)	
		12 (C^+)	
		18 (H_2O^+)	
		34 ($H_2{}^{32}S^+$/$^{34}S^+$)	Note presence of S.
		48 (SO^+)	
	363	15 (CH_3^+/NH^+)	Series of small bursts.
		16 (O^+/CH_4^+/NH_2^+)	
		28 (N_2/$C_2H_4^+$/CO^+)	

RESULTS OF THERMAL DECREPITATION ANALYSES OF SAMPLES FROM GRASS VALLEY (CONTINUED).

SAMPLE	T(°C)	MASS DETECTED	COMMENTS
GV05i	138	12 (C^+)	Single inclusion burst.
		15 (CH_3^+/NH^+)	
		16 ($O^+/CH_4^+/NH_2^+$)	
		44 (CO_2^+/N_2O^+)	
	169-300	44 (CO_2^+/N_2O^+)	Small peaks which increase in intensity
		15 (CH_3^+/NH^+)	between 182- 300°C.
			Large inclusions burst followed by a
	322	12 (C^+)	series of smaller bursts which cease by
		16 ($O^+/CH_4^+/NH_2^+$)	473 °C.
		28 ($N_2/C_2H_4^+/CO^+$)	
		44 (CO_2^+/N_2O^+)	
GV052	115	16 ($O^+/CH_4^+/NH_2^+$)	Increase in back for water peaks.
(quartz 1,2 & 3)		18 (H_2O^+)	CO^2 and Ar curves gradually increase.
	160	44 (CO_2^+/N_2O^+)	No discrete fluid inclusion bursts in this
		40 (Ar^+)	sample. All curves return to background
			at 400 °C.
GV053	79	44, 15	Small methane and nitrogen peaks.
(Quartz 7)			N_2 increasing.
	125	14, 28,44, 15	2 small peaks followed by a series of
	148	44	others.
			Large CO_2 peaks. N_2 has returned to
	194	44	background.
			Ar increasing rapidly. CO2 diminishing.
	250	40, 14, 15, 32	First water peak.
			Water peaks and second batch of CO_2
	285	16, 18	peaks.
GV053	300	16, 18, 44	Water decreasing, and small CO_2 peaks
continued			continuing.
	400	16, 18, 44	CO_2 peaks continue until 500 °C.
	500	44	

RESULTS OF THERMAL DECREPITATION ANALYSES OF SAMPLES FROM GRASS VALLEY (CONTINUED).

SAMPLE	T(°C)	MASS DETECTED	COMMENTS
GV054	100	18,16	Gradual increase of H_2O.
	201-220	12,14, 28, 30	Background of 12,14, 28 and 30 starts increasing.
	293	18, 16, 44 28	Large water burst with 44 and 28. Response starts decaying by 322 °C and is back to background by 400 °C.
GV056 (quartz 6, 7 & 8)	97-125	28	Gradual increase in 28, which reaches peak at 114, and then decreases to background.
	130	44 16, 18	First CO_2 peak. Water rising.
	240	44, 16, 18	CO_2 and water bursts. CO_2 peaks larger than water peaks.
	312	40	Ar background increasing.
	312-533	44, 16, 18,40	CO_2 and water bursts continue until 533°C.
GV057 (quartz 8)	96-500	44, 28, 14	N_2 and CO_2 peaks. No water response.

RESULTS OF THERMAL DECREPITATION ANALYSES OF SAMPLES FROM ALBERT.

SAMPLE	T(°C)	MASS DETECTED	COMMENTS
RP1 11a	138	18	Water starts increasing, and continues until
quartz vein			400°C.
with sulphides	400	33, 36	H_2S and HCl start increasing.
RP1 11	117	18, 16	Water curves start increasing.
Quartz vein 1	254	14, 28	Nitrogen curves increasing.
	303	14, 15, 28 , 44	Small inclusion bursts.
	350	36, 33	H_2S and HCl start increasing gradually.
			Water curves start decreasing.
	420	16, 18	Small argon spikes.
	454	40	
RP1 11	86	14, 28, 44	Broad nitrogen and carbon dioxide curves
Quartz vein 2			(first CO_2 pulse).
	110	18	Water increasing.
	256	18	Water reaches plateau.
	314	18	Small water peaks on back of plateau.
	350	33, 36	HCl and H_2S start increasing.
	381	44	CO_2 background increased (second CO_2
	450	44, 18, 16	pulse)
			Small CO_2 peaks (third CO_2 pulse), and
			rapid increase in water response.
RP1 11	80	28, 44, 14	Nitrogen and CO_2 curves start increasing.
Quartz vein 3			Nitrogen and CO_2 curves start decreasing.
	100	28, 44, 14	Water starts increasing.
			Nitrogen curves increase again.
	110	18	Increases.
	242	28, 14	All curves return to background.
	295	44	
	400		

RESULTS OF THERMAL DECREPITATION ANALYSES OF SAMPLES FROM SPOEDWEL.

SAMPLE	T(°C)	MASS DETECTED	COMMENTS
L1	83	14, 28, 44, 15	N_2 and CO_2 curves start increasing.
	100	18, 40	Water and argon peaks start increasing and nitrogen and CO_2 peaks start decreasing.
			Broad CO_2 peak.
			Start increasing again.
	138-150	44	Small water peaks.
	245	14, 15, 40	H2S and HCl start increasing.
	268	18	
	300	33, 36	

ABSTRACT

The Nature of Hydrothermal Fluids Associated with the Granite-hosted Spoedwel Copper Mine, Bushveld Complex, South Africa.

L. A. Freeman and L. J. Robb

Department of Geology, University of the Witwatersrand, Johannesburg, RSA.

The Spoedwel Copper Mine is situated on the farm Spoedwel 701ks, in the Groblersdal District north-west of Marble Hall. The copper mineralization occurs in the upper portion of the Lebowa Granite Suite (Nebo, Klipkloof and Makhutso granites), and is hosted by de-silicified medium-grained brick red granite, often referred to as an "episyenite" (Scoggins,1991).

The aim of this research is to elucidate the nature of the various fluids that traversed the granite pluton in the Spoedwel region, by determining the physical and chemical properties of the representative fluids trapped in fluid inclusions. The relationships between the individual fluid inclusion populations and the different pulses of ore deposition and alteration consitutes an interesting avenue of research.

The ore suite at Spoedwel is dominated by copper-bearing minerals, the most abundant being chalcopyrite, which is altered to bornite, chalcocite and covellite. The occurrence of tetrahedrite is erratic and present in minor amounts. Pyrite, sphalerite, and galena are less abundant than chalcopyrite, but never the less, form an integral part of the paragenesis at Spoedwel. Cassiterite, zircon, magnetite and sphene occur as accessory minerals, which crystalized syngenetically within the Spoedwel Granite Pluton. The Cu-Fe-Zn-S mineralization occurred later and is related to de-silicification, chloritization and haematization of the granitic host rock . The introduction of secondary fluorite occurred after extensive haematisation of feldspar crystals. Haematite veinlets are transected by younger quartz and fluorite veinlets, in which several fluid inclusions contain trapped daughter crystals of haematite.

The overall paragenetic sequence is as follows:
pyrite (white-ish yellow), cassiterite, zircon and sphene forming the orthomagmatic suite, followed by pyrite (yellow), sphalerite (transparent), galena, tetrahedrite, sphalerite (opaque) and chalcopyrite. This secondary ore suite is associated with several episodes of alteration which resulted in the conversion of chalcopyrite to bornite, chalcocite and covellite.

However, as the above sequence of mineralization suggests, ore deposition at Spoedwel is rather complicated, with more than one phase of over-printing evident. Two generations of pyrite and sphalerite are discernable, as well as two generations each of the gangue assemblage quartz, feldspar, chlorite and fluorite.

A thorough examination of polished thin sections and doubly polished thin sections (wafers) has confirmed that several different generations of fluid were responible of the formation of the deposit as it occurs today. Fluid inclusions have been observed in quartz, fluorite and transparent sphalerite crystals, preserving fractions of the magmatic fluid as well as some of the other later metamorphic fluids. Fluid inclusions in cassiterite are scarce and too small to provide meaningful analytical results.

Fluid inclusions have been categorised as primary, secondary or pseudosecondary according to the scheme of Roedder (1979) and inclusions large enough to observe phase changes in the components, and hence be suitable of microthermometric analysis, have been located and mapped. The presence of variable phase proportions in the inclusions suggests that boiling or effervescence of certain of the fluids was in process at the time of entrappment. Inclusions containing a single phase (either liquid or vapor) are found in close association with two (L+V) and three (L+V+S) phase inclusions (Plate 1). Primary inclusions, occuring randomly scattered within grains, or lining and radiating from growth zones, commonly contain cubic halite and/or rounded sylvite daughter crystals (Plate 2). However, at least four other crystals, whether as true daughters or as trapped crystals, have been noted in single inclusions. Positive identification of halite, sylvite and haematite crystals have been made, and the presence of sulphides, muscovite and chlorite is suspected. Later generations of fluid are less saline, and contain no daughter crystals (Plate 3).

The composition of the fluid phases within fluid inclusions were investigated by means of Laser Raman Spectroscopy. Spectra obtained from selected primary, secondary and pseudosecondary inclusions indicates that nitrogen was an important component of the system. The presence of carbon dioxide, water, and methane was also detected.

The results of this study are potentially valuable as aids in exploration for ore deposits in the nearby vicinity, as well as contributing to the existing database (eg. Ollila.1981; Pollard *et al*, 1991) from which a model of the mineralization in the Bushveld granites may eventually be constructed.

References

Ollila, J.T. 1981. *A Fluid Inclusion and Mineralogical Study of Tin Deposits and Rocks Associated with the Bushveld Complex at the Zaaiplaats, Union and Rooiberg Tin Mines in the Central Transvaal, South Africa.* Unpubl. PhD. Thesis. Rand Afrikaans University. pp257.

Pollard, P.J., Andrew, A.S. & Taylor, R.G. 1991. Fluid inclusion and stable isotope evidence for interaction between granites and magmatic hydrothermal fluids during formation of disseminated and pipe-style mineralization at the Zaaiplaats tin mine. *Econ. Geol.* 80: 158-171.

Roedder, E. 1979a. *Fluid inclusions as samples of ore fluids.* In: H.L. Barnes (Ed.) Geochemistry of Hydrothermal Ore Deposits. J. Wiley and sons. New York. 684-737.

Scoggins, A.J. 1991. *Kwandebele: A regional appraisal of the base metal potential of the Bushveld granites.* STK Mineral Development Division. LIB REF No. : 2958.

List of Plates

Plate 1: Photograph showing variable phase proportions in primary fluid inclusions lining a growth zone in a euhedral quartz crystal.

Plate 2: Photograph showing a portion of a pseudosecondary trail of inclusions in quartz containing large anisotropic sylvite daughter crystals.

Plate 3: Photograph showing a trail of secondary inclusions in fluorite containing no daughter crystals and variable phase proportions.

Plate 1:

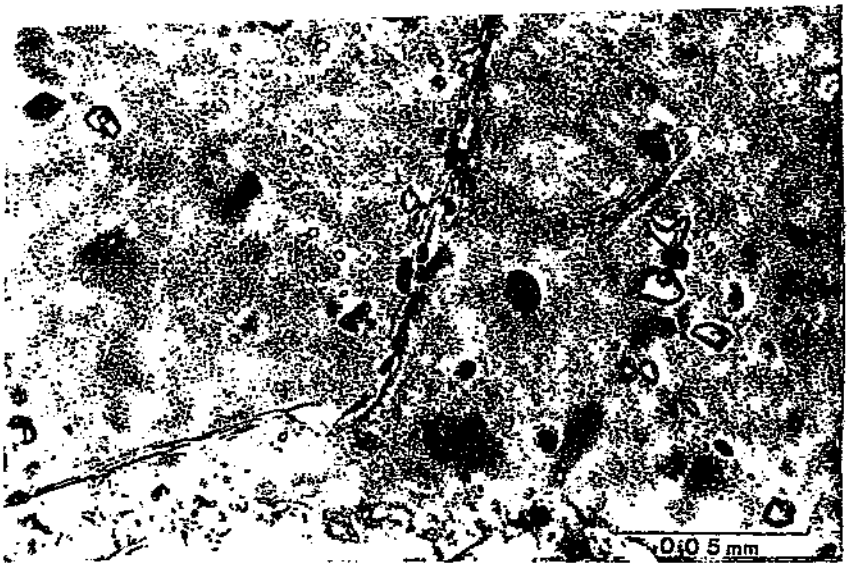


Plate 2:

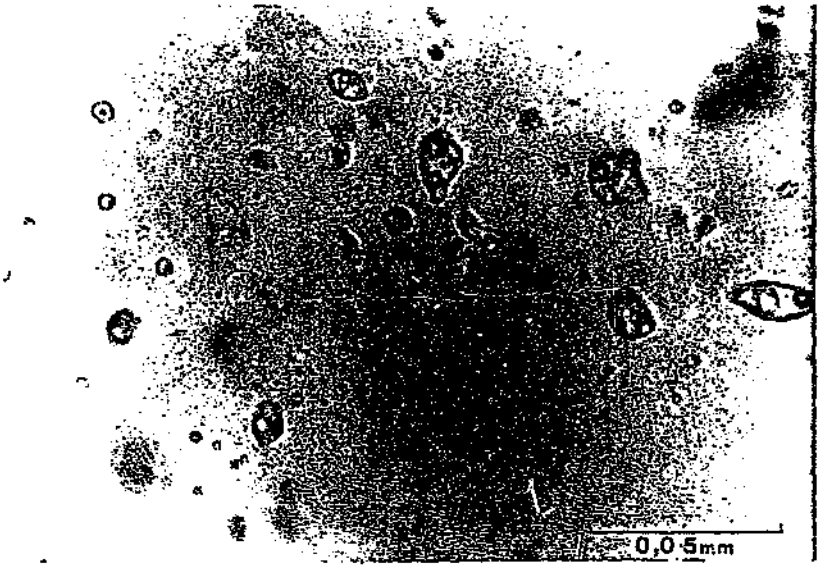
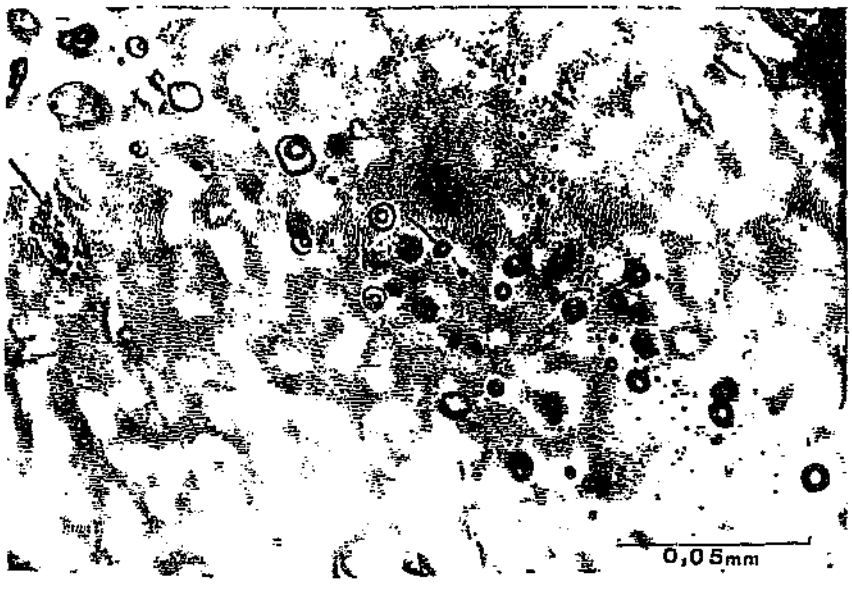


Plate 3:



FLUID MIXING AND THE FORMATION OF POLYMETALLIC MINERALISATION IN THE BUSHVELD GRANITES.

L.A.Freeman[1], L.J.Robb[1], S.E.Kesler[2] and J.R.O'Neil[2]

1. Dept. of Geology, University of the Witwatersrand, Johannesburg, RSA.
2. Dept. of Geological Sciences, University of Michigan, Ann Arbor, Michigan, USA.

Numerous small base metal deposits are known to occur in the acidic rocks of the Bushveld Complex and modern exploration programs are currently re-examining this metallotect in an attempt to refine the current working hypothesis for mineralisation in these granites. The hypothesis proposed for the origin of mineralisation is multifaceted, encompassing both spatial and temporal relationships between at least three episodes of ore formation. The first episode of mineralisation (typified by the Zaaiplaats Sn deposit) occurred at relatively high temperatures (ca. 600°C to 400°C), and resulted in the formation of orthomagmatic cassiterite, scheelite and an early generation of fluorite. At lower temperatures (200°C<T<400°C), where processes where essentially fluid dominated, a mesothermal Cu-Pb-Zn-As-Ag-Au assemblage was deposited (exemplified by the Spoedwel, Boschoek and Albert Cu and Ag deposits). A third episode of mineralisation resulted in the formation of an Fe-U-F assemblage and is recognised at several, but not necessarily all, of the deposits examined (for example, the Albert Ag deposit). The extended nature of this three-stage paragenetic sequence is considered to reflect widespread mixing between an early fluid derived by H_2O-saturation of the granitic magma and a meteoric fluid, circulation of which was stimulated by the long-lived high heat-productive capacity of the Bushveld granites, as well as exhumation of the metallotect. Support for this hypothesis is discussed below:-

1) Cathodo-luminescence images have indicated the presence of **two major episodes of fluorite precipitation at Spoedwel.** An early, possibly magmatic, stage formed as a result of cooling of acidified brines, whereas a later, low temperature, stage is believed to have precipitated as a result ofprogressive mixing of this brine with a connate component.

2) **Covellite over-printing** of Cu-bearing sulphide minerals along grain boundaries and microfractures is characteristic of retrograde thermal processes. Dissolution and replacement of chalcopyrite by covellite is considered to be the result of the imposition of an oxidizing fluid, and not simply lower temperatures.

3) Local occurrences of hydrothermal **tourmaline veins and spheroids**, similar to those of the Sn-W-Cu deposits of Cornwall (southeast England), have been recognised in the Bushveld granites. In both cases the interaction of boron-rich, magmatically derived fluids, and Fe-Mg-rich connate fluids is thought to have resulted in localised precipitation of tourmaline.

4) **Both hypersolvus (single feldspar) and subsolvus (two feldspar) granites** are now recognised in the Bushveld Complex. Subsolvus mineralogy has been identified at the Spoedwel, Albert and Grass Valley deposits, while the hypersolvus granite tend to be unmineralised. Coexisting hypersolvus and subsolvus granites are interpreted as being the products of meteoric water incursions.

5) **Fluid inclusion** characteristics suggestive of fluid mixing include; a) the occurrence of monophase liquid- and vapour-rich inclusions within two and three phase fluid inclusion assemblages which have variable phase proportions; b) broad ranges

of salinities, densities, and homogenisation temperatures in single fluid inclusion assemblages; and iii) the presence of **nitrogen, methane**, other **heavier hydrocarbons**, as well as **elevated Ar contents** in the fluids (Table 1 and Fig. 1) which have been detected by Raman Spectroscopy and Quadrupole Mass Spectrometry (QMS).

6) Fluid mixing is also indicated by the **stable isotopic signatures of fluid inclusions.** $\delta^{13}C$ values indicate at least two sources of carbon, viz. from limestones and from an externally derived organic carbon. In addition, $\delta^{18}O$ and δD values fall in a range outside that characteristic of purely magmatic fluids.

Table 1. Selected QMS analyses of fluid inclusion decrepitates from various deposits, compared to a barren granite sample. Analyses in mole %.

	CH_4	C_2H_6	Ar	N_2
GRASS VALLEY (GV02)	$2.9x10^{-3}$	$3.7x10^{-3}$	$2.1x10^{-3}$	$5.1x10^{-2}$
TOURMALINE SPHEROIDS	$5.1x10^{-2}$	$2.8x10^{-3}$	$4.8x10^{-3}$	$7.2x10^{-2}$
ALBERT SILVER MINE (RP2)	$1.3x10^{-2}$	$6.5x10^{-3}$	$4.1x10^{-3}$	$7.3x10^{-2}$
SPOEDWEL MINE (SP5)	$2.8x10^{-3}$	$4.2x10^{-3}$	$1.9x10^{-3}$	$1.7x10^{-1}$
KLIPKLOOF GRANITE	0.0	$3.2x10^{-3}$	$4.4x10^{-3}$	$9.4x10^{-2}$

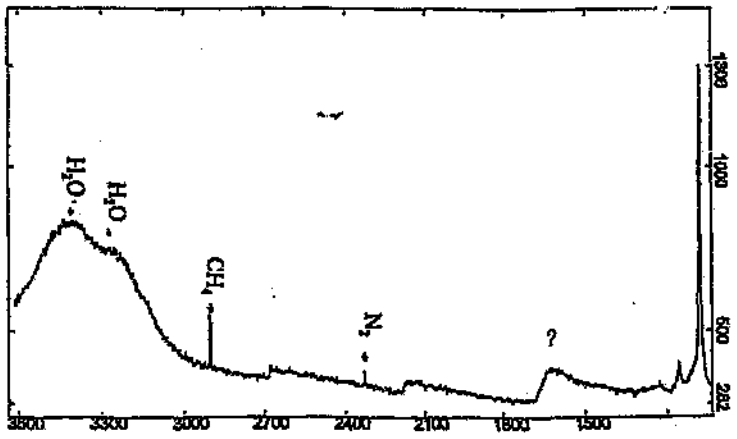


Figure 1. Raman spectrum of a fluid inclusion

The early high temperature (ca. 600°C) Sn-W assemblage was precipitated by orthomagmatic processes, as well as the circulation of magmatic fluids. With time, the pluton cooled and was subject to regional uplift and erosion. Fractures developed, acting as conduits for external fluids of meteoric and/or connate origin. The late magmatic fluids, enriched in incompatible metals (and volatiles), interacted with the connate/meteoric fluid, of contrasting chemistry and possibly also metal-charged, resulting in the localised precipitation of a secondary, lower temperature (>200°C) mineral assemblage (Cu-Pb-Zn-As-Ag-Au) in the zone of fluid mixing. As the external fluid component became progessively more dominant, the late Fe-U-F (>140°C) paragenesis formed. The extended paragenetic sequence in the acid rocks of the Bushveld Complex is adequately explained by a combination of orthomagmatic processes and sub-solidus fluid mixing.

METALLOGENY OF THE ACID PHASE OF THE BUSHVELD COMPLEX

ROBB, L.J., FREEMAN, L.A. and BAILIE, R.H.
Department of Geology, University of the Witwatersrand, Johannesburg 2050, RSA

The acid phase of the Bushveld Complex comprises a large sheet-like batholith of fractionated, alkali felspar rich granite-the Lebowa Granite Suite- intruded into a 4600m thick extrusive sequence of mainly rhyolites and pyroclastics - the Rooiberg Group. The latter was emplaced at 2061±2 Ma, while the final pulse of granite emplacement had occurred by 2054±2 Ma. Rb-Sr and Pb-Pb isotopic systems remained open for several hundred million years after emplacement indicating slow cooling and extensive fluid circulation related to the large radiogenic heat productive capacity of the mineralized portions of the batholith (up to $30\mu W.m^{-3}$)

The acid rocks are characterized by innumerable small-to medium-sized polymetallic deposits which reflect the alkalic magma composition, the high degree of *in situ* crystal fractionation and the extensive circulation of hydrothermal fluids that has occurred. A complex paragenetic sequence, comprising (Sn-W)-(Mo-Cu-Pb-Zn-As-Au-Ag)-(Fe-F-U), reflects multi-facetted control of ore deposition related to incompatible element concentration during crystallization, fluid circulation and concentration in the apical portions of the intrusion and focusing of fluid egress by major structures active during and after Bushveld emplacement. The extended paragenetic sequence, which ranges from orthomagmatic processes (Sn-W) to epithermal conditions (Fe-F-U), appears to have lasted for up to 1000 million years and is best explained in terms of long-lived, radiogenically stimulated, fluid circulation in which a dominantly magmatic fluid phase was progressively diluted by meteoric or connate components. Detailed fluid inclusion studies clearly demonstrate the characteristics of the fluid components involved in Bushveld metallogenesis.

Author: Freeman, Lauren Anne.
Name of thesis: The nature of hydrothermal fluids associated with granite-hosted, polymetallic mineralisation in the eastern lobe of the Bushveld Complex.

PUBLISHER:
University of the Witwatersrand, Johannesburg
©2015

LEGALNOTICES:

Copyright Notice: All materials on the University of the Witwatersrand, Johannesburg Library website are protected by South African copyright law and may not be distributed, transmitted, displayed or otherwise published in any format, without the prior written permission of the copyright owner.

Disclaimer and Terms of Use: Provided that you maintain all copyright and other notices contained therein, you may download material (one machine readable copy and one print copy per page)for your personal and/or educational non-commercial use only.

The University of the Witwatersrand, Johannesburg, is not responsible for any errors or omissions and excludes any and all liability for any errors in or omissions from the information on the Library website.